Development of small extracellular vesicle-based therapeutics based on the elucidation and regulation of pharmacokinetic properties

細胞外小胞の体内動態特性の解明とその制御に基づく疾患治療法の開発に関する研究

2019

Akihiro MATSUMOTO

PREFACE

Human body consists of 37 trillion cells with more than 50 different cells[1]. In order to maintain the homeostasis against different extracorporeal and intracorporeal changes, cells communicate with remote cells through the mechanism called “intercellular signaling” and controls a diverse range of cellular processes and activities. The concept that intercellular signaling in the nervous system was mediated by chemical messengers was first proposed by Dr. Otto Loewi in 1898[2]. Since then, it was found that various forms of intercellular signaling molecules were identified including neurotransmitters, hormones, chemokines and cytokines. After their great effects on human body have been uncovered, these chemical messengers are chemically or biologically synthesized and utilized to treat diseases at present. As another novel form of intercellular signaling, extracellular vesicles (EVs) have been discovered and expected for potential clinical applications.

EVs are cell-derived lipid particle secreted from various types of cells and can be found in human body fluids. According to the International Society of Extracellular Vesicles, EVs currently are roughly classified into physical characteristics, such as size: small EVs (< 100 nm or < 200 nm), or medium, large EVs > 200 nm. In particular, small EVs (sEVs), which are also called as exosomes, have gained much attraction. The presence of sEVs was firstly discovered in 1983 by Dr. Harding and his team[3]. They found that transferrin receptors associated with nanovesicles are released into the extracellular space during the maturation of reticulocyte to erythrocyte. Before that time, it was known that reticulocyte loses the transferrin receptor during the maturation process[4]. So other scientists initially considered sEV as an alternative means for cellular waste disposal and did not pay great deal of attention. The perspectives on sEV dramatically changed in 1996 when Dr. Raposo et al. reported that B cell-derived sEV display peptide-MHC-II complexes and are able to activate T responses[5]. Moreover, an epoch-making discovery was reported by Dr, Valadi et al. in 2007, showing that sEV might be involved in genetic exchange between cells by transferring mRNAs and microRNAs into other cells[6]. After that, sEVs have been regarded as one of the most important intercellular messengers which could be involved in many pathophysiological processes.

As sEV-mediated intercellular communication occurs through the transfer of sEV cargos to the recipient cells, sEVs are expected to become safe and efficient delivery vehicle and therapeutics. The feasibility of sEV-based drug delivery and therapeutics has been proven by the early studies after 2010s in which sEVs loaded with therapeutic drugs were delivered to the targeting site to treat various diseases, such as cancer, inflammatory diseases, or central nervous system diseases[7,8]. Besides, several other studies demonstrated the sEV isolated from immune cells can be applied as vaccine to induce antigen-specific immunity[9].

Pharmacokinetics of sEVs is one of the most important issues to develop sEV-based therapeutic systems[10–12]. Bioavailability at the target tissues/cells after administration of sEVs is the key determinant for the therapeutic effect of a sEV-based therapeutic system. Quantitative information regarding the elimination profile from the blood

circulation and biodistribution of sEVs is also required for a rational design of the sEV-based therapeutic systems. However, the information about these factors is limited at present.

Therefore, in this thesis, I envision sEV-based therapeutics based on elucidation and regulation of pharmacokinetic (PK) properties. In chapter I and chapter II, sEV secreted from tumor cells and dendritic cells were used to develop sEV-based cancer vaccine. Based on the elucidated *in vivo* fate of sEV, two different strategies were considered to induce strong anti-tumor immunity. In chapter III and chapter IV, PK properties, especially the clearance mechanism from blood, of sEV collected from cultured cell line and blood were quantitively analyzed. Based on the detailed PK analysis, I discovered novel sEV subpopulation which shows unique blood clearance.

ACKNOWLEDGMENTS

Firstly, I would like to express my utmost gratitude to my advisor Dr. Yoshinobu Takakura, Professor of Department of Biopharmaceutics and Drug Metabolism, Graduate School of Pharmaceutical Sciences, Kyoto University, for giving me exciting opportunities to immerse myself in pharmaceutical science at his excellent laboratory. His wonderful guidance, valuable discussion, warm support and encouragement helped me in all the time of research and writing of this thesis. Moreover, I should thank him for allowing me to work independently on interesting projects and collaborations for his ideas, and trust as well as his scientific input and advices.

I also would like to express my sincere gratitude to my research guides, Dr. Yuki Takahashi, Associate Professor of Department of Biopharmaceutics and Drug Metabolism. It was a wonderful opportunity to do my Ph.D. program under his guidance and to learn scientific mindset from his research experiences. All his encouragement, insightful comments, and hard questions were fully helpful and essential to achieve my Ph.D. research. I could not have imagined having a better advisor for my Ph.D. study.

I wish to express my deepest appreciation to Dr. Makiya Nishikawa, Professor of Laboratory of Biopharmaceutics, Faculty of Pharmaceutical Sciences, Tokyo University of Science, for his patient supervision, insightful comments, suggestions, guidance, direction, valuable discussions and supports facilitating the successful completion of this study.

I would like to thank my sincere mentor Dr. Masaki Morishita, Assistant Professor of Department of Biopharmaceutics, Kyoto Pharmaceutical University, for introducing me to the world of extracellular vesicles and for encouraging me to jump into the Ph.D. course. I appreciate him for sharing his talented research skills as well as his philosophy to sciences whenever I was in trouble. I learned a lot from him.

I would like to thank Dr. Hideo Saji, Professor of Department of Patho-Functional Bioanalysis, Graduate School of Pharmaceutical Sciences, Kyoto University, and Dr. Kohei Sano, Lecturer of Laboratory of Biophysical Chemistry, Kobe Pharmaceutical University, for the research collaboration in Chapter I_section 1 and Chapter III_section 1. They greatly contributed to the preparation of radiolabeled biotin-derivative.

I would like to thank Dr. Yasushi Ishihama, Professor of Department of Molecular and Cellular BioAnalysis, Graduate School of Pharmaceutical Sciences, Kyoto University, and his laboratory member, Dr. Hsin-Yi Chang, Yi-Wen Wu, and Mr. Kosuke Ogata for the research collaboration in Chapter III_section 2 and Chapter IV. They greatly contributed to the proteome analysis.

I would like to express my special thanks to Dr. Theresa L. Whiteside, Professor of Pathology, Immunology and Otolaryngology, UPMC Hillman Cancer Center, University of Pittsburgh Cancer Institute and her laboratory members for the warm acceptance to her laboratory as a visiting scholar. Her willingness to share experimental skills and ideas on isolation and identification of extracellular vesicle from plasma was indispensable for the

achievement of Chapter III_section 2.

I would like to thank all laboratory members, both the alumni and present members of Department of Biopharmaceutics and Drug Metabolism, Graduate School of Pharmaceutical Sciences, Kyoto University, for the exciting discussions and experimental assistances as well as for all the memorable moments we have shared in these six years. In particular, I would like to give my special thanks to Dr. Charoenviriyakul Chonlada, Ms. Aki Yamamoto, Mr. Naoki Nakagawa, Mr. Reiichi Ariizumi, Ms. Maho Asuka, and Mr. Shimpei Kitamura for the unstinting help.

I thank Japan Society for the Promotion of Science for financial support (Research Fellowship for Young Scientists) and for the financial support of research related to Chapter II and the financial support of visiting laboratories in UPMC Hillman Cancer Center, University of Pittsburgh Cancer Institute, United States. I thank Training Program of Leaders for Integrated Medical System of Kyoto University for the financial support of research related to Chapter I. I thank Graduate School of Pharmaceutical Sciences of Kyoto University for financial support to attend international academic conference.

Last not but least, I would like to thank my brothers for always helping me to see the silver lining and most importantly, my parents for their love and support throughout my career to date. They are a constant in my life and have always encouraged me to see the bigger picture for a better world. I am truly grateful to them for making me who I am today.

TABLE OF CONTENTS

LIST OF ABBREVIATIONS

The International System of Units (SI) base units and prefixes for unit names have been used and are not specified in this list.

⍙⍙Ct	Delta cycle threshold
Ab	Antibody
AnV	Annexin V
APC	Antigen presenting cell
ApoB	Apolipoprotein B
Arg1	Arginase 1
AUC	Area under the curve
B16-sEV	B16BL6-derived small extracellular vesicle
Bq	Becquerel
BMDC	Bone marrow-derived dendritic cell
BSA	Bovine serum albumin
°C	Degree Celsius
CD	Cluster of differentiation
CF	Captured fraction
CL	Clearance
Ct	Cycle threshold
DAPI	4',6-Diamidino-2-phenylindole
DC	Dendritic cell
DGC	Density gradient centrifugation
DiI	1,1'-Dioctadecyl-3,3,3',3'-tetramethylindocarbocyanine perchlorate
DiO	3,3'-Dioctadecyloxacarbocyanine perchlorate
DMEM	Dulbecco's modified eagle's medium
DNA	Deoxyribonucleic acid
DSPC	1,2-Distearoyl-sn-glycero-3-phosphocholine
DSPG	1,2-Distearoyl-sn-glycero-3-phosphoglycerol
e.g.	*exempli gratia* (Latin = for example)
EDTA	Ethylenediaminetetraacetic acid
ELISA	Enzyme-linked immuno sorbent assay
et al.	*et alii* (Latin = and others)
EV	Extracellular vesicle
FBS	Fetal bovine serum

g	Gravitational force
GAPDH	Glyceraldehyde 3-phosphate dehydrogenase
gLuc	*Gaussia* luciferase
GM-CSF	Granulocyte macrophage colony-stimulating factor
HEPES	4-(2-Hydroxyethyl)-1-piperazineethanesulfonic acid
HRP	Horseradish peroxidase
HSP70	Heat shock protein 70
i.e.	*id est* (Latin = that is)
i.v.	Intravenous
IFNγ	Interferon γ
IgG	Immunoglobulin G
IL-12p40	Interleukin-12p40
IL-2	Interleukin-2
IL-4	Interleukin-4
IL-6	Interleukin-6
iNOS	Inducible nitric oxide synthase
Lamp	Lysosomal-associated membrane protein
LDL	Low density lipoprotein
MD-mice	Macrophage-depleted mice
MFI	Mean fluorescent intensity
MHC	Major histocompatibility complex
miRNA	micro RNA
MP	Mouse plasma
MP-sEV	Mouse plasma-derived small extracellular vesicle
Mrc1	Macrophage mannose receptor 1
mRNA	messenger RNA
MRT	Mean residence time
n	Number of biological samples
NCF	Non-captured fraction
NT-mice	Non-treated mice
ODN	Oligodeoxynucleotide
OVA	Ovalbumin
PBS	Phosphate buffered saline
pDNA	plasmid DNA
PEG	Polyethylene glycol
PEI	Polyethylenimine
PG	Phosphatidylglycerol
PI	Propidium iodide

PK	Pharmacokinetic
PS	Phosphatidylserine
PSD	Phosphatidylserine decarboxylase
PSG	Penicillin-Streptomycin-Glutamine
qPCR	Quantitative polymerase chain reaction
RNA	Ribonucleic acid
RPMI	Roswell Park Memorial Institute medium
RT-PCR	Reverse transcription-polymerase chain reaction
SAV	Streptavidin
SD	Standard deviation
SDS-PAGE	Sodium dodecyl sulfate-polyacrylamide gel electrophoresis
SEC	Size exclusion chromatography
SEM	Standard error of the mean
sEV	small extracellular vesicle
TEM	Transmission electron microscopy
TGF-β	Transforming growth factor-β
Tim4	T-cell immunoglobulin and mucin domain containing 4
TNF-α	Tumor necrosis factor-α
UC	Ultracentrifugation
v/v	Volume per volume
VLDL	Very low density lipoprotein
w/v	Weight per volume

LIST OF FIGURES

LIST OF TABLES

LIST OF SUPPLEMENTARY FIGURES

LIST OF PUBLICATIONS INCLUDED IN THIS THESIS

1. **Akihiro Matsumoto**, Yuki Takahashi, Makiya Nishikawa, Kohei Sano, Masaki Morishita, Chonlada Charoenviriyakul, Hideo Saji, Yoshinobu Takakura.

   Role of phosphatidylserine-derived negative surface charges in the recognition and uptake of intravenously injected B16BL6-derived exosomes by macrophages

   Journal of Pharmaceutical Sciences, 2017, 106(1):168-175

2. **Akihiro Matsumoto**, Yuki Takahashi, Makiya Nishikawa, Sano K, Masaki Morishita, Chonlada Charoenviriyakul, Hideo Saji, Yoshinobu Takakura.

   Accelerated growth of B16BL6 tumor in mice through efficient uptake of their own exosomes by B16BL6 cells

   Cancer Science, 2017, 108(9):1803-1810.

3. **Akihiro Matsumoto**, Yuki Takahashi, Ariizumi R, Makiya Nishikawa, Yoshinobu Takakura.

   Development of DNA-anchored assembly of small extracellular vesicle for efficient antigen delivery to antigen presenting cells

   Biomaterials, 2019, 225:119518.

4. **Akihiro Matsumoto**, Yuki Takahashi, Hsin-Yi Chang, Yi-Wen Wu, Aki Yamamoto, Yasushi Ishihama, Yoshinobu Takakura.

   Blood concentrations of small extracellular vesicles are determined by a balance between abundant secretion and rapid clearance

   Journal of Extracellular Vesicles, 2019, 9:1696517. (online publication)

5. **Akihiro Matsumoto**, Yuki Takahashi, Kosuke Ogata, Naoki Nakagawa, Aki Yamamoto, Shimpei Kitamura, Yasushi Ishihama, Yoshinobu Takakura

   Discovery of phosphatidylserine-deficient small extracellular vesicle subpopulation with super long blood circulation

   Manauscript in Preparation

6. **Akihiro Matsumoto**, Maho Asuka, Yuki Takahashi, Yoshinobu Takakura

   Detailed analysis of cellular and humoral immune response by dendritic cell-derived small extracellular vesicle

   Manauscript in Preparation

LIST OF PUBLICATIONS NOT INCLUDED IN THIS THESIS

1. Takafumi Imai, Yuki Takahashi, Makiya Nishikawa, Kana Kato, Masaki Morishita, Takuma Yamashita, **Akihiro Matsumoto**, Chonlada Charoenviriyakul, Yoshinobu Takakura.

   Macrophage-dependent clearance of systemically administered B16BL6-derived exosomes from the blood circulation in mice

   Journal of Extracellular Vesicles, 2015, 4:26238. (online publication)

2. Masaki Morishita, Yuki Takahashi, **Akihiro Matsumoto**, Makiya Nishikawa, Yoshinobu Takakura.

   Exosome-based tumor antigens-adjuvant co-delivery utilizing genetically engineered tumor cell-derived exosomes with immunostimulatory CpG DNA

   Biomaterials. 2016, 111:55-65.

3. Chonlada Charoenviriyakul, Yuki Takahashi, Masaki Morishita, **Akihiro Matsumoto**, Makiya Nishikawa, Yoshinobu Takakura.

   Cell type-specific and common characteristics of exosomes derived from mouse cell lines: yield, physicochemical properties, and pharmacokinetics

   European Journal of Pharmaceutical Sciences, 2017, 96:316-322.

4. Yoshinobu Takakura, **Akihiro Matsumoto**, Yuki Takahashi.

   Therapeutic Application of Small Extracellular Vesicles (sEVs): Pharmaceutical and Pharmacokinetic Challenges

   Biological and Pharmaceutical Bulletin, accepted (2019)

5. Marie-Nicole Theodoraki, **Akihiro Matsumoto**, Inga Beccard, Thomas K. Hoffmann, Theresa L. Whiteside.

   CD44v3 protein-carrying tumor-derived exosomes in HNSCC patient's plasma as potential non-invasive biomarkers of disease activity

   OncoImmunology, in press

CHAPTER I

Cell selective delivery of tumor cell-derived small extracellular vesicle to antigen presenting cells for the efficient induction of anti-tumor immunity

Chapter I

Introduction

Tumor antigen-based immunotherapy in combination with immunostimulatory adjuvants through the activation of T cells has been shown to be a promising tumor treatment[13]. The induction of a potent antitumor immune response requires the delivery of tumor antigens to antigen-presenting cells (APCs) and the activation of APC by the adjuvants. sEVs contain proteins and nucleic acids and function in cell-cell communication as endogenous delivery carriers[6]. Since tumor cell-derived sEVs contain endogenous tumor antigens, they can be utilized for tumor antigen-based immunotherapy against various types of tumors. Moreover, since tumor-derived sEV-based immunotherapy does not require the identification and purification of tumor antigens, this therapy is advantageous compared with conventional tumor antigen-based immunotherapy[14,15]. For the successful induction of cytotoxic anti-tumor immunity by tumor cell-derived sEVs, several challenges need to be overcome, such as increased immunostimulatory activity of tumor cell-derived sEV and efficient delivery to APCs as well as elucidating the biological roles of tumor cell-derived sEV.

My laboratory has previously attempted to increase the immunostimulatory activity of tumor cell-derived sEVs by developing tumor-derived sEV-adjuvant co-delivery system for cancer vaccine[15,16]. Immunostimulatory CpG-DNA was modified to murine melanoma B16-sEVs through streptavidin (SAV)-biotin interaction. This CpG-DNA-modified sEV (CpG-sEV) successfully delivered sEVs and CpG-DNA to the same APCs, which led to the strong activation and efficient presentation of tumor antigens by the APCs.

For efficient delivery of tumor cell-derived sEV to APCs and elucidation of the biological roles of tumor cell-derived sEV, it is indispensable to quantitively analyze the *in vivo* behavior of sEV after administration[8,10,12,17]. Thus, in section 1, I conducted PK experiments to reveal the tissue distribution and cellular uptake of tumor cell-derived sEV after intratumoral administration. I subsequently considered the biological role of tumor cell-derived sEV. In section 2, I developed a delivery system which allows tumor cell-derived sEV to be selectively delivered to APCs and applied the system for cancer vaccine.

SECTION 1.

Evaluation of *in vivo* fate and biological role of B16BL6-derived small extracellular vesicle in the tumor microenvironment

I-1-1. Introduction

Several studies have investigated the role of tumor cell-derived sEVs in cancer biology[18]. Detection of primary tumor cell-derived sEVs in specific organs and determination of their role in the initiation of pre-metastatic niche formation has led to detailed research on molecular mechanisms underlying the role of these sEVs in cancer metastasis[6,19,20]. Recent studies indicate that specific proteins and microRNAs present in tumor cell-derived sEVs determined organotropic metastasis[21,22]. *In vitro* studies assessing the biological role of tumor cell-derived sEVs have shown that these EVs promote tumor progression by affecting different cell types[23,24]. To determine the actual effect of tumor cell-derived sEVs, it is important to understand their *in vivo* behavior. However, limited information is available on the transport of tumor cell-derived sEVs from tumor tissue to other organs and on cell types involved in their uptake.

For understanding the *in vivo* behavior of sEV, a sEV labeling technology that allows high sensitive and quantitative analysis would be useful[17,25]. Previously, my laboratory developed a sEV radiolabeling method based on SAV-biotin interaction by designing a fusion protein containing SAV and lactadherin (LA; a sEV-tropic protein) called SAV-LA. EVs were radiolabeled by incubating SAV-LA-modified sEVs with an iodine-125 (^{125}I)-labeled biotin derivative[17]. The radiolabeled sEVs were then intravenously injected into mice, and their PK characteristics were evaluated. In addition, my laboratory previously used fluorescently labeled sEVs to determine cell types involved in sEV uptake in the liver, spleen, and lungs[25,26]. Based on the results of these studies, I aimed to determine the *in vivo* behavior of tumor cell-derived sEVs administered exogenously by utilizing sEV radiolabeling and fluorescent labeling methods.

In this section, melanoma B16BL6 cell was selected as a model tumor cell and the effects of B16BL6-derived sEVs (B16-sEVs) on these cells were determined. In addition, the biodistribution, cellular uptake, and effect on tumor growth of B16-sEVs after intratumoral administration was examined. Finally, the effects of GW4869, an inhibitor of sEV secretion, on tumor growth was investigated. The obtained results clearly showed that B16-sEVs were efficiently taken up by B16BL6 tumor cells and accelerated the growth of these cells.

I-1-2. Materials and Methods

Mice.

Five-week-old male C57BL/6J mice were purchased from Japan SLC, Inc. (Shizuoka, Japan). Protocols for all animal experiments were approved by the Animal Experimentation Committee of the Graduate School of Pharmaceutical Sciences of Kyoto University.

Cell culture.

B16BL6 murine melanoma cells were obtained from Riken BioResource Center (Tsukuba, Japan) and were cultured in Dulbecco's modified Eagle's medium (DMEM) supplemented with 10% heat-inactivated fetal bovine serum (FBS), 0.15% sodium bicarbonate, 100 IU/mL penicillin, 100 μg/mL streptomycin, and 2 mM L-glutamine at 37°C in a humidified atmosphere containing 5% CO_2.

B16-sEV collection.

sEVs were collected from the culture supernatant of B16BL6 cells by performing differential centrifugation followed by ultracentrifugation. In brief, cell supernatants were centrifuged at 300 × *g* for 10 min, 2,000 × *g* for 20 min, and 10,000 × *g* for 30 min in order to remove cell debris and microvesicles including apoptotic bodies. The supernatant was passed through 0.22-μm syringe filter, followed by 100,000 × *g* for 1 h using a Hitachi CP80WX ultracentrifuge and P50AT2 angle rotor (Hitachi High-Technologies, Tokyo, Japan). The sEV pellet was washed in PBS, centrifuged at 100,000 × *g* for 1 h and resuspended in PBS. The amount of sEVs collected was estimated by measuring protein concentration by performing Bradford assay. Presence of sEV marker proteins Alix, HSP70, and CD81 and absence of negative marker protein calnexin in the collected sEVs was confirmed by performing western blotting with the following antibodies (Abs): rabbit anti-mouse CD81 Ab (1:200 dilution, Cat No; sc-9158, Lot; A2815, Santa Cruz Biotechnology, Dallas, TX, USA), mouse anti-mouse Alix Ab (1:20,000 dilution, Cat No; 611620, Lot; 35610, BD Biosciences, San Jose, CA, USA), rabbit anti-mouse HSP70 Ab (1:1,000 dilution, Cat No; 4872S, Lot; 10/2017, Cell Signaling Technology, Danvers, MA, USA), rabbit anti-mouse Calnexin (1:1,000, Cat No; sc-11397, Lot; 11914, Santa Cruz Biotechnology), goat anti-rabbit IgG-HRP (1:5,000 dilution, Cat No; sc-2054, Lot; C1315, Santa Cruz Biotechnology), and rabbit anti-mouse IgG-HRP (1:2,000 dilution, Cat No; 61-0120, Lot; 364278A, Thermo Fisher Scientific, Waltham, MA, USA). The membrane was then reacted with Immobilon Western Chemiluminescent HRP substrate (Merck Millipore, Billerica, MA, USA), and chemiluminescence was detected using LAS-3000 instrument (FUJIFILM, Tokyo, Japan).

Electron microscopic observation and measurement of particle size of sEVs.

The sEV suspension was added to an equal volume of 4% paraformaldehyde (Nacalai Tesque, Kyoto, Japan), and the mixture was applied to a Formvar/Carbon film-coated transmission electron microscope (TEM) grid (Alliance Biosystems, Osaka, Japan). The sample was then washed with PBS. Then, the sample was fixed by incubation with 1% glutaraldehyde for 5 min, washed with PBS, and incubated with 1% uranyl acetate for 5 min. The sample was observed under a TEM (Hitachi H-7650; Hitachi High-Technologies). As for the measurement of size distribution, qNano instrument (Izon Science Ltd., Christchurch, New Zealand) was used. NP100 nanopore was used according to the manufacturer's instructions. All sEV samples and calibration particles (Izon Science Ltd.)

were measured at around 45.0-46.5 mm stretch with a voltage of 0.5-1.0 V. Collected data were processed by Izon Control Suite software version 3.3.

Preparation of fluorescently labeled sEVs.

PKH26 red fluorescent cell linker kit and PKH67 green fluorescent cell linker kit were obtained from Sigma Aldrich (St. Louis, MO, USA). For the preparation of PKH26- or PKH67-labeled B16-sEV, PKH26 or PKH67 dye in a diluent C buffer (Sigma Aldrich) was added to the B16-sEV and incubated for 5 min at room temperature. To remove the unbound dye, the sEV + fluorescent dye was incubated with 5% BSA in PBS and ultracentrifuged at 100,000 × *g* for 1 h.

Cellular uptake assay.

B16BL6 cells (1×10^5 cells/well) were seeded onto a chamber slide (WATSON CO., LTD, Kobe, Japan) 1 day before the experiment. Next, 10 μg/mL PKH26-labeled B16-sEVs were added to the cell culture, and the cells were incubated for 4 or 24 h. The cells were washed twice with PBS, fixed with 4% paraformaldehyde for 20 min, and washed twice again with PBS. Next, the cells were treated with 100 nM 4′,6-diamino-2-phenylindole (DAPI) for 5 min to stain their nuclei and were washed once with PBS. Finally, the cells on the slide were examined using a confocal laser-scanning microscope (A1R-MP; Nikon Instech Co., Ltd., Tokyo, Japan).

In a separate experiment, 1×10^5 B16BL6 cells were seeded in a 24-well plate. After 24 h of incubation, indicated concentrations of PKH67-labeled B16-sEVs were added to the cell culture and the cells were incubated for 4 or 24 h. Next, the cells were washed twice with PBS and were harvested. Mean fluorescent intensity (MFI) of the cells was determined using a flow cytometer (Gallios Flow Cytometer; Beckman Coulter, Miami, FL, USA). Data were analyzed using Kaluza software (version 1.0, Beckman Coulter).

Tumor cell proliferation assay.

B16BL6 cells (5×10^3 cells/well) were seeded in a 96-well plate containing DMEM lacking FBS 1 day before the experiment. The cells were then incubated with the indicated concentrations of B16-sEVs or 10% normal FBS for 24 h, and cell numbers were determined using MTT assay kit (Nacalai Tesque).

Flow cytometric determination of apoptotic cells.

B16BL6 cells (1×10^5 cells/well) were seeded in a 24-well plate containing DMEM supplemented with the indicated concentrations of B16-sEVs and without FBS. After 24 h, cells both on the plate and in the medium were harvested. Apoptotic cells were determined using Alexa Fluor 488 annexin V (AnV)/propidium iodide (PI) apoptosis detection kit (Thermo Fisher Scientific) and Gallios Flow Cytometer, according to the manufacturer's instructions. Data were analyzed using the Kaluza software.

Intercellular protein analysis.

B16BL6 cells (2×10^5 cells/well) were seeded in a 12-well plate with or without the indicated concentrations

of B16-sEVs. After 24 h, the cells were washed twice with PBS and were harvested. Cell lysates were prepared by freezing and thawing the cells five times, followed by centrifugation to remove cell debris. Reduced cell lysates (2 μg) were resolved by performing sodium dodecyl sulfate-polyacrylamide (SDS-PAGE) gel electrophoresis on a 10% gel and were transferred onto a polyvinylidene fluoride membrane. Cyclin D1, Bcl-2, Bax, Akt, phosphorylated Akt (p-Akt), and GAPDH were detected by incubating the membrane with the following Abs for 1 h at room temperature: rabbit anti-cyclin D1 Ab (dilution, 1:1000, Cat No: ab134175, Lot: GR192733-13, Abcam, Cambridge, UK), rabbit anti-Bcl-2 Ab (dilution, 1:1000, Cat No: ab32124, Abcam), rabbit anti-Bax Ab (dilution, 1:1000, Cat No: ab32503, Abcam), rabbit anti-Akt Ab (dilution, 1:1000, Cat No: KAP-PK004, Lot: 09010930, Assay design, New York, NY, USA), rabbit anti-p-Akt Ab (dilution, 1:200, Cat No: sc-293125, Santa Cruz Biotechnology), and rabbit anti-GAPDH Ab (dilution, 1:10000, Cat No: ab181602, Abcam). Next, the membrane was incubated with goat anti-rabbit IgG-HRP (dilution, 1:5000, Cat No: sc-2004, Santa Cruz Biotechnology) for 1 h at room temperature. The membrane was then reacted with Immobilon Western Chemiluminescent HRP substrate (Merck Millipore), and chemiluminescence was detected using LAS-3000 instrument (FUJIFILM).

In a separate experiment, proteins present in the sEVs and cell lysates were resolved by performing SDS-PAGE gel electrophoresis and were transferred onto a polyvinylidene fluoride membrane, as described above. Survivin expression was detected by incubating the membrane with rabbit anti-survivin Ab (dilution, 1:1000, Cat No: ab182132, Lot: GR209442-2, Abcam) for 1 h at room temperature, followed by incubation with goat anti-rabbit IgG-HRP (dilution, 1:5000; Santa Cruz Biotechnology) for 1 h at room temperature. The membrane was then reacted with Immobilon Western Chemiluminescent HRP substrate, and chemiluminescence was detected using the LAS-3000 instrument.

Inhibition of B16-sEV secretion.

B16BL6 cells (8×10^6 cells/well) were seeded in a 15-cm dish and were incubated for 24 h. Next, the cells were incubated with or without 5 μg/mL GW4869 (dissolved in 5% DMSO; Cayman Chemical, Michigan, MI, USA), an inhibitor of neutral sphingomyelinases, for 24 h at 37°C. sEVs were collected, and the amount of the collected sEVs was determined by measuring protein concentration. Levels of Alix, HSP70, CD81, and calnexin in the collected samples were determined by performing western blotting, as described above.

Effect of GW4869 on tumor cell proliferation.

B16BL6 cells (1×10^4 cells/well) were seeded in a 96-well plate 1 day before the experiment. The cells were then incubated with or without 5% DMSO (vehicle), 5 μg/mL GW4869 and the indicated concentrations of B16-sEVs for 24 h, and cell numbers were estimated using the MTT assay kit.

Xenograft tumor model.

Mice were subcutaneously inoculated with 5×10^5 B16BL6 cells. Tumor size was measured using a slide caliper, and tumor volume was calculated using the following formula: tumor volume (mm^3) = (longer length × shorter length^2) × 0.5. All animal experiments were conducted when tumor volume was >100 mm^3, unless otherwise

indicated. Tumor-bearing mice were euthanized once tumor volume reached 3000 mm^3.

Preparation of ^{125}I-labeled B16-sEVs.

SAV-LA-expressing plasmid (pCMV-SAV-LA) and SAV-LA-modified sEVs were prepared, as described previously[17]. In brief, B16BL6 cells seeded in culture dishes were transfected with pCMV-SAV-LA by using polyethylenimine Max (Polysciences, Warrington, PA, USA). After 24 h, SAV-LA-modified sEVs present in the culture supernatant were collected by ultracentrifugation as described above. The amount of collected sEVs was estimated by measuring protein concentration by performing the Bradford assay. Radiolabeled sEVs were prepared by incubating the SAV-LA-modified sEVs with (3-^{125}I-iodobenzoyl) norbiotinamide, an ^{125}I-labeled biotin derivative as described previously[17].

Evaluation of the biodistribution of radiolabeled B16-sEVs after intratumoral administration in mice.

^{125}I-labeled B16-sEVs (approximately 2 μg EVs; radiation dose, 37 kBq/mouse) were injected into tumor tissues of mice having tumor volume of 100-200 or 300-500 mm^3. The mice were sacrificed at an indicated time after the injection, and their blood was collected from the vena cava. Next, their organs were collected and were washed with saline. Radioactivity of each sample was measured using Wizard 1470 automatic gamma counter (PerkinElmer, Waltham, MA, USA). Results are expressed as %ID/mL for blood samples and as %ID/organ for other samples.

Microscopic observation of the cellular uptake of B16-sEVs in tumor tissues after intratumoral administration into mice.

Tumor-bearing mice were intratumorally injected with PKH26-labeled sEVs at a dose of 10 μg sEV protein. The mice were sacrificed at an indicated time after the injection, and their tumor tissues were harvested and embedded in Tissue-Tek OCT compound (Sakura Finetek Japan, Tokyo, Japan). In addition, the organs were frozen at -80°C, and were sectioned into 10-μm-thick sections by using a freezing microtome (Leica CM3050 S; Leica Biosystems, Germany). The sections were air dried and were fixed with 4% paraformaldehyde in PBS (Nacalai Tesque). Next, the sections were washed with PBS and were incubated with 0.1% polyoxyethylene octylphenyl ether (Wako FUJIFILM, Osaka, Japan) in PBS for 10 min at room temperature to induce permeabilization. The sections were then incubated with 20% FBS in PBS for 1 h at 37°C. After washing, the sections were treated with rabbit anti-Pmel17 Ab (dilution, 1:50, Cat No: sc-377325, Santa Cruz Biotechnology) and rat anti-CD206 Ab (dilution, 1:200, Cat No: MCA2235, AbD Serotec, Oxford, UK,) for 1 h to stain B16BL6 cells and macrophages, respectively. Next, the sections were stained with Alexa Fluor 488-labeled goat anti-rabbit IgG (dilution, 1:250, Cat No: ab150077, Lot: GR248578-2, Abcam) and Alexa Fluor 488-labeled goat anti-rat IgG (dilution, 1:200, Cat No: ab150157, Lot: GR190524-2, Abcam) secondary Abs. The sections were then treated with 100 nM DAPI for 5 min to stain the nuclei, were washed once with PBS, and were examined under the confocal laser-scanning microscope (A1R-MP, Nikon Instech Co., Ltd.).

Flow cytometric analysis of the cellular uptake of B16-sEVs in tumor tissues after intratumoral administration into mice.

Tumor-bearing mice were intratumorally injected with PKH67-labeled sEVs at a dose of 20 μg sEV proteins. The mice were sacrificed at an indicated time after the injection, and their tumor tissues were harvested. The tumor tissues were minced and were digested by incubating with type 4 collagenase (Worthington Biochemical Corp, Lakewood, NJ, USA) for 15 min at 37°C. Single-cell suspensions were prepared by filtering the tissue samples through a 40-μm strainer (Greiner Bio-One, Frickenhausen, Germany). The cell suspensions were fixed with 4% paraformaldehyde in PBS. After washing with PBS, the cell suspensions were incubated with 0.1% polyoxyethylene octylphenyl ether for 10 min at room temperature to induce permeabilization. After washing, the cell suspensions were incubated with 5% FBS in PBS for 30 min at room temperature. Next, the cell suspensions were incubated with rabbit anti-Pmel17 Ab (dilution, 1:1000, Santa Cruz Biotechnology) for 1 h, followed by incubation with donkey anti-rabbit IgG H&L Alexa Fluor 647 (dilution, 1:2000, Cat No: ab150075, Lot: GR269275-1, Abcam) secondary Ab. MFI of individual cells were evaluated using the Gallios Flow Cytometer, and data were analyzed using the Kaluza software.

Effect of B16-sEVs on tumor growth.

Tumor-bearing mice were intratumorally injected with PBS or 10 μg B16-sEVs at 3-day intervals, and tumor size was measured every day.

Effect of GW4869 on tumor growth.

Tumor-bearing mice were intratumorally injected with PBS, vehicle (5% DMSO), or 1 μg GW4869 at every day, and tumor size was measured every day.

Statistical analysis.

Differences among groups were evaluated using Tukey-Kramer method, and $p < 0.05$ was considered statistically significant.

I-1-3. Results

I-1-3-a. Morphology and size distribution of B16-sEVs.

Figure 1A shows a TEM image of B16-sEVs. Round-shaped vesicles of approximately 100 nm in diameter were observed. The particle size of B16-sEVs measured by qNano was 97 ± 3 nm (Figure 1B).

I-1-3-b. *In vitro* cellular uptake of B16-sEVs by B16BL6 cells.

Figure 1C shows the confocal microscopic images of B16BL6 cells incubated with PKH26-labeled B16-sEVs. The results showed that PKH26-labeled B16-sEVs were taken up by B16BL6 cells. In addition, results of flow cytometric analysis showed that the uptake of PKH67-labeled B16-sEVs by B16BL6 cells increased with concentration and time with the set concentration conditions (Figure 1D).

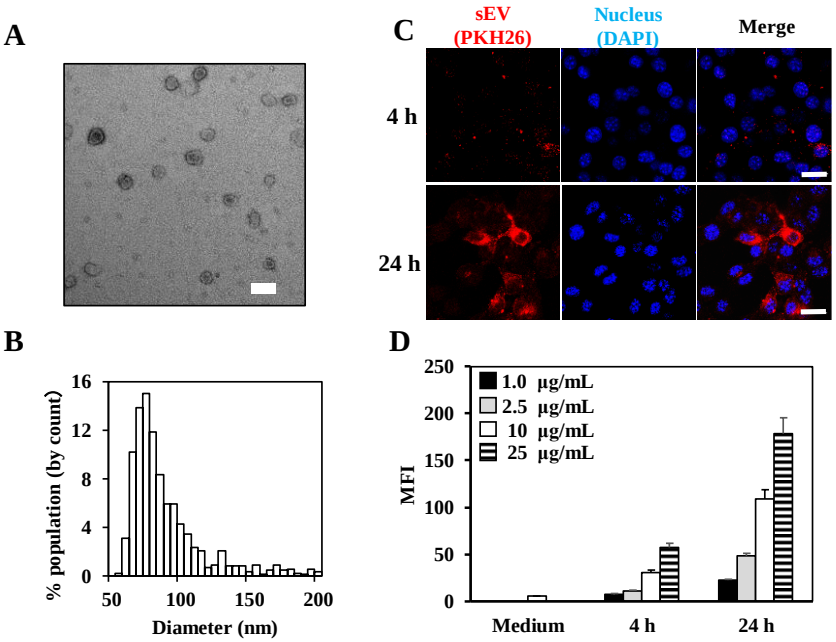

Figure 1. Characterization and *in vitro* cellular uptake of B16-sEVs.

(A) Electron microscopic image of sEVs collected from B16BL6 cells. Scale bar = 100 nm. (B) Histogram of the particle size distribution of the B16-sEVs determined using a qNano instrument. (C) Confocal microscopic observation of B16BL6 cells incubated with PKH26-labeled sEVs (red) for 4 and 24 h; scale bar = 20 μm. (D) Flow cytometric analysis of B16BL6 cells incubated with the indicated concentrations of PKH67-labeled sEVs for 4 and 24 h. Mean fluorescent intensity (MFI) was analyzed. Results are expressed as mean ± SD. (n=4).

I-1-3-c. Proliferative and anti-apoptotic effect of B16-sEVs on B16BL6 cells.

Next, I evaluated the effect of B16-sEVs on the proliferation of cultured B16BL6 cells. Treatment with B16-sEVs (2.5 and 10 μg/mL) significantly increased the number of B16BL6 cells compared with that of non-treated cells (Figure 2A). In particular, the number of B16BL6 cells treated with 10 μg/mL B16-sEVs was comparable to that of cells cultured with 10% FBS. Next, I determined the anti-apoptotic activity of B16-sEVs by staining B16BL6 cells with AnV and PI (Figure 2B). AnV-positive and PI-negative [AnV(+) and PI(-)] cells and AnV-positive and PI-positive [AnV(+) and PI(+)] cells were regarded as early apoptotic cells and late apoptotic/necrotic cells, respectively. The percentage of AnV(+) and PI(-) cells was significantly lower among B16BL6 cells treated with 2.5 μg/mL B16-sEVs than among non-treated cells (Figure 2C), suggesting that B16-sEVs inhibited the apoptosis of B16BL6 cells. In addition, B16-sEV treatment decreased the percentage of AnV(+) and PI(+) cells among B16BL6 cells; however, the decrease was not statistically significant.

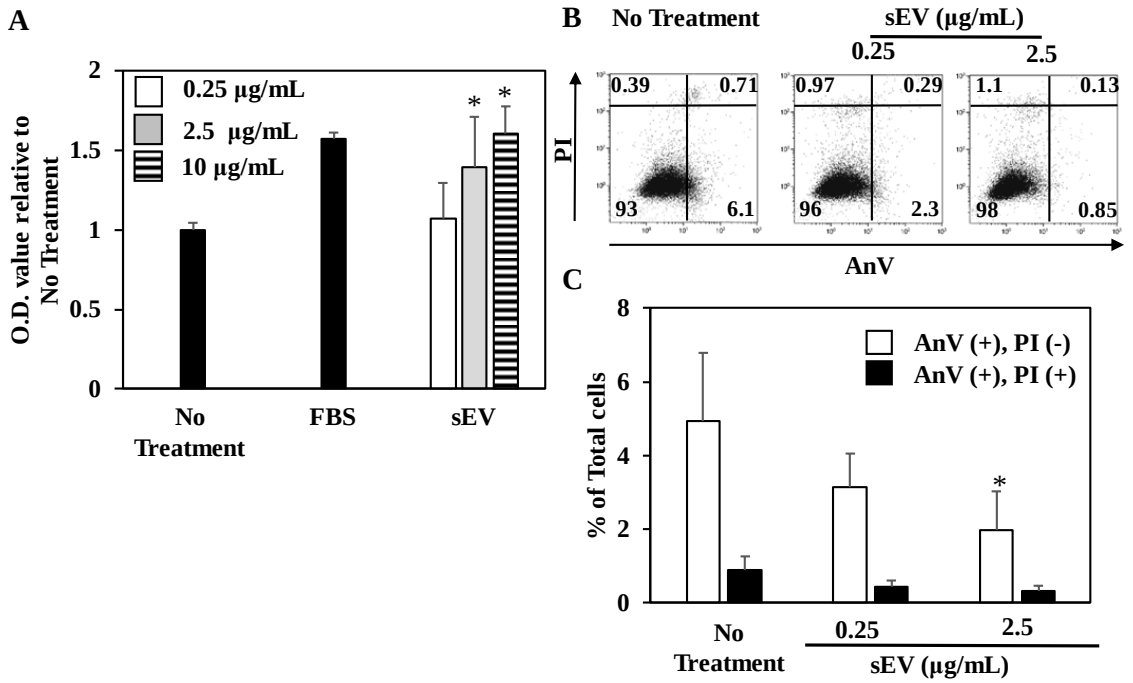

Figure 2. Effect of B16-sEVs on B16BL6 cell proliferation and apoptosis.

(A) The number of B16BL6 cells treated with the indicated concentrations of B16-sEVs was determined by performing MTT assay. (B), (C) After incubation with B16-sEVs, B16BL6 cells were stained with AnV/PI and were analyzed by performing flow cytometry. (B) Representative flow cytometry plots of B16BL6 cells treated with or without B16-sEVs. (C) Percentages of AnV-positive and PI-negative [AnV(+) and PI(-)] cells or AnV-positive and PI-positive [AnV(+) and PI(+)] cells were quantified. Results are expressed as mean ± SD. (n=4) *p < 0.05 compared with no-treatment.

I-1-3-d. Regulation of the levels of cell proliferation- and apoptosis-related proteins by B16-sEVs.

Next, I investigated the effect of B16-sEVs on the levels of intracellular proteins associated with cell proliferation (cyclin D1 and Akt) and apoptosis (Bcl-2, Bax) (Figure 3A). Cellular levels of cyclin D1, Bcl-2, and p-Akt increased, whereas those of Bax considerably decreased after treatment with B16-sEVs. Western blotting detected survivin, an apoptotic inhibitor, in both B16BL6 cells and B16-sEVs (Figure 3B).

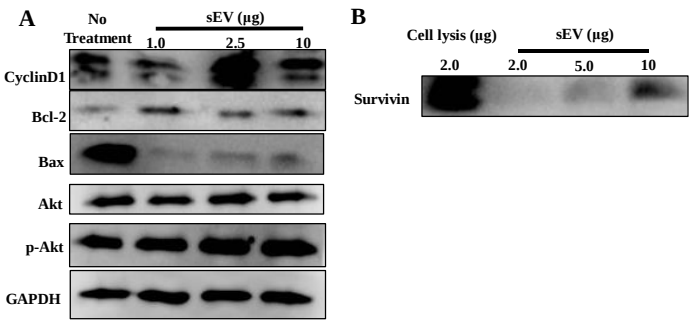

Figure 3. Changes in the intracellular levels of cell proliferation- and apoptosis-related proteins after treatment with B16-sEVs.

(A) Western blotting analysis of cyclinD1, Bcl-2, Bax, Akt, p-Akt, and GAPDH expression in B16BL6 cells treated with the indicated concentrations of B16-sEVs for 24 h. (B) Western blotting analysis of survivin expression in B16BL6 cells and B16-sEVs.

I-1-3-e. Suppressed proliferation of B16BL6 cells by GW4869-induced inhibition of B16-sEV secretion.

Figure 4A shows protein levels in sEVs collected from B16BL6 cells treated with or without GW4869. GW4869 treatment significantly decreased the amount of collected sEVs to approximately 25% of that collected from non-treated cells. Next, proteins present in sEVs collected from B16BL6 cells treated with or without GW4869 were analyzed by performing western blotting. Results of western blotting showed that sEV marker proteins Alix, HSP70, and CD81 were present and that calnexin, an endoplasmic reticulum marker, was absent in all the three groups (sEVs derived from non-treated, DMSO-treated, and GW4869-treated cells) (Figure 4B). GW4869 treatment significantly decreased the number of B16BL6 cells compared with that of non-treated and vehicle-treated cells. In contrast, treatment of GW4869-treated B16BL6 cells with 25 μg/mL B16-sEVs restored their proliferation rate (Figure 4C). These results imply that GW4869-induced inhibition of B16-sEV secretion suppressed the proliferation of B16BL6 cells.

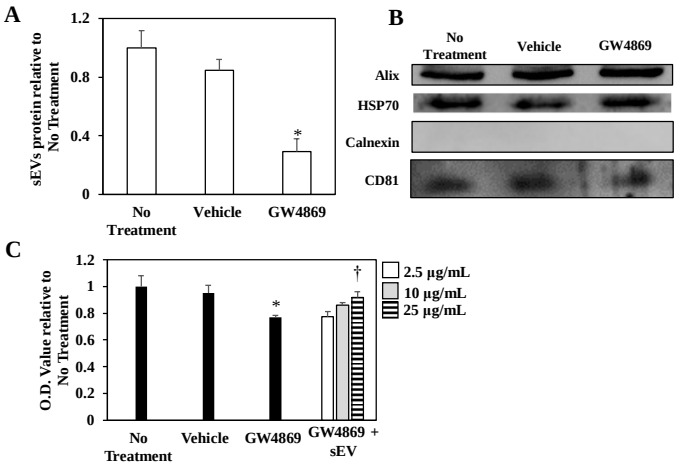

Figure 4. Effect of GW4869 on sEV secretion and B16BL6 cell number.

(A) sEVs were collected from B16BL6 cells treated with or without GW4869. The amount of collected sEVs was estimated by measuring protein concentration. (B) Western blotting of sEV marker proteins Alix, HSP70, and CD81 and sEV negative marker calnexin in sEVs isolated from B16BL6 cells treated with or without GW4869. (C) B16BL6 cells were treated with or without GW4869, and MTT assay was performed to estimate B16BL6 cell number. Moreover, B16BL6 cells were incubated with the indicated concentrations of GW4869 and B16-sEVs, and cell number was estimated. Results are expressed as the mean ± SDs. *$p < 0.05$ compared with non-treated and vehicle-treated cells; †$p < 0.05$ compared with GW4869-treated cells.

I-1-3-f. Retention at injection site and tumor growth after intratumoral administration.

The distribution of ^{125}I radioactivity after the injection of radiolabeled B16-sEVs into tumors with a volume of 100-200 (Figure 5A) or 300-500 mm^3 (Figure 5B) was measured. When radiolabeled B16-sEVs were injected into tumors with low volume (Figure 5A), a large fraction of the radioactivity remained within the tumors (approximately 57%, 43%, 33%, and 34% at 1, 4, 8, and 24 h after the injection, respectively), with limited distribution to other organs until 48 h after the injection. When radiolabeled B16-sEVs were injected into tumors with large volume (300-500 mm^3), a large fraction of the radioactivity remained within the tumors (Figure 5B), which was similar to that observed for small tumors, with radioactivity being detected in the lungs and liver (1.6% and 17% at 1 h, respectively).

I-1-3-g. *In vivo* cellular uptake of B16-sEVs in tumor tissue after intratumoral administration.

To determine cell types involved in the uptake of B16-sEVs in tumor tissue, the mice were intratumorally injected with PKH26-labeled B16-sEVs and the obtained tumor sections were stained with Abs against gp100 (a

melanoma marker) or CD206 (a macrophage marker). As shown in Figures 5C and 5D, sEVs (red dots) colocalized with stained cells (green dots), indicating that PKH26-labeled B16-sEVs were taken up by both B16BL6 cells and macrophages present in the tumor tissue. However, the uptake efficiency between B16BL6 cells and macrophages seems to be different. PKH26-labeled B16-sEVs colocalized more with B16BL6 cells than with macrophages (Figure 5C and 5D). Next, I performed flow cytometric analysis to quantitatively investigate the uptake of PKH67-labeled sEVs by B16BL6 cells in tumor tissues (Figure 5E-5H). Results of flow cytometric analysis showed that approximately 60% and 70% B16BL6 cells took up PKH67-labeled, B16-sEVs at 4 (Figures 5F and 5H) and 24 h (Figures 5G and 5H), respectively, and that approximately 27% and 30% other cells took up PKH67-labeled, B16-sEVs at 4 h (Figures 5F and 5H) and 24 h (Figures 5G and 5H), respectively.

I-1-3-h. Effect of B16-sEVs and GW4869 on tumor growth.

Figure 6A shows the time course of increase in tumor volume in tumor-bearing mice intratumorally injected with PBS or B16-sEVs. Mice injected with B16-sEVs showed significant increase in tumor growth compared with mice injected with PBS. Next, I investigated the effects of repeated intratumoral injections of GW4869 on tumor growth and survival in B16BL6-bearing mice (Figure 6B and 6C). Intratumoral injection of GW4869 significantly reduced tumor growth. In addition, GW4869 treatment prolonged the survival of tumor-bearing mice compared with that of mice in other groups; however, the difference was not statistically significant.

I-1-4. Discussion

Cyclin D1 accelerates the G1 phase of the cell cycle to increase cell proliferation[27]. Bcl-2 inhibits caspase-9 and caspase-3 activities and suppresses proapoptotic Bax proteins[28,29]. PI3K/Akt signaling pathways play a role in the survival of different cell types[30]. Therefore, B16-sEV-induced increase in the proliferation of and inhibition of the apoptosis of B16BL6 cells may involve regulation of the intracellular levels of the proteins mentioned above. (Figure 1, 2 and 3A).

Survivin enhances cell proliferation and survival and activates cyclin-dependent kinase 4 (Cdk4) to generate a cyclinD1/Cdk4 complex[31,32]. This complex promotes cell cycle progression. Moreover, alternatively spliced survivin variants interact with Bcl-2 and inhibit caspase 3 activity in the mitochondria[33]. It has been reported that survivin level in the sEVs derived from bladder cancer cells was higher than that in the lysate of the cancer cells and the sEVs enhanced the proliferation and survival of cancer cells[34]. My results showed that B16-sEVs also contained survivin; however, its level was lower than that in cell lysates (Figure 3B). B16-sEVs were efficiently taken up by B16BL6 cells (Figure 1), suggesting that survivin present in the sEVs was delivered to B16BL6 cells and might induce their proliferation and survival (Figures 2 and 3B).

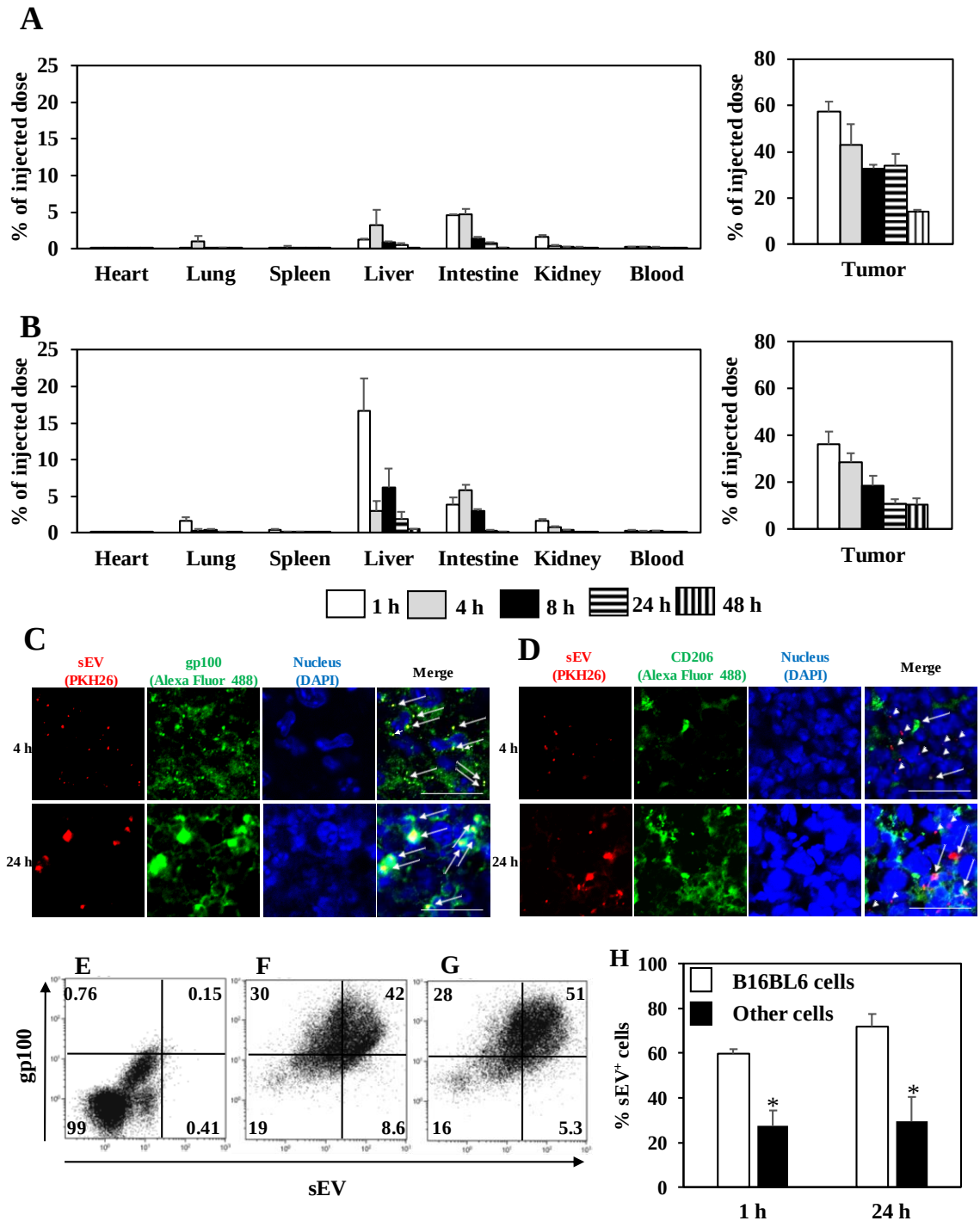

Figure 5. Biodistribution and *in vivo* cellular uptake of B16-sEVs after intratumoral administration.

(A), (B) *In vivo* distribution of ^{125}I-labeled sEVs injected into tumor tissues with a volume of (A) 100-200 or (B) 300-500 mm^3. The indicated tissues were collected at the indicated time after intratumoral injection and the radioactivity was analyzed. Results are expressed as mean ± SEM. (n=4) (C), (D) After intratumoral injection of PKH26-labeled B16-sEVs (red), tumor sections were prepared and were stained with Abs against (C) gp100 (a melanoma marker; green) and (D) CD206 (a macrophage marker; green). The sections were examined under the confocal laser-scanning microscope. Arrowheads and arrows indicate single red dots and red dots merged with green dots, respectively; scale bar = 20 μm. (E)-(G) Flow cytometric analysis of the cellular uptake of PKH67-labeled B16-sEVs in the tumor tissue after intratumoral administration. Representative flow cytometry plots of B16BL6 and other cell populations after (F) 4 and (G) 24 h in mice injected with the sEVs (E; non-treatment group). Percentages of cells in each area of the plots were quantified and are shown in the plots. (H) Percentages of sEV-positive cells at 4 and 24 h after the intratumoral injection of PKH67-labeled sEVs. Results are expressed as the mean ± SDs. (n=5) *p < 0.05 compared with other cells.

GW4869 is a potent, cell-permeable, specific, and non-competitive inhibitor of neutral sphingomyelinases[35]. sEV secretion is modulated by neutral sphingomyelinases and is inhibited by GW4869[36–38]. I treated cells with GW4869 (5 μg/mL), which is considered to have no cytotoxic effect[36]. In the present study, the degree of the reduction in sEV secretion by GW4869 was much greater than the degree of the reduction in the cell number (Figure 4A-4C), indicating that the reduced sEV secretion by GW4869 is not simply due to the reduced cell number. Moreover, reduction in the cell number by GW4869 was recovered by treating the cells with B16-sEVs (Figure 4C), suggesting that GW4869-induced suppression of B16BL6 cell proliferation might be caused by the inhibition of B16-sEV secretion.

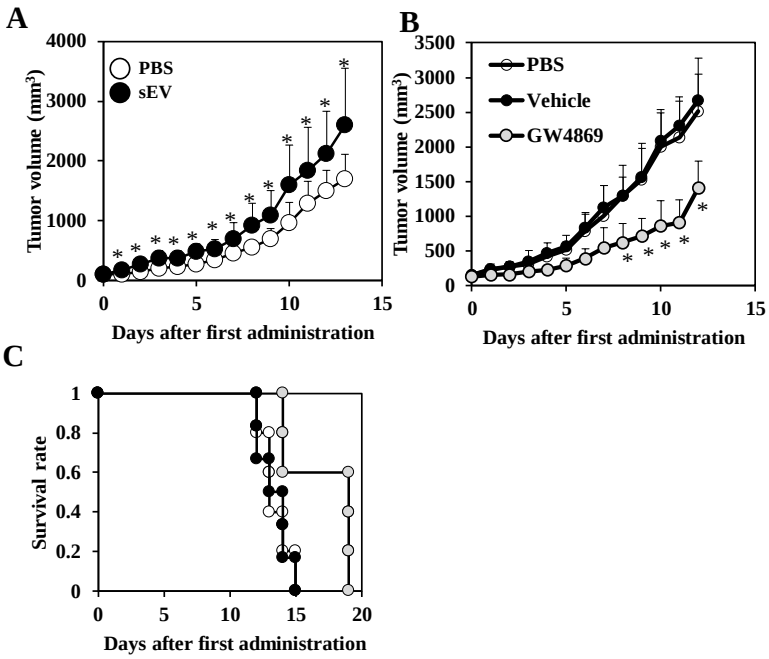

Figure 6. Effect of B16-sEVs and GW4869 on tumor progression.

(A) Effect of sEVs on tumor growth. B16-sEVs or PBS were injected into tumor tissue of tumor-bearing mice on days 0, 3, and 6. Tumor size was measured every day. Results are expressed as mean the tumor volume (mm^3) ± SD of ten mice; *$p < 0.05$ compared with PBS-treated mice. (B), (C) Effect of GW4869 on tumor growth and survival. Results are expressed as mean tumor volume (mm^3) ± SD of six mice; *$p < 0.05$ compared with PBS- and vehicle-treated mice.

Growth of tumor tissue increases vascular permeability in the tissue because of angiogenesis[39,40]. A previous study showed that biodistribution of nanoparticles having sizes comparable to those of sEVs after intratumoral injection depended on tumor size[39]. Consistently, results of the present study showed that biodistribution of radiolabeled sEVs was different between mice with different sized tumors (Figure 5A and 5B). In addition, distribution of intratumorally injected radiolabeled sEVs to the liver and lungs suggested a leakage of sEVs into blood circulation because B16-sEVs accumulate in the liver or lungs after i.v. administration[17,25,26]. The recovery rate of radioactivity was approximately 60%. This might be because of the leakage of the radiolabeled sEVs from the tumor tissue to the surrounding skin or muscle.

Tumor tissues contain stromal cells as well as tumor cells, and tumor cell-derived sEVs may be taken up by both these cells. In the present study, I evaluated the uptake of B16-sEVs by B16BL6 cells and macrophages, a type of stromal cells. B16-sEV uptake by macrophages was investigated because macrophages play a major role in the uptake of exogenously administered sEVs[26]. Flow cytometric analysis and microscopic observation showed that B16BL6 cells efficiently took up B16-sEVs compared with other cells in the tumor tissue (Figure 6). This might be because sEVs are more efficiently taken up by cells similar to the producing cells than other cells[41,42], suggesting that B16-sEVs have tropism toward B16BL6 cells. Research on uptake mechanism of cancer cell-derived sEVs by their producing cells is required in the future study.

Tumor cell-derived sEVs induce tumor progression both *in vitro* and *in vivo*[41–43]. Significant increase in tumor volume after the intratumoral injection of B16-sEVs (Figure 6A) suggests that these sEVs induced tumor progression. In contrast, intratumoral injection of GW4869 inhibited tumor progression (Figure 6B and 6C). Because B16-sEVs remain in the tumor tissue and are mainly taken up by B16BL6 cells (Figure 5), it can be suggested that these sEVs promote B16BL6 cell proliferation and tumor progression under physiological conditions.

I-1-5. Summary of section 1 of chapter I

In this section, I found that B16BL6 cells secreted and took up their own sEVs to induce their proliferation and inhibit their apoptosis, thus promoting tumor progression. These findings provide important information for elucidating the physiological functions of EVs as well as for establishing sEV delivery strategy.

SECTION 2.

Development of DNA-anchored assembly of small extracellular vesicle for efficient antigen delivery to antigen presenting cells

I-2-1. Introduction

In section 1 of chapter I, I revealed that B16-sEV was mainly taken up by B16BL6 cells instead of APCs (*e.g.* dendritic cells, macrophages). In order to achieve strong induction of anti-tumor immunity, I considered targeting sEV to APC by increasing and decreasing the uptake by APCs and B16BL6 cells, respectively. For APC-specific targeting, it has been observed that APCs can efficiently take up micrometer-sized particles through phagocytosis or macropinocytosis; however, non-APCs are generally unable to take up such particles[44,45]. Furthermore, micrometer-sized particles show prolonged retention in the injection site after local injection compared with nanometer-sized particles[46]. Recently, DNA nanotechnology has facilitated the development of micrometer-sized colloidal superstructures in which DNA-modified nanoparticles are crosslinked with each other through DNA[47,48]. Since sEVs are sized approximately 100 nm and can be modified with DNA, I speculated that the formation of a sEV assembly where a DNA-induced colloidal superstructure is formed by sEVs can achieve an efficient and sustained delivery of tumor-cell derived sEVs to APCs to induce a potent tumor antigen-specific immune response.

In this section, I newly prepared a DNA-anchored sEV assembly in which tumor-cell derived sEVs were assembled with each other by cross-linker DNA-induced DNA hybridization. Since the design and amount of cross-linker DNA is likely to affect the assembly efficiency, CpG-sEV was combined with different amounts of cross-linker DNA with various sequences, and the resulting products were observed using transmission electron microscopy (TEM). The CpG-sEV assembly prepared in the optimized conditions was selectively taken up by APCs compared to non-APCs, and the CpG-sEV assembly strongly activated the APCs. Moreover, when compared with the simple suspended CpG-sEV, CpG-sEV assembly more effectively induced a tumor antigen-specific immune response *in vivo*.

I-2-2. Materials and Methods

Mice.

Five-week-old male C57BL6/J or five-week-old male ICR mice were purchased from Japan SLC, Inc. The protocols of all the animal experiments were approved by the Animal Experimentation Committee of the Graduate School of Pharmaceutical Sciences of Kyoto University.

Cell culture.

B16BL6 murine melanoma cells were obtained from Riken BioResource Center. NIH3T3 cells (mouse embryonic fibroblast) and RAW264.7 cells (mouse macrophage-like cells) were obtained from American Type Culture Collection (Manassas, VA, USA). Mouse dendritic DC2.4 cells were kindly provided by Dr. K. L. Rock (University of Massachusetts Medical School, Worcester, MA, USA). Cells were cultured in the medium and conditions previously described[49].

sEV collection and characterization.

sEVs were collected from the culture supernatant of B16BL6 cells by performing differential centrifugation followed by ultracentrifugation. In brief, culture supernatant was spun at 300 × *g* for 10 min, 2,000 × *g* for 20 min, and 10,000 × *g* for 30 min, followed by 0.22-μm filtration. The clarified medium was centrifuged at 100,000 × *g* for 1 h for three times (Himac CP80WX ultracentrifuge, Hitachi Koki, Tokyo, Japan; P50AT2 angle rotor, Hitachi Koki). The pellet was collected by resuspension in PBS. SAV-LA modified sEVs (SAV-sEV) and *Gaussia* luciferase (gLuc)-LA modified sEVs (gLuc-sEV) were isolated from the culture supernatants of B16BL6 cells transfected with pCMV-SAV-LA and pCMV-gLuc-LA. CpG-sEV and fluorescently-labeled CpG-sEV were prepared by incubating SAV-sEV with biotinylated CpG-DNA samples, followed by purification based on 100,000 × *g* for 1 h as described in a previous paper[50]. The prepared sEVs were characterized using the Bradford assay, western blotting, qNano instrument (Izon Science Ltd.), TEM, and zetasizer Nano ZS (Malvern Instruments, Malvern, UK), as described previously[50,51]. Doses of sEVs used in the experiments are shown as protein amount of sEVs estimated by Bradford assay. TEM images were analyzed using ImageJ software (Rasband, W.S., US National Institutes of Health, Bethesda, Maryland, USA) For binding stability of biotinylated CpG-DNA to sEV, sEV labeled with fluorescein-labeled CpG-DNA was incubated in 10% mouse serum in PBS solution at 37°C with gentle agitation. Samples were collected at the indicated time points. Collected samples were applied to size exclusion chromatography (SEC) and the elute was collected in 14 sequential fractions of 1 mL. The SEC column (1.5 cm × 12 cm mini-columns; Bio-Rad, Herculues, CA, USA; Econo-Pac columns) was packed with sepharose 2B (Sigma Aldrich) to make a 10 mL column bed before the sample apply. Fluorescence intensity in each fraction was measured to evaluate the release of CpG-DNA from sEV.

sEV labeling with fluorescence.

Lipophilic dye PKH26 or PKH67-labeled sEV was prepared by PKH26 red fluorescent cell linker kit or PKH67 green fluorescent cell linker kit (Sigma Aldrich). sEV samples resuspended in a buffer provided in the kits were mixed with the PKH dyes and were incubated for 5 min at room temperature. Next, the samples were added to PBS supplemented with 5% bovine serum albumin (BSA) and were ultracentrifuged at 100,000 × *g* for 1 h to remove free dyes. Exo-green-labeled-sEV was prepared by Exo-green fluorescent dye (System Biosciences Inc., Mountain View, CA, USA) according to the manufacture's protocol.

Oligodeoxynucleotides (ODNs).

All ODNs were purchased from Integrated DNA Technologies (Coralville, IA, USA). The sequences of the

ODNs used are listed in Table 1. For the preparation of the cross-linker DNA, ODNs dissolved in 150 mM NaCl were mixed at a final concentration of 450 μM for each ODN. The mixtures were then incubated at 95°C for 2 min and slowly cooled down to 4°C using a thermal cycler.

Preparation of CpG-sEV assembly.

CpG-sEV (1 μg of protein) was incubated with the indicated annealed cross-linker DNA at the indicated ratio. The samples were then incubated at 4°C for 30-60 min and observed by TEM. In a separate experiment, CpG-sEV assembly was treated with DNaseI (5U/sample; Takara Bio Inc., Shiga, Japan) at 37°C for 30 min. The sample was observed by TEM.

***In vitro* cellular uptake assay and cytokine release assay.**

For the cellular uptake assay, cells were seeded in a cell culture plate and incubated for 24 h before use. Then, PKH67-labeled sEV (10 μg/mL) samples were added to the cells. After incubation for the indicated time periods, the cells were washed twice with PBS and harvested. The mean fluorescent intensity (MFI) of the cells was determined using a flow cytometer (Gallios Flow Cytometer; Beckman Coulter). Data were analyzed using Kaluza software (version 1.0, Beckman Coulter). In the assessment of endocytosis, the cells were pre-treated with 5-(N-ethyl-N-isopropyl) amirolide (EIPA) or cytochalasin D for 30 min prior to the treatment with PKH67-labeled sEV samples (10 μg/mL). In a separate experiment, DC2.4 cells were seeded onto a chamber slide (Watson Co., Ltd, Kobe, Japan) for 24 h before the experiment. Next, PKH26-labeled sEV (10 μg/mL) samples were added to the chamber slide for incubation. The cells on the slide were observed using a fluorescence microscope (BioZero BZ-X710, Keyence, Osaka, Japan). For the cytokine release assay, the amount of tumor necrosis factor (TNF)-α and interleukin (IL)-6 in the culture medium of the DC2.4 cells treated with sEV samples were measured by ELISA, as previously described[15].

Detection of fluorescence or gLuc-labeled CpG-sEV after intradermal injection.

Anesthetized ICR mice received an intradermal injection of the indicated Exo-green-labeled CpG-sEV samples (5 μg/shot). Bright field and fluorescence images of mice were acquired using LAS-3000 instrument (FUJIFILM) at the pre-determined time points. In a separate experiment, the indicated gLuc-labeled CpG-sEV samples (5 μg/shot) were injected into anesthetized mice via intradermal injection. The mice were sacrificed, and the injection sites were excised. The excised skin tissues were homogenized and the gLuc activity was measured. The amount of sEVs in the skin samples was normalized to the injection dose based on the gLuc activity and expressed as a percentage of the injected dose/tissue (%ID/tissue).

Quantitative measurement of mRNA expression.

The indicated CpG-sEV samples were injected into the mice via an intradermal injection at the indicated dose. At 12 and 48 h, the mice were sacrificed, and the injection sites were excised. Total RNA in the excised skin was extracted by sepasol-RNA I super G (Nacalai Tesque) according to the manufacture's protocol. Then, 50 ng of

extracted mRNA was used as a template for reverse transcription according to the manufacture's protocol (ReverTra Ace® qPCR RT Master Mix; TOYOBO CO., LTD, Osaka, Japan). For qPCR reaction, 5 ng of the cDNA was used according to the manufacture's protocol (KAPA SYBR® FAST qPCR Kits; Kapa Biosystems,Wilmington, MA, USA). The qPCR conditions were as follow[15]; stage 1 (1 round); 95°C for 10 min, stage 2 (40 round); 95°C for 15 s, and 60°C for 12 s, melt curve; 95°C for 15 s, 60°C for 1 min, and 95°C for 15 s. The primers used for amplification are listed in Table 2. The threshold cycle (CT) information was generated from a qPCR system (Applied Biosystems® StepOne Real-Time PCR Systems; Thermo Fisher Scientific). The obtained CT information was analyzed by ΔΔCT method. Briefly, the first ΔCT was calculated as follow: ΔCT = CT[a target gene (CXCL10, CXCL6, IL-6, IL-12p40)]-CT[a reference gene (β-actin)]. The ΔΔCT was calculated as follow: ΔΔCT = CT[a target sample (CpG-sEV, Ctrl CL DNA + CpG-sEV, CpG-sEV assembly] -CT[a reference sample (NT)]. The results were shown as the fold change of target gene expression in a target sample relative to a reference sample, normalized to a reference gene.

Evaluation of anti-tumor immunity.

Under anesthesia with isoflurane, C57BL6/J mice were intradermally immunized with the indicated CpG-sEV samples (3 μg/shot) in 30 μl of PBS. Mice were immunized three times on days 0, 4, and 8. Seven days after the final immunization, the mice were sacrificed and the serum and splenocytes were collected. B16BL6-specific IgG, IgG1, and IgG2a levels were measured as previously described[6]. The release of interferon-γ (IFN-γ) from the collected splenocytes incubated with mitomycin C-treated B16BL6 was evaluated as previously described[6].

Tumor inoculation in a preventive model.

Mice were intradermally immunized three times with the indicated CpG-sEV samples (3 μg/shot) on days 0, 4, and 8. Seven days after the final immunization, the mice were subcutaneously inoculated with 5×10^5 of B16BL6 cells and the tumor size was measured, as previously described[6].

Statistical analysis.

The statistical differences among the groups were evaluated using Tukey-Kramer method, and $P<0.05$ was considered statistically significant.

Table 1. Sequences of ODNs used in this study.

Underlined residues are phosphonothioate backbone.

ODN		Sequences (5'→3')	Conjugation	Length (mer)
3'Bio-TEG-CpG DNA		GCTGCTGACCACTGTCCATGACGTTCCTGATGCT	3'-biotin triethylene glycol	34
5'Fluoresein, 3'Bio-TEG-CpG DNA		GCTGCTGACCACTGTCCATGACGTTCCTGATGCT	5'-fluoresein 3'-triethylene glycol	34
CpG DNA used for Sense CpG Exo preparation	Sense	GCTGCTGACCACTGTCCATGACGTTCCTGATGCT	3'-biotin triethylene glycol	34
	Anti sense	CAGTGGTCAGCAGCTCCATGACGTTCCTGATGCT	3'-biotin triethylene glycol	34
T0 DNA	Sense	CAGTGGTCAGCAGCAGTCTAGCTTGTGCAG		30
	Anti sense	CAGTGGTCAGCAGCCTGCACAAGCTAGACT		30
Ctrl T0 DNA	Sense	GCTGCTGACCACTGAGTCTAGCTTGTGCAG		30
	Anti sense	GCTGCTGACCACTGTGCACAAGCTAGACT		30
T10 DNA	Sense	CAGTGGTCAGCAGC(T)$_{10}$AGTCTAGCTTGTGCAG		40
	Anti sense	CAGTGGTCAGCAGC(T)$_{10}$CTGCACAAGCTAGACT		40
T10A10 DNA	Sense	CAGTGGTCAGCAGC(T)$_{10}$AGTCTAGCTTGTGCAG(A)$_{10}$		50
	Anti sense	CAGTGGTCAGCAGC(T)$_{10}$CTGCACAAGCTAGACT(A)$_{10}$		50
T30 DNA	Sense	CAGTGGTCAGCAGC(T)$_{30}$AGTCTAGCTTGTGCAG		60
	Anti sense	CAGTGGTCAGCAGC(T)$_{30}$CTGCACAAGCTAGACT		60
T30A30 DNA	Sense	CAGTGGTCAGCAGC(T)$_{30}$AGTCTAGCTTGTGCAG(A)$_{30}$		90
	Anti sense	CAGTGGTCAGCAGC(T)$_{30}$CTGCACAAGCTAGACT(A)$_{30}$		90
T50 DNA	Sense	CAGTGGTCAGCAGC(T)$_{50}$AGTCTAGCTTGTGCAG		80
	Anti sense	CAGTGGTCAGCAGC(T)$_{50}$CTGCACAAGCTAGACT		80
T50A50 DNA	Sense	CAGTGGTCAGCAGC(T)$_{50}$AGTCTAGCTTGTGCAG(A)$_{50}$		130
	Anti sense	CAGTGGTCAGCAGC(T)$_{50}$CTGCACAAGCTAGACT(A)$_{50}$		130

Table 2. The primers used for RT-PCR in this study.

Gene	Primers	Sequences (5'→3')
IL-6	Sense	GTTCTCTGGGAAATCGTGGA
	Anti sense	TGTACTCCAGGTAGCT ATGG
CCL5	Sense	CCAATCTTGCAGTCGTGTTTG
	Anti sense	ACCCTCTATCCTAGCTCATCTC
CXCL10	Sense	AAGTGCTGCCGTCATTTTCT
	Anti sense	CCTATGGCCCTCATTCTCAC
IL-12p40	Sense	ACTCCCCATTCCTACTTCTCC
	Anti sense	CATTCCCGCCTTTGCATTG
β-actin	Sense	CATCCGTAAAGACCTCTATGC
	Anti sense	ATGGAGCCACCGATCCACA

I-2-3. Results

I-2-3-a. Preparation and characterization of CpG-sEV assembly.

Firstly, the sEV markers, size distribution, zeta potential, and morphology of CpG-sEV were measured and checked (Supplementary figure 1). By measuring both the sEV protein level and the fluorescence intensity of CpG DNA, it was estimated that 1 μg of sEV was modified with approximately 1 pmol (12 ng) of CpG DNA. I also checked the labeling stability of CpG-DNA to sEV in mouse serum. SEC analysis revealed that CpG-DNA of CpG-sEV sample was eluted at fraction 4, which corresponded to sEVs, irrespective of the incubation time, suggesting that CpG-DNA bound to sEV with high stability (Supplementary figure 2). Next, I preliminarily designed two different ways to assemble CpG-sEV; one involved linking the CpG-sEV via a cross-linker DNA (Figure 7A), and the other involved linking the CpG-sEV directly using two different CpG-DNAs with complementary nick sites at the 5'-end (Figure 7B). TEM analysis revealed that the former design formed an CpG-sEV assembly more efficiently than the latter (Supplementary figure 3). Thus, I focused on the former design (Figure 7A) for further studies. The micro-sized superstructure disappeared after DNase treatment (Supplementary figure 4A), suggesting that the superstructure was specifically formed by DNA hybridization. Moreover, the colocalization of PKH26-labeled CpG-sEV and fluorescein-labeled linker DNA suggests that CpG-sEV assembled with each other via CL DNA to create a micro-sized assembly (Supplementary figure 4B). Different lengths of cross-linker DNA were prepared by varying the length of the thymine repeat (T0, T10, T30, and T50 DNA) or adenine to alter flexibility (T10A10, T30A30, and T50A50 DNA) (Figure 8A). After mixing CpG-sEV and various cross-linker DNAs, the formation of CpG-sEV assembly was observed when the T0, T10, T10A10, T30A30, or T50A50 DNA was used, while the T30 or T50 DNA did not result in assembly formation (Figure 8B). Compared to the assembly with the use of T10 DNA or T30A30 DNA, the amount of the assembly with the use of T0 DNA and T10A10 DNA appeared to be more. In addition, the size of the assembly with use of T0 DNA and T10A10 DNA appeared to be larger than the assembly with the use of T10 DNA or T30A30 DNA. Moreover, the T0 DNA in particular formed an assembly with a high reproducibility in the repeated four independent experiments. Thus, I chose T0 DNA (termed as "cross linker (CL) DNA" hereafter) for further experiments. Next, a scrambled control cross-linker DNA (Ctrl CL DNA) which did not hybridize with CpG-sEV was prepared for the establishment of the optimal ratio of CL DNA to CpG-sEV (Figure 8A). The observation of the CpG-sEV assembly by TEM and image analysis indicated that increase of CL DNA resulted in formation of increased amount of CpG-sEV assembly and that 100 pmol of CL DNA was sufficient for assembly formation with 1 μg of CpG-sEV (Figure 8C). Thus, further functional experiments were conducted with the CpG-sEV assembly at a ratio of CpG-sEV (1 μg) : CL DNA (100 pmol).

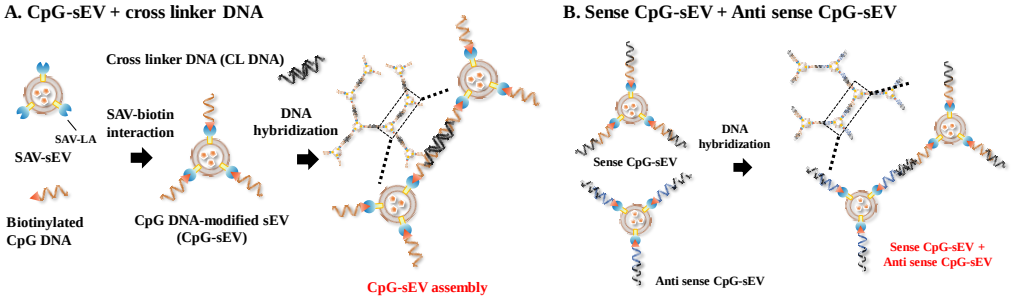

Figure 7. Schematic representation of the preparation of the CpG-sEV assembly.

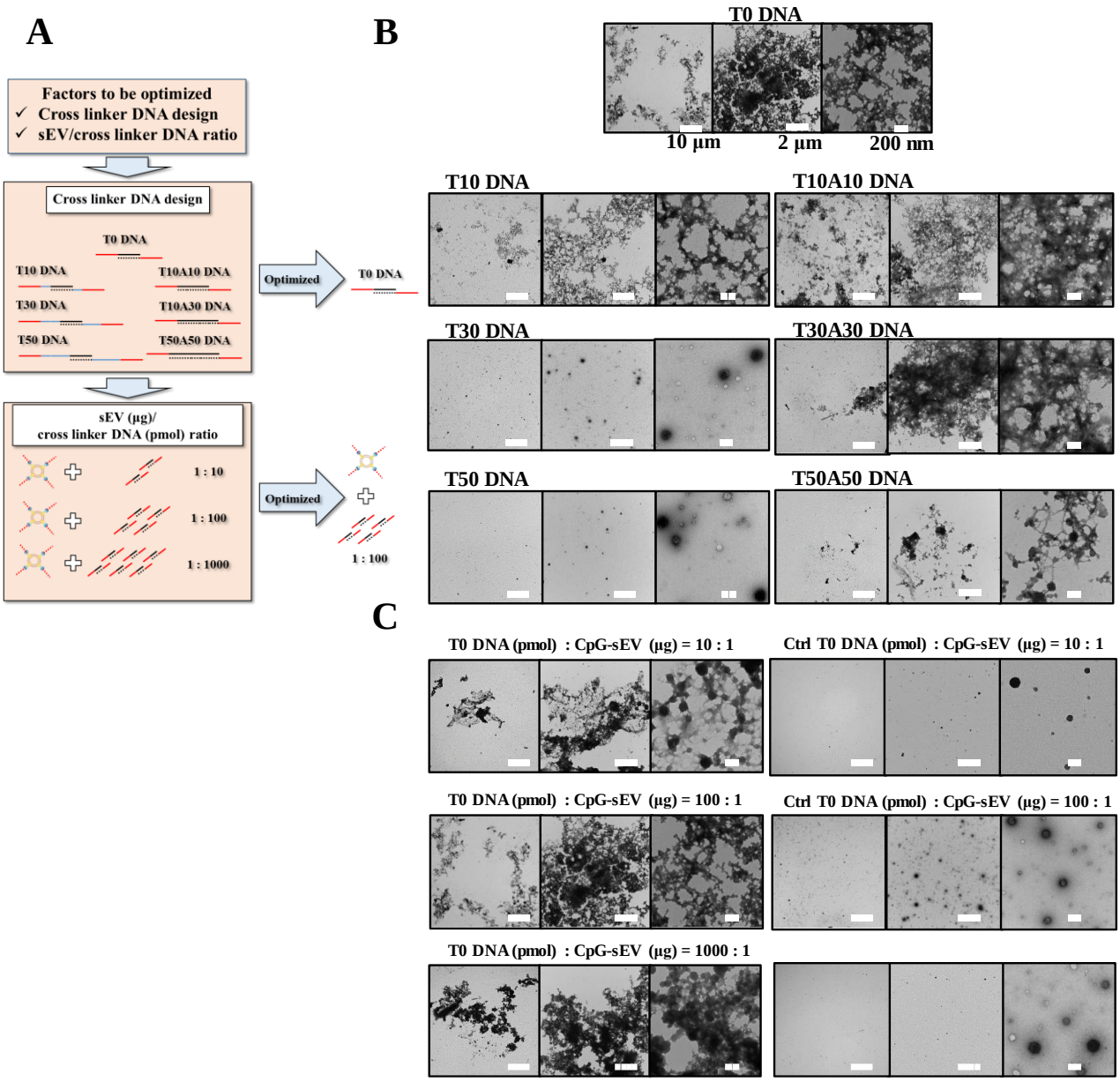

Figure 8. Effect of linker DNA design on the formation of CpG-sEV assembly.

(A) Schematic representation of the optimization of CpG-sEV assembly preparation. (B) TEM image of CpG-sEV assembly formed with cross-linker DNA of different lengths. CpG-sEV (1 μg) was incubated with different cross-linker DNAs (100 pmol). The sequences of the cross-linker DNA are summarized in Table 1. T0 DNA was selected for subsequent experiments. (C) The effect of the CpG-sEV : T0 DNA ratio on the formation of the CpG-sEV assembly. CpG-sEV (1 μg) was incubated with different amounts of T0 DNA or Ctrl T0 DNA (10, 100, 1000 pmol).

I-2-3-b. *In vitro* cellular uptake of CpG-sEV assembly.

Next, the CpG-DNA or sEVs were labeled with fluorescein or PKH67, respectively, and the uptake of sEV samples by APCs and non-APCs was evaluated. Irrespective of the fluorescent probes, the MFI values of the DC2.4 cells, used as a model APC, treated with labeled CpG-sEV assembly was significantly higher than those treated with the corresponding CpG-DNA or Ctrl CL DNA + CpG-sEV (Figure 9A, 9B), indicating that the cellular uptake of CpG-sEV (CpG-DNA and sEV) was increased by assembly formation. The simultaneous uptake of fluorescein-labeled CpG-DNA or CL DNA with PKH26-labeled sEVs by the same DC2.4 cells was observed after the addition

of CpG-sEV assembly (Figure 9C, 9D). Next, the uptake of CpG-sEV assembly by RAW264.7, another model APC, or B16BL6, and NIH3T3 cells, used as model non-APCs, was evaluated (Figure 9E-9G). In the RAW264.7 cells, the MFI values of cells treated with the CpG-sEV assembly almost doubled compared with those cells treated with CpG-sEV or Ctrl CL DNA + CpG-sEV. In the case of B16BL6 or NIH3T3 cells, the MFI values of the cells treated with the CpG-sEV assembly were significantly decreased or hardly changed, respectively. The uptake mechanism of CpG-sEV assembly by DC2.4 cells was also evaluated using several endocytosis inhibitors (Figure 10). The uptake of CpG-sEV, Ctrl CL DNA + CpG-sEV, and CpG-sEV assembly was inhibited when the DC2.4 cells were treated with cytochalasin D or EIPA.

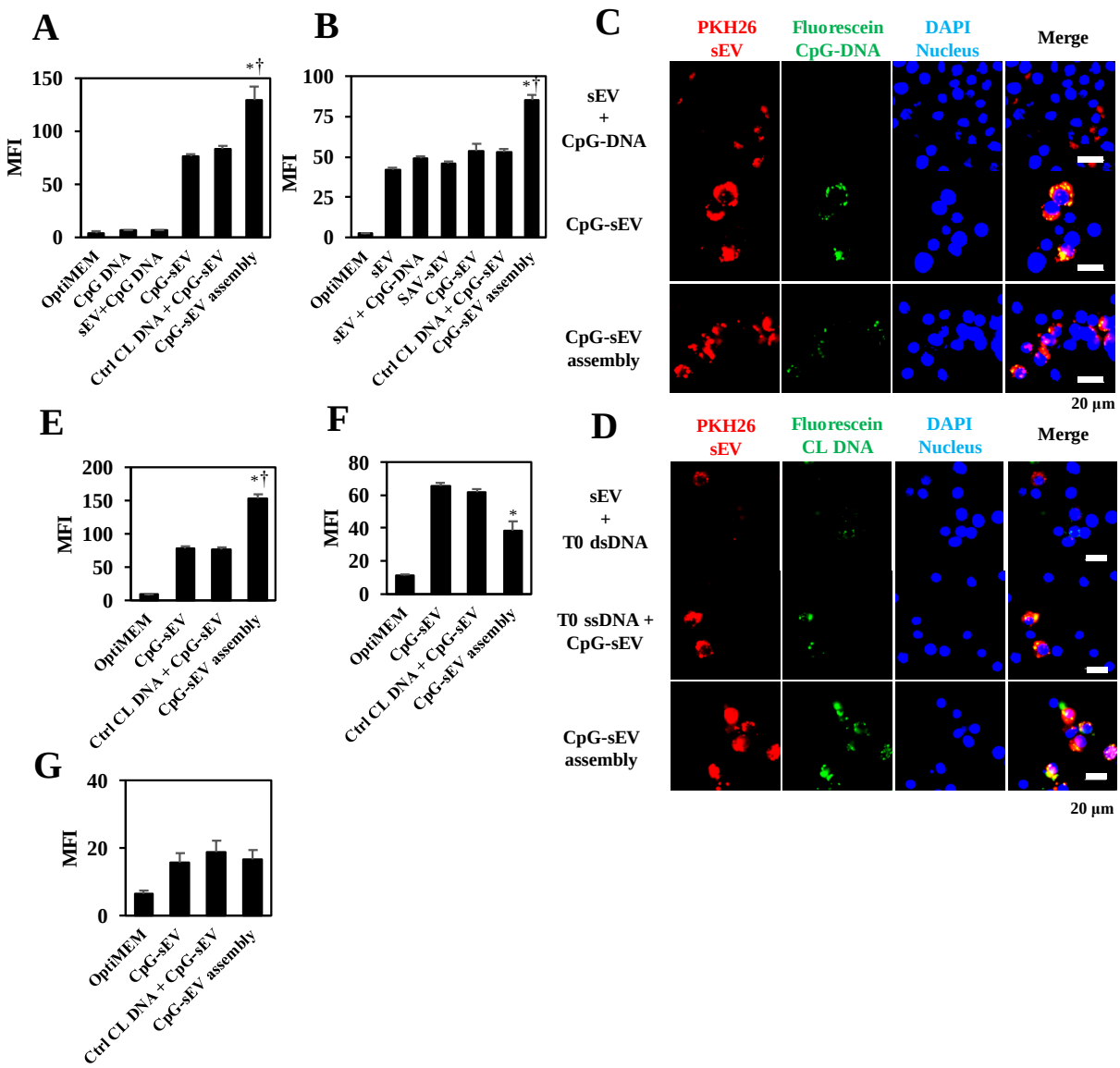

Figure 9. Increased and selective cellular uptake of CpG-sEV assembly by APC

(A), (B) Flow cytometric analysis of DC2.4 cells after the addition of 10 μg/mL of (A) fluorescein-labeled biotinylated CpG-DNA (10 nM) or (B) PKH67-labeled sEV samples. The mean fluorescent intensity (MFI) was calculated as an index of cellular uptake. (C), (D) Fluorescent microscopic image of DC2.4 cells incubated with the 10 μg/mL of CpG-sEV assembly. (C) red = PKH26-labeled sEVs, green = fluorescein-labeled biotinylated CpG-DNA, blue = DAPI. (D) red = PKH26-labeled sEVs, green = fluorescein-labeled CL DNA, blue = DAPI. (E)-(G) Flow cytometric analysis of (E) RAW264.7 cells, (F) B16BL6 cells, and (G) NIH3T3 cells after the addition of PKH67-labeled sEV samples. Results are expressed as the mean ± SD (n = 4). † $P<0.05$ v.s. CpG-sEV at the same concentration. * $P<0.05$ compared with Ctrl CL DNA + CpG-sEV.

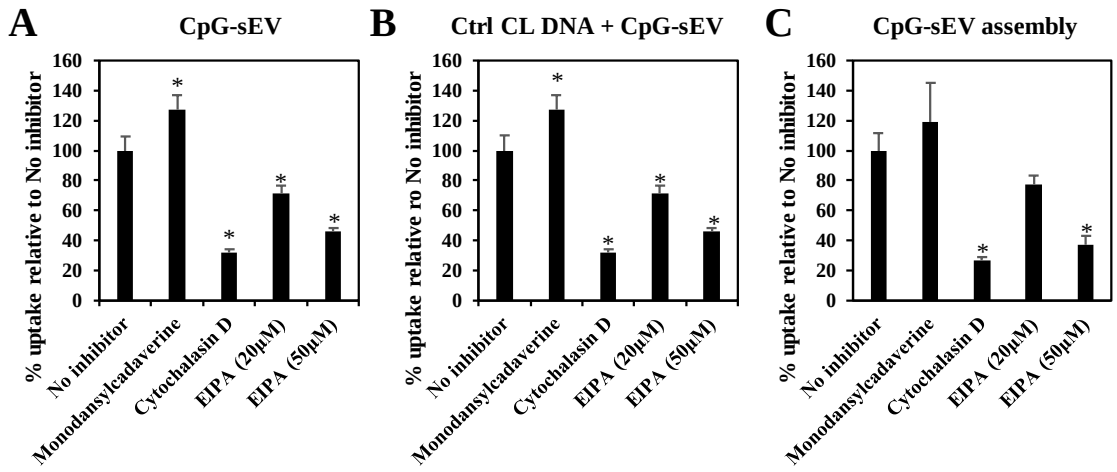

Figure 10. Effect of endocytosis inhibitors on *in vitro* cellular uptake of sEV samples by DC2.4 cells.

Flow cytometric analysis of DC2.4 cells after the addition of 10 μg/mL of (A) PKH67-labeled CpG-sEV, (B) Ctrl CL DNA + PKH67-labeled sEV, or (C) PKH67-labeled CpG-sEV assembly. DC2.4 cells were pre-treated with the indicated endocytosis inhibitors. The mean fluorescence intensity (MFI) was calculated as an index of cellular uptake. Results are expressed as the mean ± SD (n = 4). † $P < 0.05$ v.s. no inhibitor

I-2-3-c. Cytokine release by DC2.4 cells after stimulation by CpG-sEV assembly.

Next, the release of cytokines (TNF-α, IL-6) from DC2.4 cells treated with sEV, SAV-sEV, sEV + CpG-DNA, CpG-sEV, Ctrl CL DNA + CpG-sEV, or CpG-sEV assembly was evaluated (Figure 11). Significantly higher amounts of TNF-α and IL-6 were released from DC2.4 cells treated with CpG-sEV assembly compared to the other groups. Contrastingly, CL DNA had little effect on TNF-α and IL-6 secretion (Figure 12).

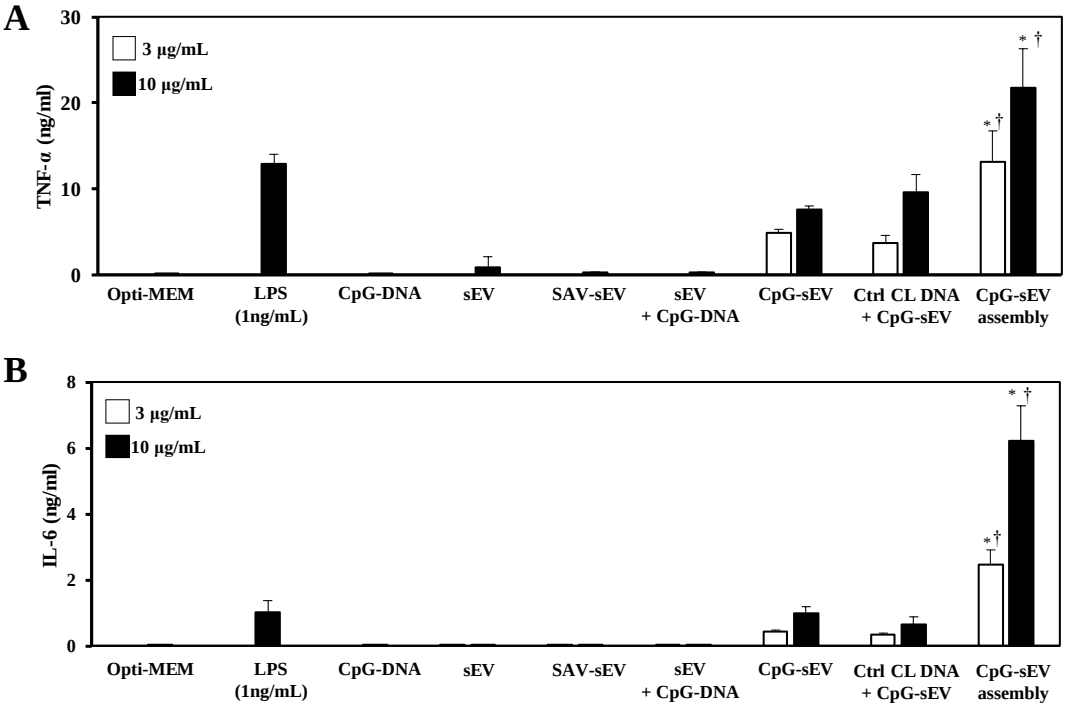

Figure 11. Enhanced cytokine release from DC2.4 cells stimulated with the CpG-sEV assembly.

(A) TNF-α and (B) IL-6 secretion from DC2.4 cells 8 h after treatment with the CpG-sEV assembly. Results are expressed as the mean ± SDs (n = 4). † $P<0.05$ v.s. CpG-sEV at the same concentration. * $P<0.05$ compared with Ctrl CL DNA + CpG-sEV.

I-2-3-d. Retention at injection site and immunostimulatory activity after intradermal injection.

Based on the results of cellular uptake assay and cytokine release assay, I have decided to focus on CpG-sEV, Ctrl CL DNA + CpG-sEV, and CpG-sEV assembly for further *in vivo* assay. Exo-green-labeled CpG-sEV, CpG-sEV assembly, or Ctrl CL DNA + CpG-sEV were intradermally injected in mice and their retention at the injection site was observed by *in vivo* imaging (Figure 13A). At early time points (1 h), the fluorescence signals were comparable among the groups; at late time points (24 and 48 h), more intense fluorescence signals were detected at the CpG-sEV assembly injection site. This result was not dependent on the dermal site of injection, that is, whether the right, middle, or left part of the back was injected. The prolonged retention in the injection site was further quantitatively confirmed by using gLuc-labeled CpG-sEV samples (Figure 13B). At 8 h and later time points after injection, gLuc activity at the injection site was significantly higher for CpG-sEV assembly than for the other groups. In addition, gLuc activity was comparable between CpG-sEV and Ctrl CL DNA + CpG-sEV. To evaluate whether the formation of CpG-sEV assembly affected the immune response *in vivo*, I evaluated the mRNA expression of several cytokines (IL-6 and IL12-p40) and chemokines (CXCL5 and CXCL10) at the injection sites 12 or 48 h after the injection (Figure 14). The mRNA expression levels of both cytokines and chemokines were higher in the CpG-sEV assembly compared with CpG-sEV and Ctrl CL DNA + CpG-sEV, except in the case of IL12-p40 at 12 h.

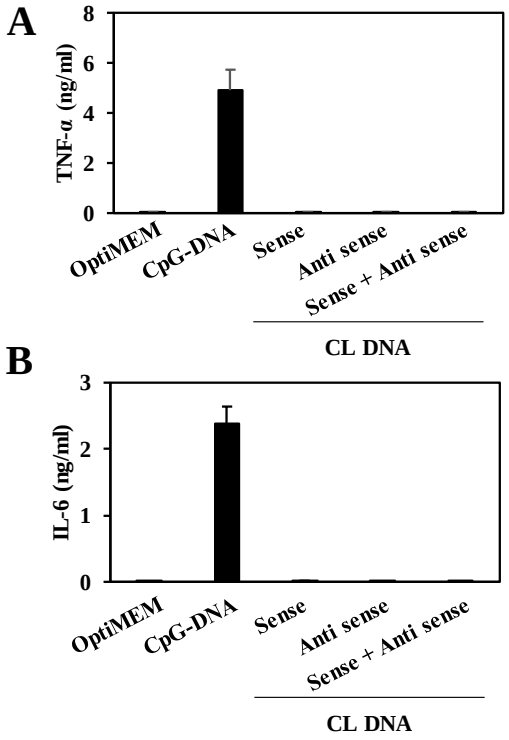

Figure 12. Cytokine release from DC2.4 cells stimulated with CL DNA.

DC2.4 cells were treated with 5 μM of the indicated DNA samples for 8 h. (A) TNF-α or (B) IL-6 levels in the supernatant was measured by ELISA. Results are expressed as the mean ± SD (n = 4)

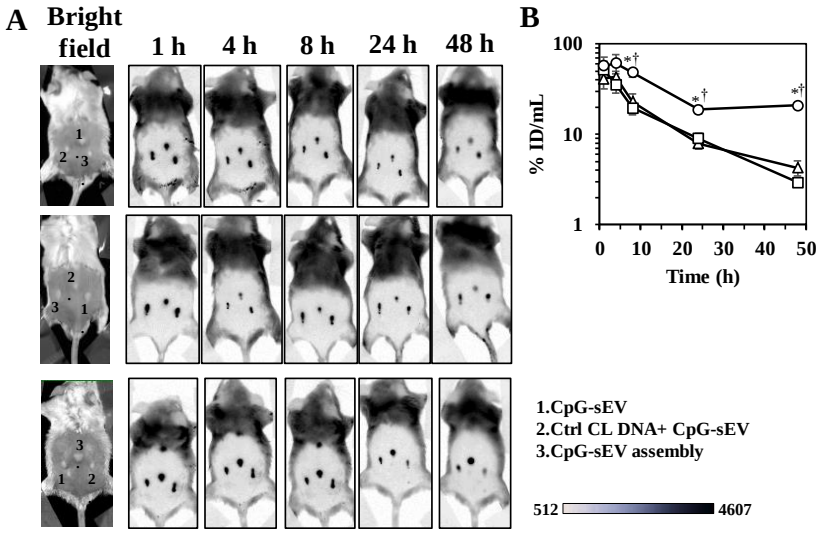

Figure 13. Prolonged tissue residence of CpG-sEV assembly after intradermal injection.

(A) Clearance of sEV in the skin after intradermal injection in mice. Exo-green-labeled CpG-sEV samples (5 μg/shot) was administered into tumor tissue and the fluorescence distribution around the shaved back was photographed. (B) The skin tissue around the injection site was excised and the gLuc activity was measured at the indicated time points after the intradermal injection of 5 μg/shot of the gLuc-labeled CpG-sEV samples. Results are expressed as mean ± SD (n = 3). † $P<0.05$ v.s. CpG-sEV at the same timepoint. * $P<0.05$ compared with Ctrl CL DNA + CpG-sEV at the same timepoint.

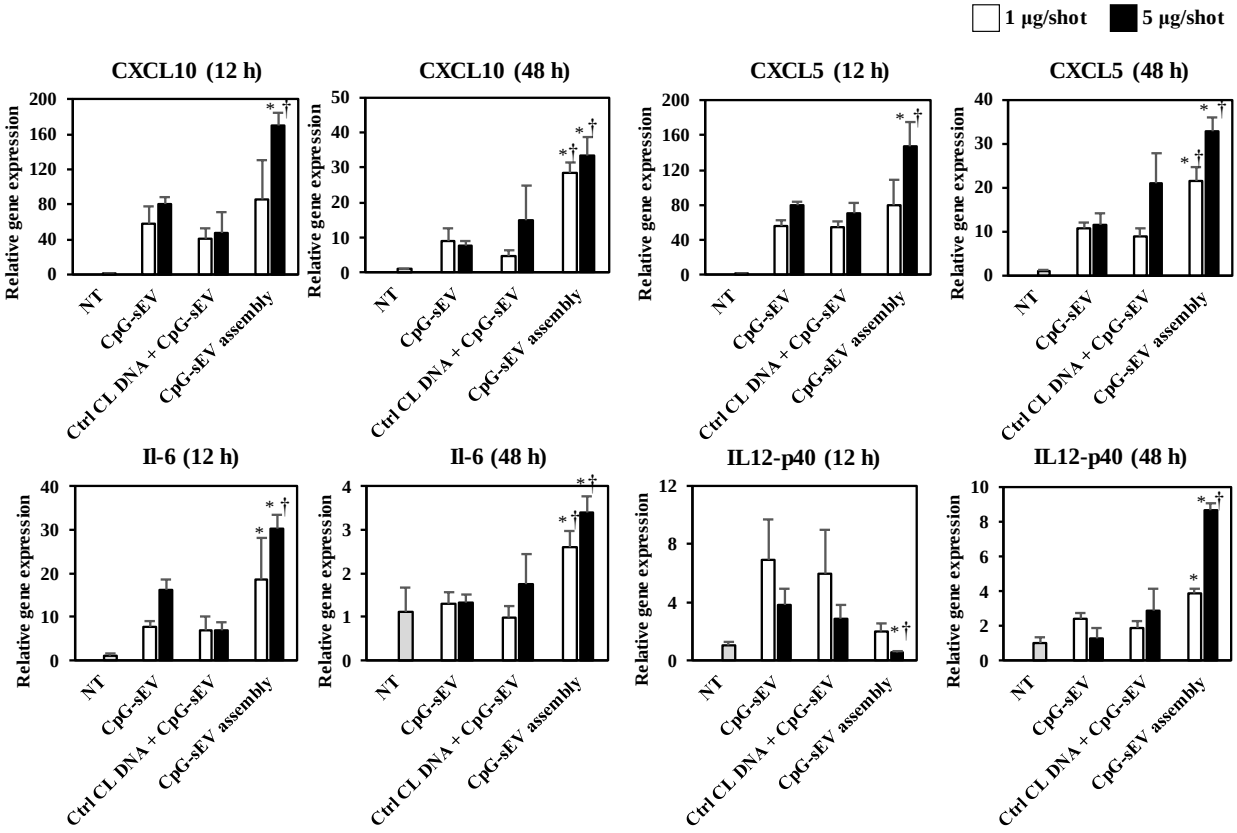

Figure 14. Enhanced immunostimulatory activity of the CpG-sEV assembly after intradermal injection.

The skin tissue around the injection site was excised and total mRNA was extracted 12 and 48 h after the intradermal injection of the CpG-sEV samples. The indicated mRNA was quantified by RT-PCR. Results are expressed as the mean ± SD (n = 4). † P<0.05 v.s. CpG-sEV at the same concentration. * P<0.05 compared with Ctrl CL DNA + CpG-sEV.

I-2-3-e. Induction of B16BL6-specific immune response and protective anti-tumor immunity by CpG-sEV assembly.

Next, mice were intradermally injected with PBS, SAV-sEV, CpG-sEV, Ctrl CL DNA + CpG-sEV, or CpG-sEV assembly. Immunization with the CpG-sEV assembly increased the amount of B16BL6-specific IgG Abs in mice compared to those immunized with CpG-sEV (Figure 15A). Furthermore, the evaluation of B16BL6-specific Ab revealed an increase in the Th-1-related IgG2a isotype in mice immunized with CpG-sEV assembly (Figure 15B). Contrastingly, enhancement of the Th-2-related IgG1 isotype was not observed after immunization with the CpG-sEV assembly, which was comparable to that with CpG-sEV (Figure 15C). Next, in order to investigate the T-cell activation after administration of CpG-sEV assembly, the Th-1 type cytokine IFN-γ secretion from T-cell in the murine splenocytes after re-stimulation with mitomycin C-treated B16BL6 cells was measured[15,52–54]. After re-stimulation with mitomycin C-treated B16BL6 cells, the splenocytes of mice immunized with CpG-sEV assembly induced higher amounts of IFN-γ than those of mice immunized with PBS and SAV-sEV samples (Figure 15D). Next, the enhanced protective anti-tumor immunity induced by CpG-sEV assembly was measured (Figure 15E). Consequently, immunization with CpG-sEV assembly significantly inhibited tumor growth in mice compared to that with PBS and SAV-sEV.

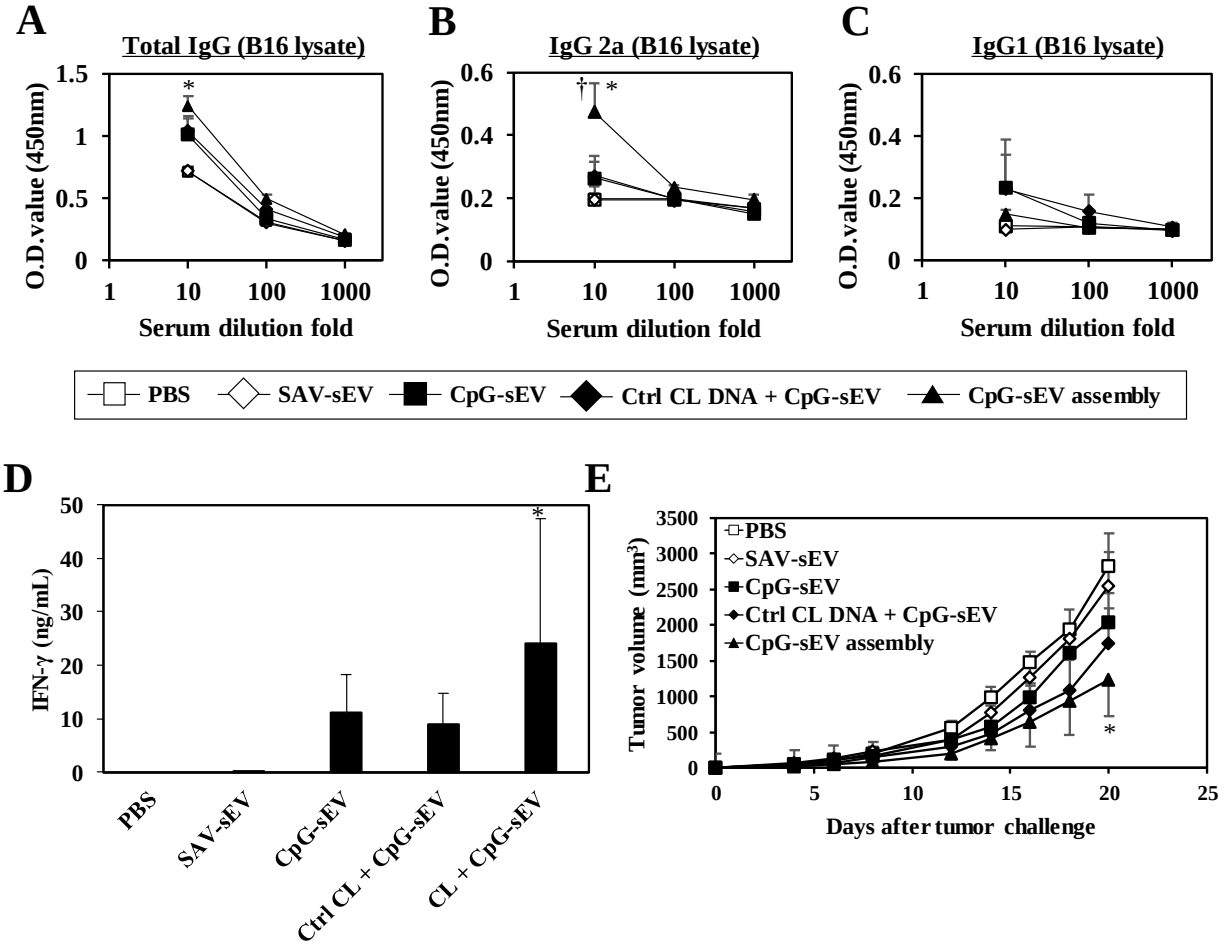

Figure 15. Induction of potent B16BL6-specific cellular and humoral immunity and enhanced protective anti-tumor immunity induced by CpG-sEV assembly.

Mice were intradermally immunized three times with 3 μg/shot of the indicated samples. (A)-(C) For the humoral immune responses, plates were coated with B16BL6 and incubated with serum from immunized mice. (A) Total mouse immunoglobulin G (IgG), (B) mouse IgG2a, and (C) mouse IgG1 were detected. Results are expressed as the mean ± SD (n = 4). † $P<0.05$ v.s. CpG-sEV at the same concentration. *$P<0.05$ compared with Ctrl CL DNA + CpG-sEV. (D) For the cellular immune response induced by the indicated samples, splenocytes were collected 7 days after the final immunization and stimulated with mitomycin C-treated B16BL6 for 3 days. The levels of released IFN-γ in the culture media were measured. (E) Seven days after the final immunization, the mice were subcutaneously inoculated with B16BL6 cells and the tumor volume was measured. Results are expressed as mean ± SD (n = 6). * $P<0.05$ compared with the PBS and SAV-sEV groups.

I-2-4. Discussion

Ever since nanoparticle assembly using DNA hybridization was initially reported by Mirkin et al. in 1996, DNA-nanoparticle hybrid materials and assemblies have been widely investigated using different nanoparticle materials such as gold nanoparticles and liposomes and different assembly designs[55]. Currently, this concept has been successfully applied to understanding the lipid membrane fusion, the development of biosensors (*e.g.* detection of DNA mutation), and drug delivery[47,48]. sEVs are a potential candidate for drug delivery and therapeutic treatment. However, to the best of my knowledge, no studies have reported on sEV assembly. This could be due to the lack of stable DNA labeling on the surface of sEVs. Thus, by using a stable DNA labeling method based on a previously developed SAV-biotin interaction[17], I successfully prepared a CpG-sEV assembly after optimization (Figure 7, 8,

Supplementary figure 1-4). Moreover, recent research on sEV-based immunotherapy significantly improved by mixing sEV with adjuvant, followed by loading the CpG-DNA adjuvant to sEV membrane. In this study, I hypothesized that CpG-sEV assembly could be superior to CpG-DNA and improve sEV-based tumor immunotherapy (Figure 16).

The formation of the CpG-sEV assembly is likely to be affected by the solvent (*e.g.* solvent types, solvent temperature, and solvent concentration), the particle concentration and physicochemical properties of particle (e.g. particle size, rigidity, and zeta potential), as well as the cross-linker DNA design (sequence length, flexibility, and ratio to sEVs)[48,56,57]. Due to its therapeutic applications, I decided to focus on the cross-linker DNA design for CpG-sEV assembly formation. The results indicated that T0 DNA, the shortest and simplest design considered in this study, formed the largest CpG-sEV assembly with the highest reproducibility (Figure 8). I initially assumed that CpG-sEV would repulse each other due to the coulomb force derived from the negative charge of sEVs (Supplementary figure 1) and therefore the longer cross-linker DNAs would permit a more efficient assembly. Considering that CpG-sEV are cross-linked with more sites when shorter cross-linker DNA was used (Figure 8), easier access to DNA hybridization in the case of short cross-linker DNAs can outweigh the repulsive coulomb force to obtain a stable CpG-sEV assembly.

Recent studies investigating the sEV uptake mechanism have revealed that sEVs are taken up by cells via endocytosis, such as phagocytosis, macropinocytosis, caveolin-mediated endocytosis, or clathrin-mediated endocytosis, and that the uptake mechanism is dependent on the recipient cells[58]. Experiments using uptake inhibitors suggested that CpG-sEV assembly was taken up by DC2.4 cells through either phagocytosis or macropinocytosis (Figure 10). Particle size is one of the key physicochemical factors for cellular uptake of nanoparticle. It is assumed that the size difference may be the reason for the increased and selective cellular uptake of CpG-sEV assembly by APCs[44,45] (Figure 9).

After internalization through the phagocytosis pathway, CpG-sEV assembly could be encapsulated in the phagosome and be delivered directly to the lysosome for digestion[58]. However, in the case of macropinocytosis, CpG-sEV assembly could be delivered to lysosomes via endosomes, where TLR9, a ligand for CpG-DNA, is localized[59,60]. Increased cytokine release by assembly formation implies that CpG-sEV may be taken up via macropinocytosis (Figure 11, 12). After the CpG-sEV assembly was delivered to endosome, the CpG-sEV assembly might be disassembled to CpG-sEV because of low pH environment in the endosome[16]. The increased surface area of CpG-sEV might also contribute to the increased recognition of CpG-DNA by TLR9 and increased cytokine release.

The skin is rich in APCs, such as Langerhans cells, and is a suitable injection site for the induction of anti-tumor immunity[61]. I demonstrated a prolonged retention time in CpG-sEV assembly after intradermal injection (Figure 13). After intradermal injection, sEVs diffuse and are cleared to regional lymphatic vessels and blood capillaries, or are taken up by local cells[62,63]. Particles with a size range of 10-200 nm (sEVs are within this size range) can enter lymphatic vessels and blood capillaries by directly diffusing through the endothelial cell junctions, while micro-sized particles are restricted to diffuse from the injection site[44]. As the complementary DNA-DNA interaction is based on the hydrogen bonding, the stability of DNA-DNA interaction is greatly affected by the DNA concentration. After intradermal injection of the CpG-sEV assembly, the solvent will diffuse from the injection site

much faster than the CpG-sEV assembly, making the concentration of CpG-sEV assembly in the injection site higher. On the other hand, endogenous DNase in the skin should be considered to disassemble the CpG-sEV assembly. Thus, it was assumed that CpG-sEV assembly, which is larger than the size range of 10-200 nm, remained at the injection site and was gradually degraded by endogenous DNase in the skin as shown in Figure 13B.

After the delivery of antigens and adjuvants to the dermal-resident APCs, the APCs matured and secreted several chemokines and cytokines to initiate a subsequent immune response. For instance, the secretion of CXCL10 induces a Th1-favored proinflammatory response, CXCL5 recruits neutrophils, IL-12p40 induces Th-1 and CTL responses, and IL-6 leads to the maturation of B cells and induces Th17 responses[64,65]. Based on the *in vivo* results, it was assumed that CpG-sEV assembly was efficiently taken up by the dermal-resident APCs and induced the maturation of APCs (Figure 14), followed by the induction of a B16BL6-specific immune response and protective antitumor immunity (Figure 15). These results suggest that the intradermal immunization with CpG-sEV assembly elicited stronger antitumor immunity than that induced by intradermal immunization with CpG-sEV.

A sEV assembly-based delivery system is advantageous compared to conventional gold nanoparticle or liposome assembly-based delivery systems due to their lower cytotoxicity and tumor antigen loading[14–16,66]. Furthermore, compared to dispersed microvesicles of the same diameter, the CpG-sEV assembly has a larger surface area. This means the CpG-sEV assembly can deliver more CpG-DNA than the microvesicles. To further improve the assembly design, the assembly and disassembly should be controlled in order to precisely control the size of the assembly. A previous study successfully controlled the efficiency of the assembly by optimizing the DNA modification efficiency on gold nanoparticles[67,68]. It could also be likely that CpG-sEV concentration affects the assembly size. Thus, future studies should attempt to mix CpG-sEV at different CpG-DNA modification ratios at different concentrations. Moreover, since the heterogeneity of sEV might also be a barrier to prepare sEV assembly

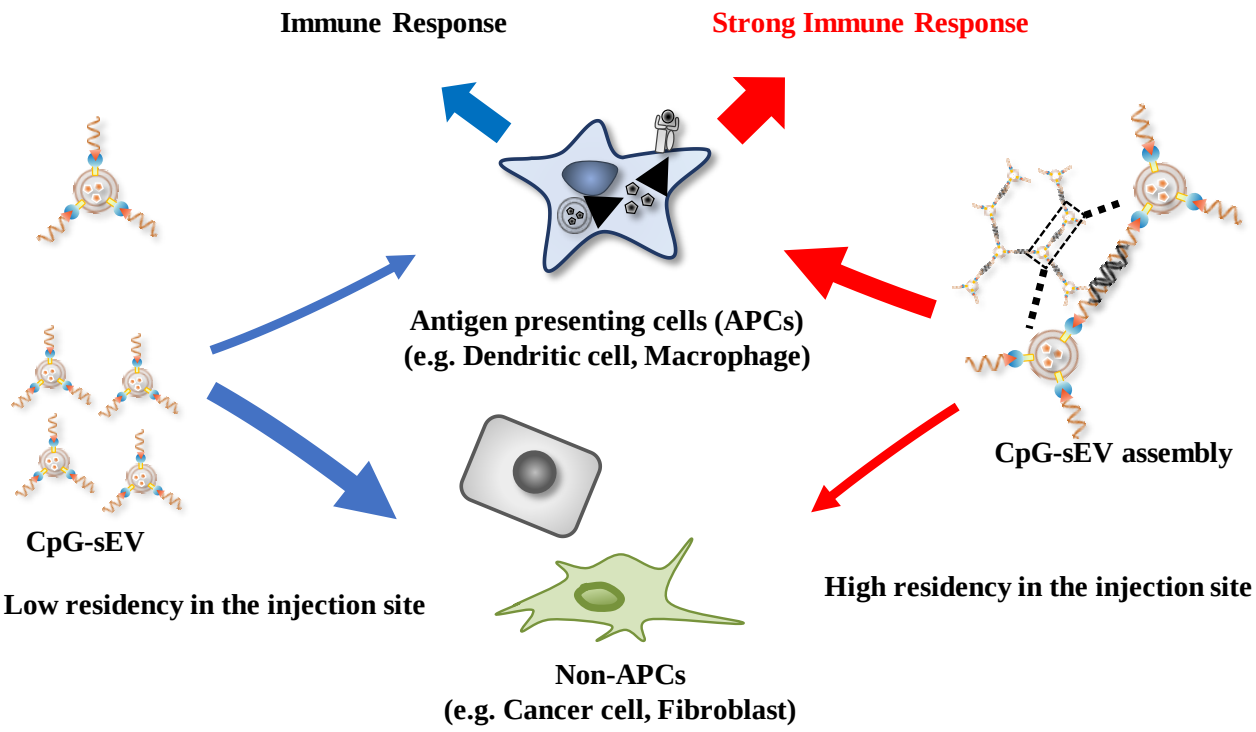

Figure 16. Schematic image of enhanced immune response by CpG-sEV assembly.

with uniform size, isolation protocol, such as size exclusion chromatography and field flow fractionation, should also be considered to fractionate into sEV subpopulation[69]. For the disassembly, an external stimulus, such as light or complementary cross-linker DNA, is able to program reversible assembly with high specificity[57,70]. Controlling the size and disassembly of the CpG-sEV assembly would enhance antitumor immunity induced by tumor-cell derived sEVs. Thus, the optimization of these properties should be examined in future studies.

I-2-5. Summary of section 2 of chapter I

In this section, I have newly designed DNA-anchored micrometer-sized assembly of tumor-cell derived sEVs-modified with CpG-DNA for the first time in order to improve tumor-cell derived sEV-based tumor immunotherapy. I have demonstrated that CpG-sEV assembly shows the ability to encourage selective uptake by dendritic cells and increased retention time at the site of intradermal injection. Immunization with CpG-sEV assembly exerted stronger immune activation and antitumor effects than simple CpG-sEV. These findings propose a novel insight for sEV bioengineering as well as a useful tumor-cell derived sEV-delivery system that can be used for tumor immunotherapy.

I-2-6. Supplementary figures of section 2 of chapter I

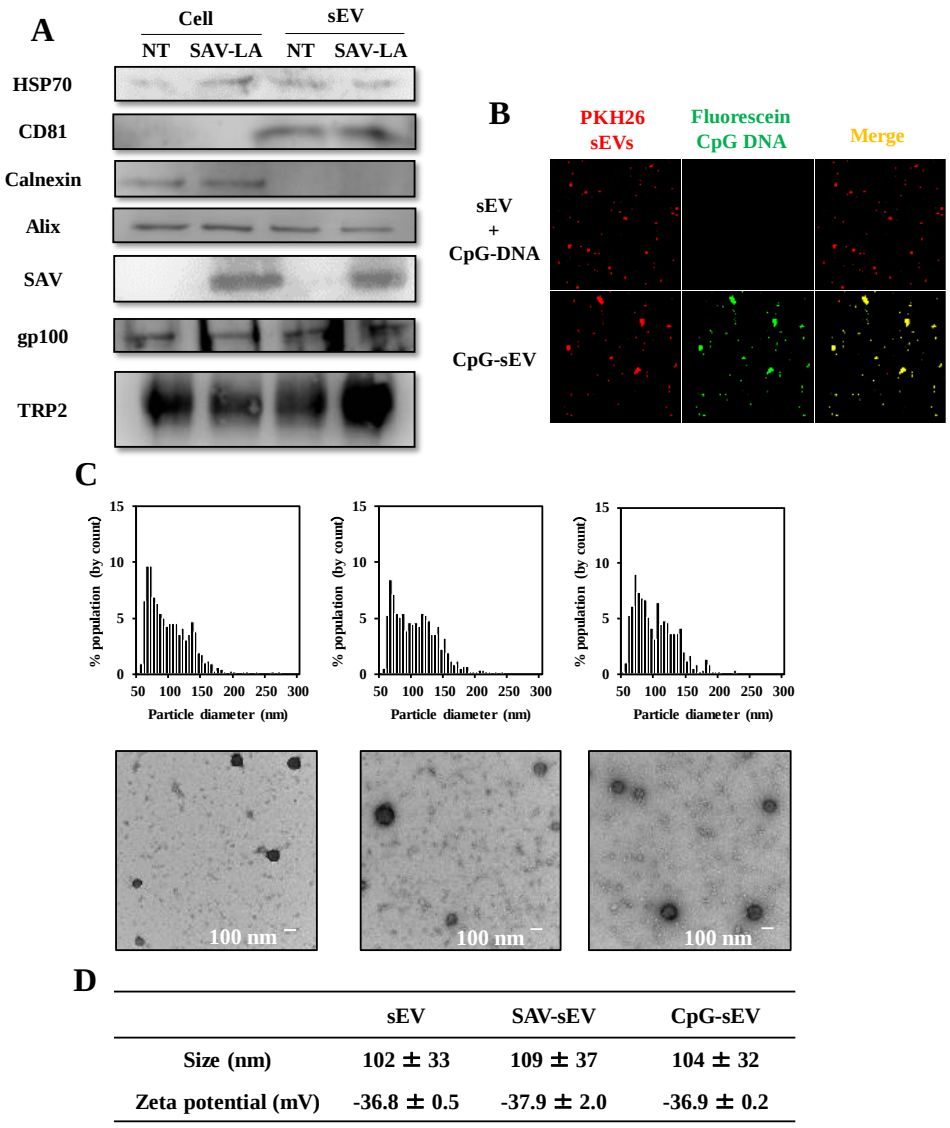

	sEV	SAV-sEV	CpG-sEV
Size (nm)	102 ± 33	109 ± 37	104 ± 32
Zeta potential (mV)	-36.8 ± 0.5	-37.9 ± 2.0	-36.9 ± 0.2

Supplementary figure 1. Characterization of CpG-sEV.

(A) Western blotting analysis. (B) Fluorescent microscopic observation of sEV mixed with biotinylated CpG DNA and CpG-sEV (green = fluorescein-labeled biotinylated CpG DNA, red = PKH26-labeled sEV). (C) Histograms of particle size distribution and TEM images. (D) Particle size and zeta potential of sEV, SAV-sEV, and CpG-sEV. Results are expressed as the mean ± SD (n = 3).

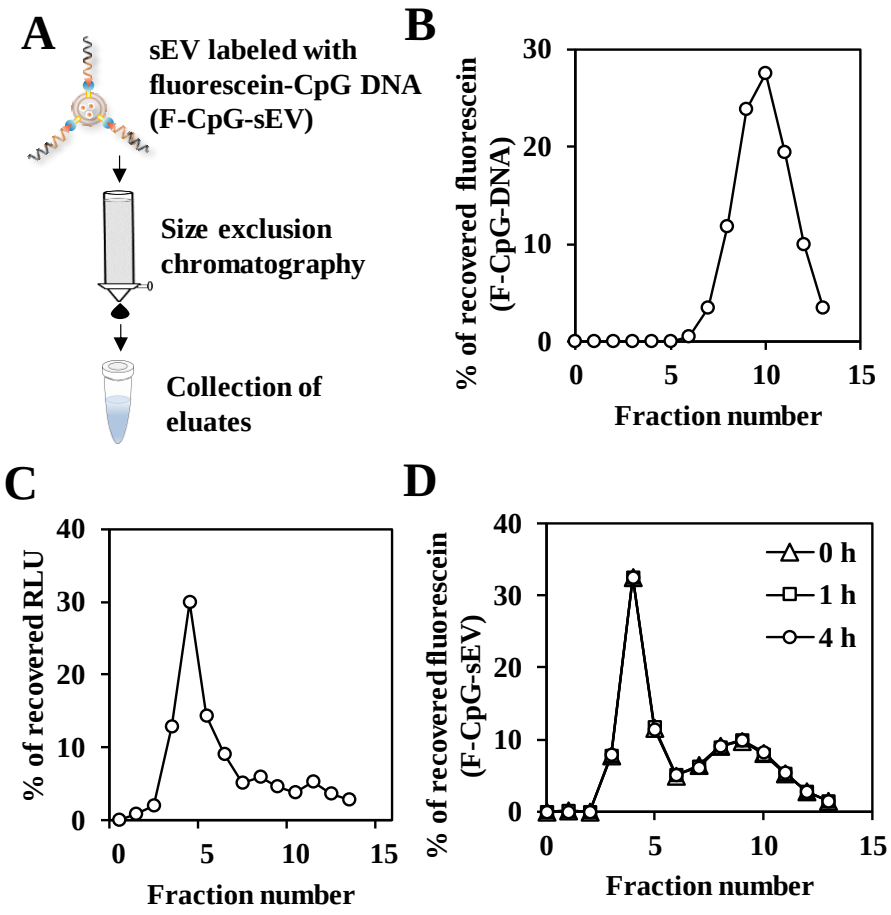

Supplementary figure 2. Binding stability of CpG-DNA to sEV.

(A) After sEV labeled with fluorescein-CpG DNA (F-CpG-sEV) was incubated with 10% mouse serum in PBS for the indicated time, the sample was proceeded into size exclusion chromatography (SEC) analysis. The fluorescence intensity or the gLuc enzyme activity of each fraction was measured. Elution profile of (B) F-CpG-DNA and (C) gLuc-LA-sEV is shown, respectively. (D) Elution profile of F-CpG-sEV incubated with 10% mouse serum in PBS.

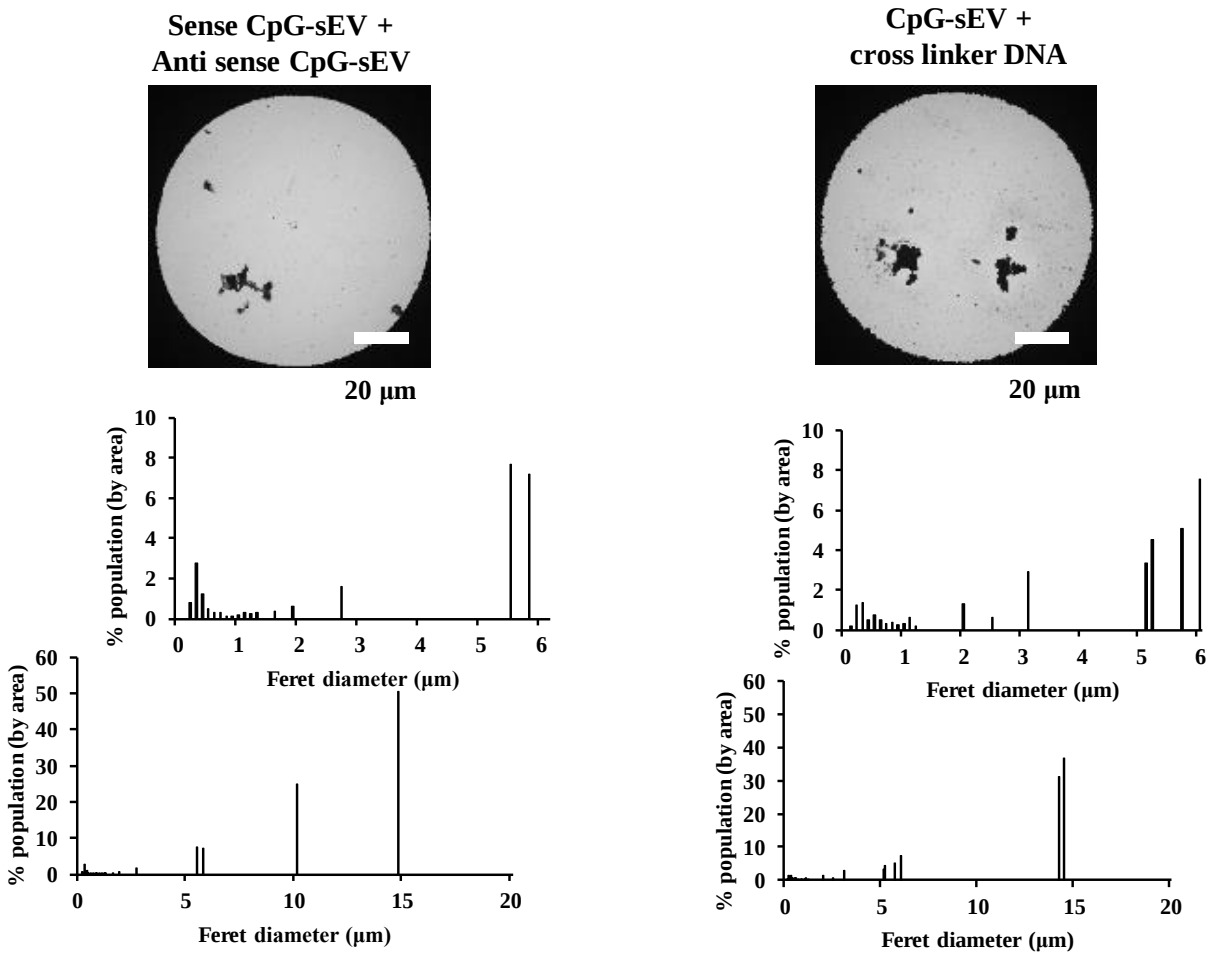

Supplementary figure 3. Comparison of CpG-sEV assembly design.

TEM images of sense CpG-sEV + anti-sense CpG-sEV, and CpG-sEV + cross linker DNA (T0 DNA). Histograms of particle size distribution obtained by analyzing the TEM images. Vertical axis of histograms shows % population by area.

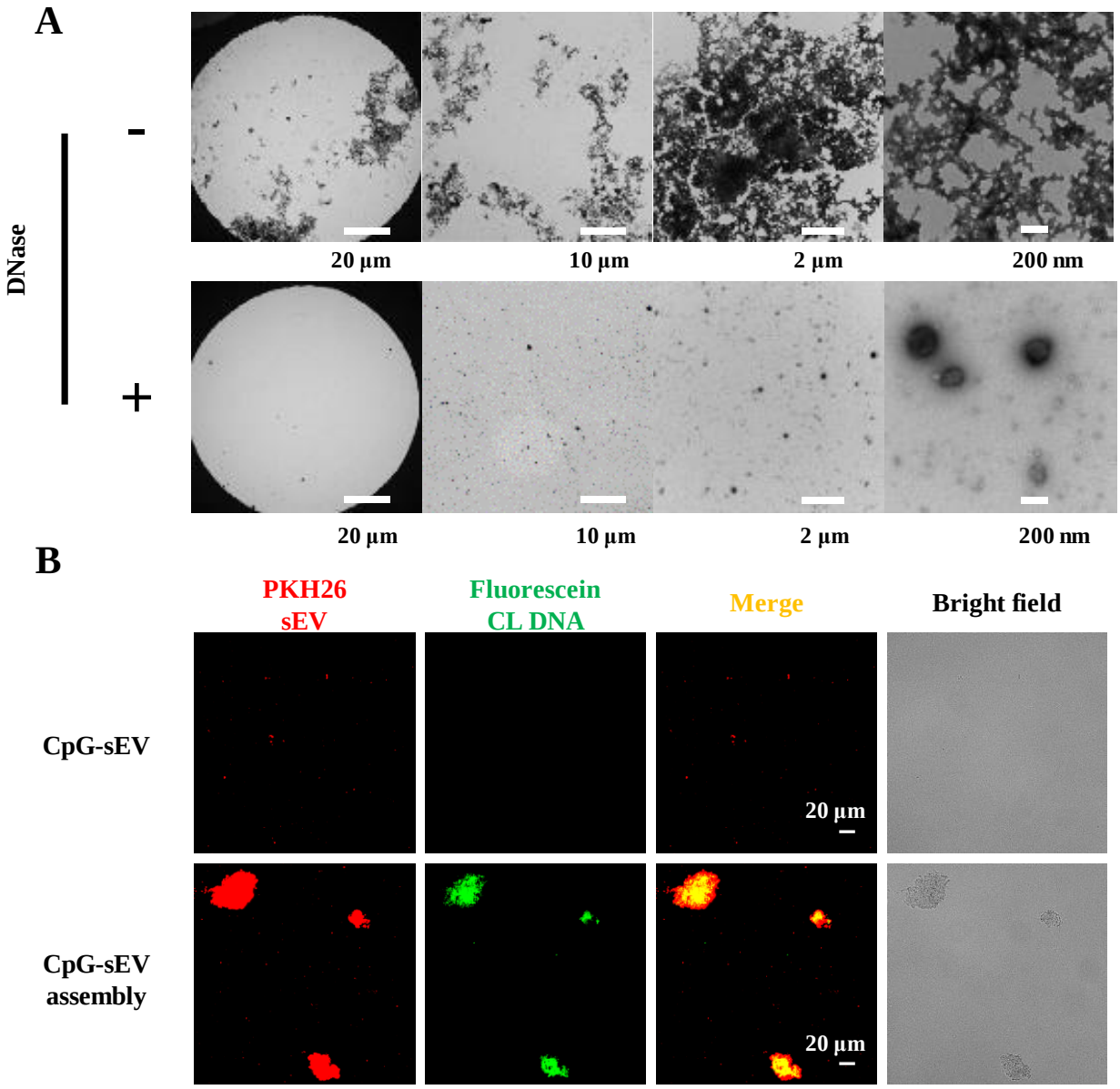

Supplementary figure 4. Confirmation of DNA CL linker-dependent formation of CpG-sEV assembly.

(A) TEM images of CpG-sEV assembly before/after DNase treatment. (B) Fluorescent microscopic observation of sEV mixed with biotinylated CpG-DNA and CpG-sEV (red = PKH26-labeled CpG-sEV, green = fluorescein-labeled CL DNA).

CHAPTER II

Development of cancer vaccine by utilizing dendritic cell-derived small extracellular vesicle with high immunostimulatory activity

II-1. Summary of chapter II

Small extracellular vesicle (sEVs) originating from dendritic cells (DCs) is expected as a novel candidate for tumor antigen-based cancer immunotherapy[71]. This is because DC-derived sEV (DC-sEV) contain several immunologically relevant components, such as antigen, MHC class I and II molecules complexed with antigen epitopes, and co-stimulatory molecules (CD80, CD86). Murine DC-sEVs have been shown to be able to stimulate antigen-specific T cell response both *in vitro* and *in vivo* and to enhance anti-cancer immunity *in vivo*[72–74]. Clinical trials to evaluate DC-sEV for cancer immunotherapy have been conducted. Although the feasibility and safety of DC-sEV was proven, DC-sEV failed to induce sufficient antitumor immunity for tumor regression[71,75]. In order to improve the DC-sEV-induced antitumor immunity, production of DC-sEV with ability to induce potent antigen-specific humoral and cellular immune responses through understanding the immune stimulatory properties of DC-sEV is pivotal. However, there is no preceding study investigating how to prepare DC-sEV with highly immune activity based on the understanding.

Recent reports have stressed the importance of boosting innate immunity for maintaining the T cell activity[76,77]. In the tumor microenvironment, macrophages, key immune cells for the natural immunity, exhibit immunosuppressive M2-type phenotype and secret immunosuppressive cytokine (such as IL-4 and TGF-β), thereby suppressing the T cell activity[78]. It has not been studied so far whether DC-sEV can boost the innate immunity.

For the adaptive immunity, DC-sEVs could induce antigen-specific T cell responses by mainly APCs -independent and -dependent mechanisms[9,79]. For APCs-independent mechanism, DC-sEVs could directly activate T cell through the sEV MHC/peptide complex binding to T cells. For APC-dependent mechanism, after DC-sEVs are taken up by the immature APCs, the loaded immunostimulatory molecules and antigens induced the immature APCs to get matured and cross present the antigen to MHC. However, research to elucidate such mechanisms has not been well conducted.

In this chapter, I demonstrate that activated-DC_{OVA}-sEV, which has high immunostimulatory activity and loaded OVA protein, can interact with macrophages, DCs, and T cells to boost both innate and adaptive immunity. The activated-DC_{OVA}-sEV strongly activated the macrophages and dendritic cells in a TLR4-dependent mechanism. I also found the APC-dependent mechanism was the primary pathway for T cell activation compared to the APC-independent mechanism. These result suggest that DC-sEV could be used as a cancer vaccine material which could elicit strong anti-tumor immunity.

CHAPTER III

Pharmacokinetic analysis of small extracellular vesicle clearance from blood after intravenous administration

Chapter III

Introduction

To develop sEV-based drug delivery systems, it is indispensable to understand the *in vivo* fate of sEVs after their administration. Previously, my laboratory developed a sEV-labeling method by designing a fusion protein named gLuc-LA to investigate the blood clearance of cultured cell-derived sEVs after i.v. administration in mice[25]. When gLuc-LA-labeled sEVs derived from 5 different cell lines including B16BL6 cells were administered to normal mice via i.v. injection, sEVs were rapidly cleared from the blood circulation with a blood half-life the in α phase ($t_{1/2\alpha}$) < 10 min and distributed mainly to the liver[80]. Moreover, it was also found that the clearance of sEVs was dramatically delayed in macrophage-depleted mice[26]. These results were consistent with other reports investigating the sEV *in vivo* fate based on different sEV producing cultured cell lines or different labeling methods[10–12]. Therefore, macrophages, especially macrophages in the liver, play pivotal roles in the clearance of intravenously injected sEVs, although there is little information regarding the mechanism through which sEVs are cleared by macrophages.

Over the last decade, it was considered by several researchers that *in vivo* behavior of endogenous sEV in the blood is quite different from that of exogenously administrated cultured-cell derived sEV. Such researchers consider that endogenous sEV in the blood should show long blood circulation based on the following two observations[69,81,82]; that 1) endogenous sEV concentration in blood is high because large amounts of sEV can be isolated from blood, and that 2) endogenous sEV in the blood needs to circulate around the blood, reach the target site, and be taken up by recipient cells to release their cargos and induce cellular responses in the body, such as metastasis, immune regulation, or metabolism. If these observations are true and endogenous sEV show long blood circulation, it is assumed that endogenous sEV in the blood could be utilized as a promising drug carrier. However, because of the technological limitations, information on the dynamics of endogenous sEV in the blood has never been evaluated.

Therefore, in chapter III, I explored the *in vivo* fate of sEV in detail. In section 1, the recognition and cellular uptake mechanism of sEV by macrophages was identified. In section 2, novel protocols for PK analysis were established to experimentally considered the dynamics of endogenous sEV in the blood.

SECTION 1.

Role of phosphatidylserine-negative surface charges in the recognition and uptake of small extracellular vesicle by macrophages

III-1-1. Introduction

To manipulate the *in vivo* fate of sEVs after administration, it is necessary to understand the mechanism by which macrophages recognize and take up sEVs. Phosphatidylserine (PS) is a negatively charged phospholipid localized at the inner leaflet of the plasma membrane[83]. It has been reported that apoptotic cells expose PS on the outer leaflet of the plasma membrane and that they are engulfed by macrophages through the recognition of the exposed PS[84,85]. As sEVs also have PS on their surface[86,87], I hypothesized that macrophages take up sEVs by PS recognition.

In this section, I investigated PS involvement in the recognition and uptake of sEVs by macrophages. A PS-binding protein, AnV, was used to mask PS on the sEV membrane. Then, three types of liposomes with different charges were used to investigate PS involvement or the surface charge in the uptake of sEVs by macrophages. To examine to what extent PS might be responsible for the removal of intravenously administered sEVs from the blood circulation, gLuc-LA-labeled sEVs were prepared as a highly sensitive probe. Subsequently, radiolabeled sEVs prepared by incubating sEVs modified with SAV-LA, a fusion protein comprising SAV and LA, with (3-^{125}I-iodobenzoyl) norbiotinamide were utilized to quantitatively analyze the effect of PS on the tissue distribution of sEVs[17].

III-1-2. Materials and Methods

Mice.

Five-week-old male Balb/c mice were purchased from Japan SLC, Inc. All protocols for the animal experiments were approved by the Animal Experimentation Committee of the Graduate School of Pharmaceutical Sciences of Kyoto University.

Cell culture.

B16BL6 murine melanoma cells were obtained from the Riken BioResource Center and cultured in DMEM supplemented with 10% heat-inactivated fetal bovine serum (FBS), 0.15% sodium bicarbonate, 100-IU/mL penicillin, 100-μg/mL streptomycin, and 2 mM L-glutamine at 37°C in humidified air containing 5% CO_2. Mouse

peritoneal macrophages were collected and cultured using a previously described method with modifications[88]. In brief, mice were stimulated via the intraperitoneal administration of 2 mL of 4.05% thioglycolate medium. Three days after administration, mice were sacrificed, and 5 mL of ice-cold PBS were injected into the peritoneal cavity. After 2 min, the peritoneal lavage fluid was collected and centrifuged at 260 × *g* for 10 min to sediment cells. Cells were seeded in 96-well culture plates at a density of 2×10^5 cells/well prior to use.

Preparation of fluorescently labeled sEVs.

sEVs were collected from culture supernatant of B16BL6 cells by ultracentrifugation following differential centrifugation as described previously[89]. The presence of sEV marker proteins Alix, HSP70, and CD81 in the sEVs was confirmed by western blot analysis. The sEV samples were negative for calnexin, an endoplasmic reticulum marker, suggesting that the sEVs samples contained little contamination from cell debris[89]. PKH26 red fluorescent cell linker kit and a PKH67 green fluorescent cell linker kit for general cell membrane labeling were obtained from Sigma Aldrich. sEVs were labeled with PKH26 or PKH67 dyes as previously described[25,26]. In brief, sEVs resuspended in buffer from the kit were mixed with PKH dyes and incubated for 5 min at room temperature. Then, the samples were added to PBS containing 5% bovine serum albumin (BSA) and subjected to ultracentrifugation at 100,000 × *g* for 1 h to remove free dye.

Preparation of liposomes.

1,2-Distearoyl-sn-glycero-3-phosphocholine (DSPC) was obtained from Tokyo Chemical Industry (Tokyo, Japan). Brain PS and 1,2-distearoyl-sn-glycero-3-phospho-(1′-rac-glycerol) (DSPG) were obtained from Avanti Polar Lipids, Inc. (Alabaster, AL, USA). Cholesterol was obtained from Nacalai Tesque. Phosphatidylcholine (PC)-rich, PS-rich, and phosphatidylglycerol (PG)-rich liposomes were prepared according to the method of Terpstra et al[84]. PC-rich, PS-rich, and PG-rich liposomes were composed of DSPC:Brain PS:DSPG:cholesterol at molar ratios of 2:0:0:1, 1:1:0:1, and 1:0:1:1, respectively. Liposomes were extruded through 0.1-μm pore size polycarbonate membranes using a mini-extruder device (Avanti Polar Lipids). The mean diameters ± standard deviations (SDs) of liposomes were as follows: PC-rich, 99 ± 1 nm; PS-rich, 101 ± 1 nm; and PG-rich, 110 ± 1 nm. The mean zeta potentials ± SDs of liposomes were as follows: PC-rich, −12.9 ± 0.9 mV; PS-rich, −51.5 ± 1.1 mV; and PG-rich, −53.9 ± 2.5 mV. Liposomes were stored under nitrogen gas at 4°C until use.

Measurement of particle size and zeta potential in sEVs and liposomes.

A qNano instrument (Izon Science Ltd.) was used to measure the particle size distribution of the sEVs and liposomes. A Zetasizer Nano ZS (Malvern Instruments) was used to determine the zeta potential of the liposomes.

Electron microscopic observation of sEVs.

The sEV suspension was added to an equal volume of 4% paraformaldehyde (Nacalai Tesque), and the mixture was applied to a Formvar/Carbon film-coated TEM grid (Alliance Biosystems). The sample was then washed with PBS. Then, the sample was fixed by incubation with 1% glutaraldehyde for 5 min, washed with PBS,

and incubated with 1% uranyl acetate for 5 min. The sample was observed under a TEM (Hitachi H-7650; Hitachi High-Technologies).

Fluorescent microscopic observation .

For this, 1 μg of PKH26-labeled sEVs were mixed with 3 ng of Alexa Fluor 488-labeled AnV (Thermo Fisher Scientific) resuspended in HEPES buffer containing 2.5 mM $CaCl_2$ and incubated at room temperature for 15 min. The samples were observed under a fluorescence microscope (BioZero BZ-X710; Keyence).

***In vitro* cellular uptake assay.**

Mouse peritoneal macrophages seeded in 96-well plate were incubated with PKH67-labeled sEVs mixed with or without the indicated concentration of AnV. Cells were then incubated at 37°C for 2 h, washed twice with PBS, and harvested. A flow cytometer (Gallios Flow Cytometer; Beckman Coulter) was used to determine the mean fluorescent intensity (MFI) of the cells. The data were analyzed using Kaluza software (version 1.0, Beckman Coulter). In a separate set of experiment, mouse peritoneal macrophages seeded in 96-well plates were incubated with PKH67-labeled sEVs either 37°C or 4°C for 2 h. Then cells were washed twice with PBS and harvested for the measurement of MFI as described above. In another separate set of experiments, mouse peritoneal macrophages seeded in 96-well plates were incubated with the indicated concentrations of liposomes in FBS-free RPMI for 30 min prior to the addition of PKH67-labeled sEVs. The concentration of liposomes added to macrophages was normalized based on the cholesterol concentrations. Cells were then incubated at 37°C for 2 h, washed twice with PBS, and harvested for the measurement of MFI as described above.

Preparation of B16-sEVs labeled with gLuc-LA or SAV-LA.

pCMV-gLuc-LA encoding gLuc-LA and pCMV-SAV-LA encoding SAV-LA were prepared as previously described[17,25]. B16BL6 cells seeded on culture dishes were transfected with plasmid DNA using polyethylenimine "Max" (Polysciences) as described previously[25,26]. Twenty-four hours after transfection, sEVs in the culture supernatant were purified as previously described[17,25,26,89]. The amount of sEVs collected was estimated by measuring protein concentrations using the Bradford assay.

Blood clearance.

Five-week-old mice were injected with 0.8 mg of liposomes into the tail vein at the indicated concentration. After 2 min, 5 μg of gLuc-LA-labeled sEVs were injected, and blood samples were collected at the indicated time points. Serum was obtained by centrifuging clotted whole blood samples at 8,000 × *g* for 20 min at 4°C. The serum was diluted with PBS and mixed with a sea pansy luciferase assay system (Picagene Dual; Toyo Ink, Tokyo, Japan). The chemiluminescence was measured with a luminometer (Lumat LB 9507; EG&G Berthhold, Bad Wildbad, Germany). gLuc activity was used to normalize the amount of sEVs in samples to the injected dose (ID), which was expressed as a percent of the injected dose/mL (% ID/mL).

Evaluation of the tissue distribution of sEVs in mice by using radiolabeled sEVs.

Radiolabeled sEVs were prepared by the previously described method[17]. In brief, SAV-LA–modified sEVs were incubated with ^{125}I-labeled biotin [(3-^{125}I-iodobenzoyl) norbiotinamide]. ^{125}I-labeled B16-sEVs (approximately 4 μg of sEV, 37 kBq/mouse) were injected into the tail vein of mice 2 min after the pre-administration of 0.8 mg of liposomes. Five minutes after the administration of sEVs, mice were anesthetized, and blood was collected from the vena cava. Then, organs were collected and washed with saline. The radioactivity of each sample was measured using a Wizard 1470 automatic gamma counter (PerkinElmer). The results were expressed as % ID/mL for blood samples or % ID/organ for other samples.

Pharmacokinetic analysis.

The time-course data were analyzed based on a two-compartmental model. The sEV concentration in the blood is described as a function of time by equation (1), and the parameters A, B, α, and β in the equation were determined using the nonlinear least-squares program MULTI to fit a curve to the blood concentration-time profile.

$$C_{(t)} = A \cdot e^{-\alpha t} + B \cdot e^{-\beta t} \quad (1)$$

The half-lives in the α phases ($t_{1/2}\alpha$) were calculated from these parameters. The area under the curve (AUC), mean residence time (MRT), and clearance (CL) were calculated for each animal by integration from 5 to 240 min.

Statistical analysis.

Differences were evaluated using the Tukey–Kramer method, and $p < 0.05$ was considered statistically significant.

III-1-3. Results

III-1-3-a. Effect of AnV on the physicochemical properties of sEVs.

After the incubation of PKH26-labeled sEVs with Alexa Fluor 488-labeled AnV, the co-localization of the red signal of sEVs with the green signal of AnV was observed (Figure 27A), suggesting that AnV bound to the sEVs. Figure 27B shows the histogram of the particle size distribution of the sEVs incubated with or without AnV. The distribution of sEVs with AnV was almost identical to that of sEVs without AnV. The particle sizes of sEVs mixed with AnV (AnV-sEV) and unmodified sEVs were 88 ± 32 and 93 ± 34 nm, respectively. In addition, transmission electron microscopic observation also revealed no apparent differences in the morphology of the sEVs between the AnV-sEV and unmodified sEVs (Figure 27C).

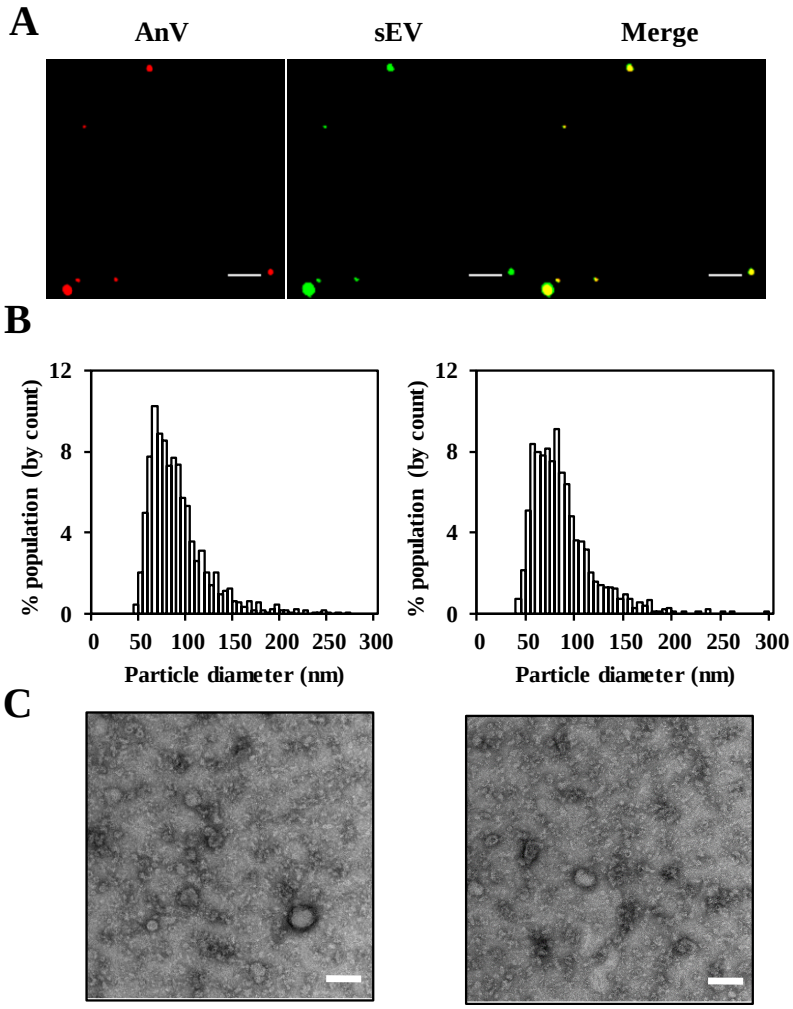

Figure 17. Binding of AnV to sEVs.

(A) Fluorescent microscopic observation of PKH26-labeled sEVs incubated with Alexa Fluor 488-labeled AnV. Scale bar = 20 μm. (B) Histogram of the particle size distribution of the sEVs determined using a qNano. Left; sEVs. Right; sEVs mixed with AnV (AnV-sEV). (C) Transmission electron microscopic images of sEVs. Left; sEVs. Right; AnV-sEV. Scale bar = 100 nm.

III-1-3-b. *In vitro* cellular uptake of AnV-sEVs by macrophages.

To evaluate PS involvement in the uptake of sEVs by macrophages *in vitro*, PKH67-labeled sEVs were firstly incubated with mouse peritoneal macrophages at either 37°C or 4°C for 2 h and cellular uptake was analyzed by measuring the MFI of the cells. The MFI of mouse peritoneal macrophages incubated at 4°C was much lower than that of mouse peritoneal macrophages incubated at 37°C (Figure 28A). Next, PKH67-labeled AnV-sEVs was incubated with mouse peritoneal macrophages in culture and cellular uptake was analyzed. The MFI of mouse peritoneal macrophages incubated with AnV-sEVs was significantly lower than that of mouse peritoneal macrophages incubated with unmodified sEVs (Figure 28B). The uptake of sEVs was reduced by addition of AnV in a dose-dependent manner and reduced to 66% of no treatment group by addition of 30 μg/mL of AnV. These results suggest that AnV suppressed the uptake of PKH67-labeled sEVs by macrophages.

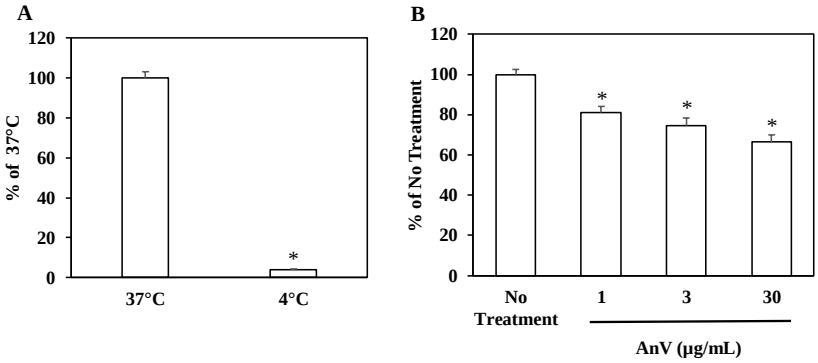

Figure 18. Effect of AnV on the cellular uptake of sEVs by macrophages.

(A) Mouse peritoneal macrophages were incubated PKH67-labeled sEVs at either 37°C or 4°C. (B) Mouse peritoneal macrophages were incubated with PKH67-labeled sEVs mixed with or without the indicated concentration of AnV. Results are expressed as the mean ± SD of four wells. *p < 0.05 compared to the (A) 37°C or (B) No Treatment.

III-1-3-c. Inhibition of cellular uptake of sEVs by negatively charged liposomes.

Next, the influence of negative surface charges of sEVs on their recognition by mouse peritoneal macrophages was evaluated using liposomes with different lipid contents (Figure 29). Pre-treatment with PS-rich liposomes reduced the MFI of macrophages incubated with PKH67-labeled sEVs in a concentration-dependent manner. When 660 μg/mL PS-rich liposomes were added, the MFI of macrophages decreased to 33% of that of non-treated macrophages. Macrophages pre-treated with PG-rich liposomes revealed the same tendency as macrophages pre-treated with PS-rich liposomes. On the contrary, PC-rich liposomes hardly affected the uptake of sEVs by

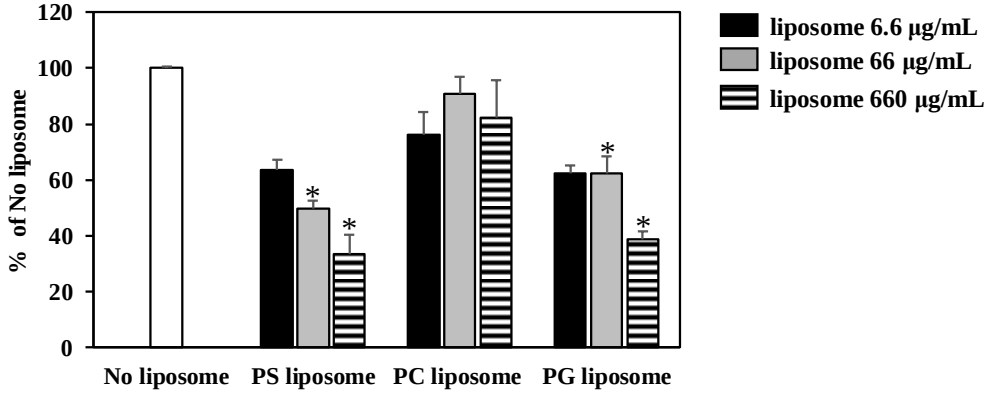

Figure 19. Effect of liposomal surface charges on the uptake of sEVs by macrophages.

Mouse peritoneal macrophages were incubated with PKH67-labeled sEVs 30 min after liposome addition. Results are expressed as mean ± SD. (n=4) *p < 0.05 compared to the PBS and PC-liposome group at the same concentrations.

macrophages.

III-1-3-d. Delayed blood clearance of B16-sEVs by pre-injection of negatively charged liposomes.

To evaluate the effect of PS on the time-course of the serum concentration of intravenously administered sEVs, mice underwent i.v. administration of gLuc-LA-labeled B16-sEVs 2 min after the pre-administration of liposomes. As shown in Figure 30, the serum gLuc activity was significantly higher in mice pre-treated with PS-rich or PG-rich liposomes than that in mice pre-treated with PBS or PC-rich liposomes in every time points. Figure 31 summarizes the PK parameters. The AUCs in the PS-rich liposome–treated and PG-rich liposome-treated mice were approximately 10- and 8-fold higher than that in the PBS-treated mice, respectively. The CLs in the PS-rich liposome-treated and PG-rich liposome-treated mice were approximately 11% and 13% of that in the PBS-treated mice, respectively. On the contrary, there were no apparent differences in $t_{1/2\alpha}$ and MRT among mice pre-treated with ant types of liposomes. These results suggest that pre-injection of negatively charged liposomes delayed blood clearance of B16-sEVs.

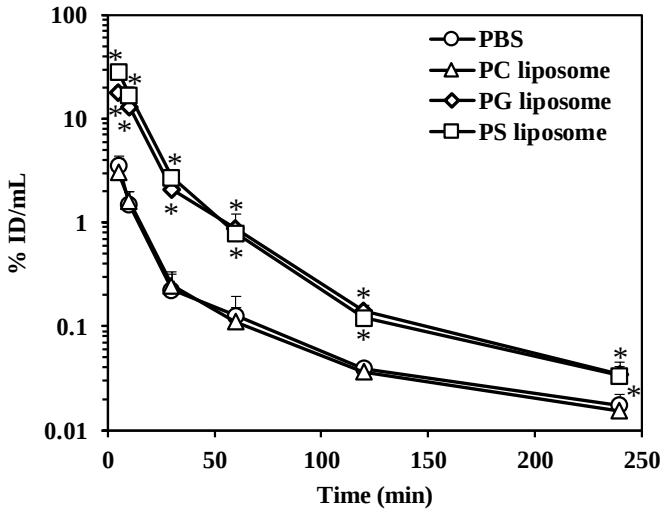

Figure 20. Blood clearance of sEVs after i.v. administration.

gLuc activity in the serum of mice pre-treated with PBS (circle), PC-rich liposomes (triangle), PG-rich liposomes (diamond), or PS-rich liposomes (square) was sequentially measured after the i.v. injection of gLuc-LA-labeled sEVs. Results are expressed as the mean of the percentage of injected dose/mL (% ID/mL) ± SD of four mice. *$p < 0.05$ compared to the PBS and PC-rich liposome-treated groups.

III-1-3-e. Decreased liver accumulation of radiolabeled B16-sEVs by pre-injection of PS-rich liposomes.

Figure 32 shows the tissue distribution of ^{125}I-labeled B16-sEVs in mice pre-treated with PBS or liposomes. In all three groups, radioactivity extensively accumulated in the liver. Approximately 40% of the radioactivity was accumulated in the liver of mice pre-treated with PBS or PC-rich liposomes. Radioactivity in the livers of mice pre-treated with PS-rich liposome was significantly lower (approximately 26%) than that in the livers of mice pre-treated with PBS or PC-rich liposomes, suggesting that the liver accumulation of sEVs was suppressed by PS-rich liposomes. In addition to the liver, a significant difference in radioactivity was observed in the blood between the PS-rich liposome-treated group and the other two groups. Radioactivity in the blood was 3.26, 3.60, and 10.5% ID/mL in PBS-treated, PC-rich liposome-treated, and PS-rich liposome-treated mice, respectively. Pre-administration of liposomes hardly changed the radioactivity of other organs.

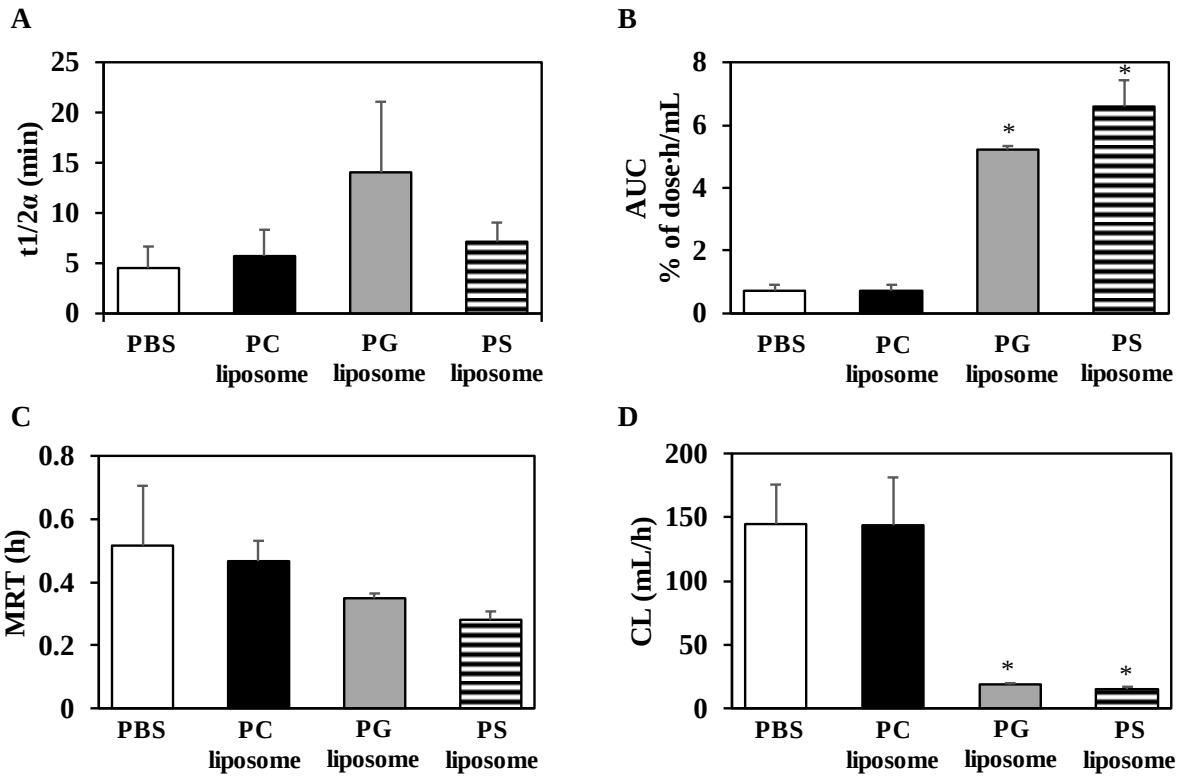

Figure 21. Effect of liposome treatment on the PK parameters of sEVs.

(A) Half-lives in the initial phase ($t_{1/2\alpha}$) (min). (B) AUC from 5 to 240 min (% of dose·h/mL). (C) MRT (h). (D) Clearance (mL/h). Results are expressed as the mean ± SD of four mice.*$p < 0.05$ compared to the PBS and PC-rich liposome-treated groups.

III-1-4. Discussion

In this study, PS involvement in the uptake of sEVs by macrophages was investigated. As it is assumed that macrophages accumulate sEVs by recognizing molecules on the surface of sEVs, it is highly likely that membrane proteins or lipids are involved in the uptake of sEVs by macrophages. Although the effect of the membrane proteins of sEVs on their uptake by macrophages was reported[90], the involvement of lipids in their uptake by macrophages has yet to be studied. Regarding to the lipid content in sEVs, lipidomics revealed that sEVs contained sphingomyelins, PC, phosphatidylethanolamines, and PS[86]. In addition, it was reported that PS of sEVs derived from PC-3 cells comprised approximately 31.1% of the total phospholipid content, making it the second most common phospholipid existing in PC-3-derived sEVs[87].

AnV is an intracellular protein widely used to detect apoptotic cells in combination with propidium iodide[91]. AnV is also used to inhibit the uptake of apoptotic cells by macrophages by masking PS[92,93]. In the present study, binding of AnV to B16-sEVs was confirmed, which suggests the existence of PS on the surface of B16-sEVs (Figure 27). On the other hand, the great reduction in the uptake of PKH67-labeled sEVs by macrophages incubated at 4°C suggests that sEVs were taken up by macrophages mainly in an energy-dependent pathway (Figure 28A). Moreover, the significant reduction in the uptake of PKH67-labeled sEVs by macrophages following incubation with AnV suggests that PS on the surface of sEVs was involved in the *in vitro* cellular uptake of sEVs by macrophages (Figure 28B).

Macrophages specifically recognize PS or non-specifically recognize the negative charge of PS. Such

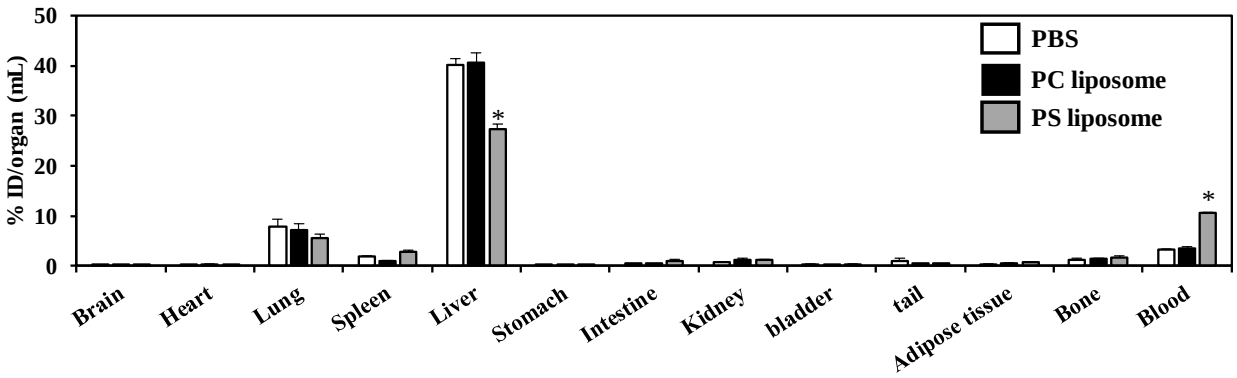

Figure 22. *In vivo* distribution of ^{125}I-labeled sEVs after i.v. injection into mice pre-treated with liposomes.

Results are expressed as the mean ± SEM in four mice. *p < 0.05 compared to the mice treated with PBS and PC-rich liposome-treated groups.

recognition mechanisms are widely studied in various kinds of macrophages, including peritoneal macrophages[94]. Concerning the specific recognition of PS, several receptors expressed on macrophages such as immune receptor expressed on myeloid cells 1, CD300f, T-cell immunoglobulin and mucin domain 4, brain-specific angiogenesis inhibitor 1, and stabilins directly bind to PS[85,95–97]. In addition, other receptors specifically recognize PS via soluble PS-binding bridging molecules, such as growth arrest-specific 6[98]. It is assumed that these receptors or PS-binding bridging molecules interact with the hydrophilic head of PS[99]. On the contrary, the negative charge of PS is also recognized by macrophages. Class B scavenger receptor 1 and CD36 tightly bind to negatively charged substances, such as phosphatidylinositol, oxidized low-density lipoprotein, and PS[100]. As the *in vitro* cellular uptake of PKH67-labeled sEVs by macrophages was inhibited in both the PS rich liposome-treated and PG-rich liposome-treated groups, it is assumed that the negative charge on the sEVs contributed to their recognition by macrophages (Figure 29). In addition, the negatively charged phospholipids of sEVs largely comprised PS[87]. Taken together, the negative charge of PS played a role in the uptake of sEVs by the peritoneal macrophages in culture. However, the inhibition of the uptake of PKH67-labeled sEVs by AnV was weak (Figure 28B). This may, in part, due to the low concentration of AnV. Bennett et al. inhibited the uptake of apoptotic cells by macrophages to about 50% at 100 μg/mL of AnV, while I inhibited the uptake of sEVs at 30 μg/mL of AnV[92].

Kupffer cells play pivotal roles in the accumulation of intravenously administered B16-sEVs in the liver[26]. Using liposomes and radiolabeled sEVs, it was found that the distribution of intravenously administered B16-sEVs to the liver was inhibited by the pre-administration of PS-rich liposomes (Figure 30-32), indicating that Kupffer cells in the liver recognize PS on sEVs, facilitating their uptake[26]. The spleen is another organ rich in macrophages. However, the distribution of sEVs to the spleen was not reduced by the pre-administration of PS-rich liposomes. Macrophages in the spleen consist of red pulp macrophages, marginal metallophilic macrophages, and marginal zone macrophages[101]. Marginal metallophilic macrophages and marginal zone macrophages were reported to engulf sEVs from B cells through the recognition of sialic acids[102]. Considering that each type of macrophages exhibits different phenotypes, the uptake of sEVs by splenic macrophages may be mediated by PS-independent pathways such as the recognition of sialic acids. Further research is needed to elucidate the mechanism by which sEVs are accumulated in the spleen.

The distribution of sEVs to the lungs was hardly changed by pre-treatment with liposomes, suggesting that

the accumulation of intravenously administered sEVs in the lungs was not dependent on PS. Vascular endothelial cells were responsible for the lung accumulation of intravenously injected B16-sEVs[26]. These findings imply that the uptake of B16-sEVs by endothelial cells in the lungs is not dependent on PS. When sEVs from human breast cancer cells distributed to the lungs, integrin on the surface of sEVs mediated the uptake by endothelial cells[21]. Therefore, the distribution of B16-sEVs to the lungs could be explained by molecules other than PS, such as surface protein[103].

III-1-5. Summary of section 1 of chapter III

In this chapter, it was demonstrated the involvement of negative charges derived from PS in the uptake of sEVs by macrophages. The present findings provide information useful for elucidating the physiological functions of sEVs and developing sEVs-based drug delivery systems.

SECTION 2.
Quantitative pharmacokinetic analysis of the mass balance of secretion and clearance of endogenous small extracellular vesicle in the blood

III-2-1. Introduction

Considering that sEVs in the blood circulate around the body to reach recipient cells, understanding the dynamics of blood sEV concentration is indispensable. As a reasonable hypothesis to explain the dynamics of blood sEV, I propose the "balance hypothesis" herein, in which sEVs are constantly secreted into and cleared from the blood, and that the balance between these two processes determines their concentration. However, due to technical hurdles in measuring sEV clearance and secretion rate in the blood, this hypothesis has never been evaluated.

To estimate the clearance rate of blood sEVs, I considered two technological hurdles must be overcome, specifically the isolation of intact blood sEVs and sEV-specific labeling with high sensitivity. The "default standard strategy" for analyzing the blood clearance of cultured cell-derived sEVs starts with sEV isolation followed by sEVs labeling with a lipophilic fluorescent dye (*e.g.* carbocyanine dyes such as DiO and DiI)[10]. For the isolation step, physiochemically intact sEVs are desirable because this property is a critical determinant of nanoparticle clearance from blood circulation[104]. However, due to the concurrent presence of lipoprotein particles and plasma proteins, isolation of physiochemically-intact sEVs from blood is very challenging[105]. Moreover, nonspecific labeling of co-isolated lipoprotein particles in addition to blood sEVs by lipophilic fluorescent dye also hinders the use of the "default standard strategy"[106].

sEVs are secreted by diverse cells from different organs into blood with theoretically different secretion rate[69,81,82,107]. Thus, it is very difficult to directly analyze sEVs secretion into blood. Recently, the secretion rate of cell culture-derived sEVs has been proposed using a stable CD63-pHluorin-expressing cell line[108]. However, such methodology cannot be applied to evaluate the sEV secretion rate in blood. In this study, I proposed novel kinetic approaches to estimate the secretion/clearance rate of mouse plasma-derived sEVs (MP-sEVs) and validated the "balance hypothesis".

To overcome the two hurdles to estimating MP-sEVs clearance rate, an isolation method based on size exclusion chromatography (SEC) was selected to obtain physiochemically-intact sEVs and chimeric gLuc (*Gaussia* luciferase, a reporter protein) proteins were used to specifically label MP-sEVs[25,26,51,80]. After estimating the clearance rate, PK analysis was applied to indirectly calculate the total secretion rate of sEVs into blood assuming that they are produced and secreted at zero-order kinetics. I finally validated the hypothesis using a macrophage-depleted mouse model in which sEVs clearance is markedly disrupted[26].

III-2-2. Materials and Methods

sEV isolation from mouse plasma.

Na/EDTA-treated mouse plasma from Balb/c mice (Lot: 22071, 24734) was obtained from Innovative Research (MI, USA). Plasma specimens were subjected to sequential centrifugation (2,000 × *g* for 10 min and 10,000 × *g* for 30 min). Clarified plasma was passed through a 0.22-μm filter to remove large microvesicles and large lipoproteins and used for subsequent sEV isolation[69]. SEC-based isolation was conducted in reference to the previous paper with minor modifications[109]. In brief, sepharose 2B (Sigma Aldrich) was packed into 1.5 cm × 12 cm mini-columns (Bio-Rad; Econo-Pac columns) to make a 10-mL column bed. The column was blocked with 2% bovine serum albumin (BSA) solution and washed with phosphate saline buffer (PBS). Then, the filtered plasma sample (1 mL) was loaded onto the column and the eluate was collected (fraction 0). Subsequently, 1 mL of PBS was repeatedly subjected to collect the following fractions, which were sequentially numbered. For ultracentrifugation (UC)-based isolation, filtered plasma was spun at 100,000 × *g* for 1 h (Himac CP80WX ultracentrifuge, Hitachi Koki; P50AT2 angle rotor, Hitachi Koki) to obtain pellets. The pellets were then washed with PBS and recovered in PBS as the sEV-enriched fraction. For polyethylene glycol (PEG)-based isolation, filtered plasma was mixed with an equal volume of 16% PEG6,000 (Wako FUJIFILM). The mixture was then incubated overnight at 4°C with gentle agitation. Then, the mixture was centrifuged at 4,000 × *g* for 1 h to obtain pellets. The pellets were resuspended in PBS and spun at 100,000 × *g* for 1 h. The fraction was then recovered in PBS as the sEV-enriched fraction. The number of isolated sEVs was measured based on protein content based on the Bradford assay.

Plasmid DNA (pDNA) encoding gLuc, gLuc-lactadherin (gLuc-LA), gLuc-perfringolysin-O (gLuc-PFG), and gLuc-lysenin (gLuc-Lys).

pDNA encoding gLuc and gLuc-LA was obtained as previously described[25,26,51]. The coding sequence of perfringolysin-O (PFG; high affinity to cholesterol) and lysenin (Lys; high affinity to sphingomyelin) was synthesized by FASMAC (Atsugi, Japan). The chimeric sequences of gLuc-PFG and gLuc-Lys were prepared by a 2-step PCR method as described previously[25]. The sequences encoding fusion proteins were subcloned into the BamH1/Xba1 site of the pcDNA3.1 vector (Thermo Fisher Scientific) to construct pCMV vectors encoding corresponding fusion proteins.

sEV isolation from B16BL6 cells.

B16BL6 murine melanoma cells were obtained and cultured as described previously[25,26,50,51]. B16BL6 cells were transfected with pDNA using polyethylenimine (PEI) “Max” (Polysciences) in accordance with a previous report[25]. After transfection, the medium was replaced with Opti-MEM (Thermo Fisher Scientific) and cultured for 24 h. The conditioned medium was collected and subjected to sequential centrifugation (300 × *g* for 10 min, 2,000 × *g* for 20 min, and 10,000 × *g* for 30 min) to remove cell debris and large vesicles. In addition, the medium was filtered with a 0.22-μm filter. The clarified medium was spun at 100,000 × *g* for 1 h (Himac CP80WX

ultracentrifuge). The supernatant was then collected for subsequent experiments. The pellet was resuspended in PBS and spun again at 100,000 × *g* for 1 h. The sEVs were recovered in PBS.

Preparation of chimeric gLuc protein-enriched sample.

The recovered supernatant during sEV isolation from B16BL6 cells, described previously herein, was passed through an Amicon Ultra 100K (Merck Millipore) to remove the remaining vesicles or protein aggregates. The flow-through medium was the concentrated by ultrafiltration (Amicon Ultra 10K for gLuc protein and Amicon Ultra 30 K for gLuc-LA, gLuc-PFG, and gLuc-Lys, respectively).

Chimeric gLuc-protein labeling of B16BL6/mouse plasma-sEVs.

Clarified mouse plasma or concentrated B16BL6 condition medium was mixed with gLuc, gLuc-LA, gLuc-PFG, or gLuc-Lys. After the mixture was incubated under the indicated condition (incubation time and incubation temperature), samples were applied to SEC for the purification of labeled sEVs from unbound proteins. Labeled sEVs were mixed with a sea pansy luciferase assay reagent (Picagene Dual; Toyo Ink, Tokyo, Japan). The chemiluminescence was then measured with a luminometer (Lumat LB 9507; EG&G Berthold). Labeling efficiency (RLU/s/μg) was calculated as luciferase activity (RLU/s/mL) divided by protein concentration (μg/mL).

Labeling stability of chimeric gLuc proteins to MP-sEV in mouse serum.

sEVs labeled with chimeric gLuc proteins were incubated in 10% mouse serum in PBS solution at 37°C with gentle agitation. Samples were collected at the indicated time points. The stability of gLuc enzyme activity was evaluated by measuring gLuc enzyme activity in the collected samples. Samples were applied to SEC and the eluate was collected in 14 sequential fractions of 1 mL. gLuc enzyme activity in each fraction was measured to evaluate the release of gLuc proteins from sEVs.

Characterization of MP-sEVs.

Electron microscopy-based morphologies, vesicle sizes, and surface charges of the sEV samples were evaluated as described previously[25,26]. The morphology of sEV and LDL/VLDL was distinguished by referring to the reported morphology and size of MP-sEV[109–111]. To analyze size distribution of the sEV samples, TEM images were analyzed using ImageJ software (Rasband, W.S., U.S. National Institutes of Health, Bethesda, Maryland, USA). qNano instrument (Izon Science Ltd.) was also used for size distribution measurement. NP150 nanopore was used according to the manufacturer's instructions. All sEV samples and calibration particles (Izon Science Ltd.) were measured at 47.0 mm stretch with a voltage of 0.5-0.8 V. Collected data were processed by Izon Control Suite software version 3.3. For immunoelectron microscopy, gLuc-LA-labeled MP-EVs were fixed with 4% paraformaldehyde in PBS. Then, the sample was applied to a carbon formvar film-coated TEM grid (Alliance Biosystems) and incubated for 20 min. The grid was washed with 50 mM glycine in PBS and blocked with 5% BSA in PBS. The grid was stained with rabbit anti-gLuc Ab (1: 500 dilution, Cat No; E89023S, Lot; 0041211, New England Biolabs Inc., Madison, WI, USA) for 30 min. After washing with 0.5% BSA in PBS, the sample was

incubated with a 10-nm protein A-gold conjugate (BB Solution, Cardiff, UK) for 20 min, followed by immerse fixation by 1% glutaraldehyde in PBS. Following washing with distilled water, the grid was stained with uranyl acetate and observed by TEM. For sodium dodecyl sulfate-polyacrylamide gel electrophoresis (SDS-PAGE) of sEVs samples was performed as described previously[103]. For gLuc zymography, each sample was electrophoresed under nonreducing conditions on SDS polyacrylamide gels. The chemiluminescence was observed by LAS3000 instrument (FUJIFILM). For protein staining, the gel was stained with Lumitein™ Protein Gel reagent (Biotium, Inc., Landing Parkway Fremon, CA, USA) according to the manufacturer's protocol. The stained gel was observed using the LAS-3000 instrument (FUJIFILM). Western blotting analysis of sEV markers (CD63, Alix, HSP70) was conducted as described previously[26,51,103]. The following Abs were used; rabbit anti-mouse CD63 Ab (1:200 dilution, Cat No; sc-15363, Lot; B0311, Santa Cruz Biotechnology), mouse anti-mouse Alix Ab (1:20,000 dilution, Cat No; 611620, Lot; 35610, BD Biosciences), rabbit anti-mouse HSP70 Ab (1:1,000 dilution, Cat No; 4872S, Lot; 10/2017, Cell Signaling Technology), and mouse anti-rabbit IgG-HRP (1:2,000 dilution, Cat No; sc-2357, Lot; A0316, Santa Cruz Biotechnology), rabbit anti-mouse IgG-HRP (1:2,000 dilution, Cat No; 61-0120, Lot; 364278A, Thermo Fisher Scientific). For detection of surface markers of gLuc-LA-labeled-MP-sEVs (AnV, CD63, Lamp2), protein A/G magnetic beads (2.5 μL, Cat No; 88802, Lot; TJ273976, Thermo Fisher Scientific) was incubated with gLuc Ab at 1:25 dilution for 1 h at room temperature with gentle agitation. After the beads were washed with PBS, the beads were resuspended in 50 μL of PBS with 2 μg of sEV sample for 1 h incubation. The sEVs captured on beads were magnetically separated, washed with PBS and resuspended in 500 μL of PBS. For detection of surface molecules of the sEV, 50 μL aliquots of sEVs captured on beads were incubated with the indicated fluorescent labeled protein or Ab for 1 h with gentle agitation. The used fluorescent labeled protein or Ab are as follow; FITC-labeled AnV (1:25 dilution, Cat No; 640905, Lot; B284572, Biolegend), Alexa fluor 488-labeled Lamp2 Ab (1:25 dilution, Cat No; 53-1072-80, Lot; 1944990, Thermo Fisher Scientific), PE-labeled CD63 Ab (1:25 dilution, Cat No; 143903, Lot; B288704, Biolegend). After the sEVs on beads were washed with PBS, the fluorescence was detected by Gallios™ flow cytometry (Beckman Coulter). Data were analyzed using Kaluza software (version 1.0, Beckman Coulter).

Liposome preparation (PS, PG, and clodronate liposomes).

Phosphatidylserine (PS)-rich liposomes and phosphatidylglycerol (PG)-rich liposomes were prepared by a thin film hydration method as described in section 1 of chapter III. Liposomes containing disodium clodronate tetrahydrate (clodronate; Tokyo chemical industry Co., LTD, Tokyo, Japan) were prepared according to the previous report[26]. In brief, 43 mg of L-a-phosphatidylcholine (Sigma Aldrich) and 4 mg of cholesterol (Nacalai Tesque) were dissolved in chloroform and dried under reduced pressure. The lipid membranes were hydrated in 5 mL of PBS containing 0.7 M clodronate and sonicated with a tip-type sonicator (US-300; Nihonseiki Kaisha Ltd, Tokyo, Japan). Clodronate that was not encapsulated in liposomes was removed by ultracentrifugation, and the liposome pellet was resuspended in 2 mL of PBS. Liposomes were stored at 4°C until use.

Immunoprecipitation.

Coating an anti-ApoB Ab (Cat No; NB200527, Lot; 2007015, Novus Biologicals, Littleton, CO, USA) with magnetic beads was performed by mixing 10 μL of magnetic beads (pierce™ ProteinA/G magnetic beads; Thermo Fisher Scientific) with the 10 μL anti-ApoB Ab, which was then gently agitated on a shaker at room temperature for 1 h. Anti-ApoB Ab-coated magnetic beads were washed twice with PBS using a magnet and resuspended in sEV samples (4 μg in 50 μL), which were then gently agitated on a shaker at room temperature for 1 h. Next, the beads were collected using a magnet and the supernatant (non-captured fraction) was harvested. The magnet beads were washed twice with PBS and resuspended in PBS (captured fraction). The captured fraction and non-captured fraction were used for downstream assays.

Concentration of gLuc-LA-labeled-MP-sEVs ($^{gLuc\text{-}LA}$MP-sEVs) from the SEC eluate.

Protein A/G magnetic beads (50 μL; Thermo Fisher Scientific) was incubated with gLuc Ab at a 1:25 dilution for 1 h at room temperature with gentle agitation. After the beads were washed with PBS, the beads were resuspended in 150 μL of PBS with 80 μg of $^{gLuc\text{-}LA}$MP-sEV sample for 1 h incubation. The sEVs captured on beads were magnetically separated and washed with PBS. The sEV-beads complexes were treated with 100 mM glycine buffer (pH 2.0) for 10 min with gentle agitation. Then the tubes were placed on a magnet and supernatants were carefully collected. Immediately after the supernatant collection, 250 mM NaOH was added for neutralization.

PKH26 labeling of $^{gLuc\text{-}LA}$MP-sEV.

For labeling of the indicated $^{gLuc\text{-}LA}$MP-sEVs loaded onto gLuc Ab-conjugated magnetic beads, PKH26 dye (Sigma Aldrich) in a diluent C buffer (Sigma Aldrich) was added to the sEV-bead complexes and incubated for 5 min at room temperature. The sEVs on beads were washed with 5% BSA in PBS followed by PBS washing 3 times to remove the free dye. Then, $^{gLuc\text{-}LA}$MP-sEV labeled with both PKH26 was eluted from the beads as described above.

Estimation of sEV clearance from blood.

All protocols for animal experiments were approved by the Animal Experimentation Committee of the Graduate School of Pharmaceutical Sciences of Kyoto University. Macrophage-depleted mice were prepared by i.v. injection of clodronate-encapsulated liposome and confirmed by methods described previously[26]. Apparent worsening health status of mice was not observed after the treatment. The clearance of $^{gLuc\text{-}LA}$MP-sEVs from blood, after their i.v. administration into the tail vein of mice (the indicated MP-sEV amount in 200 μL/dose), was measured based on a luciferase activity as described previously[26,51]. In brief, blood samples were collected at the indicated time points. Blood was centrifuged at 8,000 × *g* for 20 min to obtain serum. The gLuc enzyme activity of serum was measured as described above. The obtained data were analyzed by two-compartment PK model. Compartment PK analysis is an established mathematical analysis widely used to kinetically simulate the *in vivo* behavior of drug after administration[112]. In two-compartment i.v. model, intravenously administered drug circulate around the body under several assumptions as follows; 1. The body is divided into central (blood circulation) and peripheral compartment, 2. Intravenously administered drug enters and instantaneously distributes to the central

compartment, 3. Drug concentrations in the compartments equal to the amounts divided by volumes (*i.e.*, concentration in the plasma $C_c = \frac{X_c}{V_c}$; C_c: concentration in the central compartment, X_c: drug amount in the central compartment, V_c: volume of distribution of central compartment), 4. drug in the central compartment transfer to the peripheral compartment and vice versa with a first-order fractional constant k_{12}: first-order rate constants for distribution from central compartment to peripheral compartment, and k_{21}: first-order rate constants for distribution from peripheral compartment to central compartment. 5. Drug only in central compartment is eliminated with a rate constant k_{el}, first-order elimination rate constants from the body. Mass balance in central and peripheral compartment can be described as follows:

$$\frac{dX_c}{dt} = k_{21} \cdot X_p - k_{12} \cdot X_c - k_{el} \cdot X_c \quad (1)$$

$$\frac{dX_p}{dt} = k_{12} \cdot X_c - k_{21} \cdot X_p \quad (2)$$

X_p is drug amount in the peripheral compartment. The parameter X_c can be depicted by integrating the differential equation described above as follows:

$$X_c(t) = \frac{X_0 \cdot (\alpha - k_{21})}{(\alpha - \beta)} \exp(-\alpha t) + \frac{X_0 \cdot (k_{21} - \beta)}{(\alpha - \beta)} \exp(-\beta t) \quad (3)$$

where parameter α and β are defined as follows:

$$\alpha + \beta = k_{12} + k_{21} + k_{el} \quad (4)$$

$$\alpha\beta = k_{21} \cdot k_{el} \quad (5)$$

Drug concentration $C_c(t)$ at time (t) can be defined as dividing $X_c(t)$ by volume of distribution of the central compartment V_c.

$$C_c(t) = A \cdot \exp(-\alpha t) + B \cdot \exp(-\beta t) \quad (6)$$

where parameter A and B are defined as follows:

$$A = \frac{X_0 \cdot (\alpha - k_{21})}{V_c \cdot (\alpha - \beta)} \quad (7)$$

$$B = \frac{X_0 \cdot (k_{21} - \beta)}{V_c \cdot (\alpha - \beta)} \quad (8)$$

In the current study, C_c was defined as plasma sEV concentration (C_{sEV}) and the parameters A, B, α, and β were determined using the nonlinear least-squares program MULTI[113] to fit a calculated curve to the obtained blood concentration–time profile from 5 to 240 min.

Estimation of sEV secretion into blood.

To estimate the sEV secretion rate, a two-compartment PK model with i.v. infusion analysis was applied. Under this model, drug is constantly entering the central compartment at zero-order kinetics. Mass balance can be described as follows:

$$\frac{dX_c}{dt} = k_0 + k_{21} \cdot Xp - k_{12} \cdot Xc - k_{el} \cdot Xc \quad (10)$$

$$\frac{dX_p}{dt} = k_{12} \cdot Xc - k_{21} \cdot Xp \quad (11)$$

where parameter k_0 is defined as first-order rate constants for infusion. At a steady state, the rate of changes in parameters Xc and Xp are zero, hence

$$k_0 = k_{el} \cdot X_c = k_{el} \cdot V_c \cdot C_c \quad (12)$$

C_c was defined as plasma sEV concentration (C_{sEV}) in this study. Hence, C_{sEV} is defined as follows:

$$C_{sEV} = \frac{k_0}{k_{el} \cdot V_c} \quad (13)$$

Biodistribution of gLuc-LA-labeled MP-sEV after i.v. administration.

For the cellular uptake of $^{gLuc\text{-}LA}$MP-sEV in the accumulated organs, mice received an i.v. injection of sEVs labeled with PKH26. Four hours after the injection, mice were sacrificed for liver collection. The harvested organs were frozen at -80°C, and the frozen sections were cut with a freezing microtome (Leica CM3050 S; Leica Biosystems, Germany). The sections were air dried and fixed with 4% paraformaldehyde in PBS. After washing with PBS, sections were stained with Alexa fluor 488-labeled anti-mouse F4/80 Ab (1:50 dilution, Biolegend) for 1 h at 37°C. The specimens were washed 3 times with PBS and observed under a fluorescence microscope (Biozero BZ-8000; Keyence).

Quantitation and characterization of steady state MP-sEVs.

SEC was used to isolate the MP-sEV-enriched fraction from plasma. To remove LDL contaminants, fractions 4 and 5 of the SEC eluate were subsequently subjected to Optiprep™ (Axis-Shield Poc, Oslo, Norway)-density ultracentrifugation. Briefly, 13, 17, 20, 25, and 60% Optiprep solutions (13%; 1.060 g/mL (1 mL), 17%; 1.072 g/mL (2 mL), 20%; 1.081 g/mL (2 mL), 25%; 1.096 g/mL (2 mL), and 60%; 1.201 g/mL (2 mL), respectively) were sequentially layered in an ultracentrifugation tube to form the gradient. Then, samples (2 mL) were layered onto the top or bottom and ultracentrifugation was performed at 180,000 × *g* for more than 24 h. Samples were collected in 11 sequential fractions of 1 mL from top to bottom. Fractions corresponding to sEV density were collected for further protein quantitation and proteome analysis.

Affinity capture of MP-sEV using Tim4-conjugated beads.

After Tim4-conjugated beads (30 μL, Cat No; 291-79721, Lot, CAL1998, Wako FUJIFILM) were washed with the wash buffer according to manufacturer's instruction, the beads were incubated with 2 μg of sEV sample in

50 μL PBS for 1 h incubation with gentle agitation. The tubes were placed on a magnet and supernatants were carefully collected. After the beads were washed with PBS, the beads were assayed by flow cytometry or the sEVs on the beads were eluted by the elution buffer (20 mM Tris-HCl, pH 7.4, 150 mM NaCl, 2 mM EDTA) and used for the downstream assay.

sEV proteome analysis.

Isolated sEV-related proteins were reduced with 10 mM dithiothreitol (Wako FUJIFILM) for 30 min, alkylated with 50 mM iodoacetamide (Sigma Aldrich) for 30 min, and digested with Lys-C (Wako FUJIFILM, 1:50 enzyme-to-protein ratio) for 3 h followed by trypsin (Promega, 1:50 enzyme-to-protein ratio) overnight in 50 mM ammonium bicarbonate (Wako FUJIFILM). Digestion was stopped by the addition of trifluoroacetic acid to a final concentration of 0.5%. The peptide mixture solution was desalted with reversed-phase StageTips[114] and 250 ng of peptides were injected onto a nanoLC/MS/MS system consisting of an Ultimate 3000 RSLCnano nanoLC pump and Q-Exactive tandem mass spectrometer (Thermo Fisher Scientific). Peptides were separated by a self-pulled analytical column (150 mm length × 100 μm i.d.) packed with ReproSil-Pur C18-AQ materials (3 μm, Dr. Maisch GmbH, Ammerbuch-Entringen, Germany), using a 65-min gradient of 5–40% B (solvent A was 0.5% acetic acid and solvent B was 0.5% acetic acid in 80% acetonitrile) at a flow rate of 500 nL/min. The applied ESI voltage was 2.4 kV and the MS scan range were m/z 350–1500 at a resolution of 70.000 (at m/z 200) in the orbitrap using an AGC target value of 3×10^6 charges. The top 10 precursor ions were selected for subsequent MS/MS scans in the HCD (higher-energy collision) cell and acquired at a resolution of 17.500 (at m/z 200) in the orbitrap using an AGC target value of 1×10^5 charges and an underfill ratio of 1%. Dynamic exclusion was applied with an exclusion time of 30 s. Peptides were identified with Mascot version 2.6.1 (Matrix Science, London, UK) against the SwissProt Database (version 2017_04) with a precursor ion mass tolerance of 5 ppm and a product ion mass tolerance of 0.02 Da. Up to two missed trypsin cleavages were allowed. Cysteine carbamidomethylation was set as a fixed modification and methionine oxidation was allowed as a variable modification. Peptides were primarily considered identified if the Mascot score was greater than the 95% confidence limit based on the identity score of each peptide. False discovery rates less than 1% were estimated by searching against a randomized decoy database. The label-free quantification of peptides was based on the peak area on the extracted ion chromatograms.

Statistical analysis.

Differences between two groups and multiple groups were evaluated using the student t-test and Tukey-Kramer test, respectively, and $p < 0.05$ was considered statistically significant.

III-2-3. Results

III-2-3-a. Preparation and characterization of MP-sEVs isolated by SEC.

The separation of sEVs from soluble proteins by SEC was confirmed by the elution pattern of purified murine melanoma B16-sEVs and soluble proteins (BSA and gLuc-LA protein) (Supplementary figure 5). B16-sEVs were most abundant in fraction 4. Therefore, I decided to isolate fraction 4 as the sEV-enriched fraction and used it for downstream experiments unless otherwise mentioned. Physicochemical properties, as well as the protein composition, of MP-sEVs-enriched SEC eluate were characterized and compared with those of MP-sEVs-enriched pellets collected by UC and PEG-based methods (Figure 33A). SEC eluate sample appeared to be relatively free of albumin, ApoB100, ApoE, and apo A-I (band at approximately 70, 500, 37, and 25 kDa, respectively) compared to those isolated by other methods (Figure 33B). Aggregation was observed in UC and PEG samples, as reflected by size histogram (Figure 33C), while SEC eluate was enriched in unclustered, morphologically intact membrane vesicles, which were probably MP-sEVs. Based on these results, SEC was chosen as an MP-sEV isolation method.

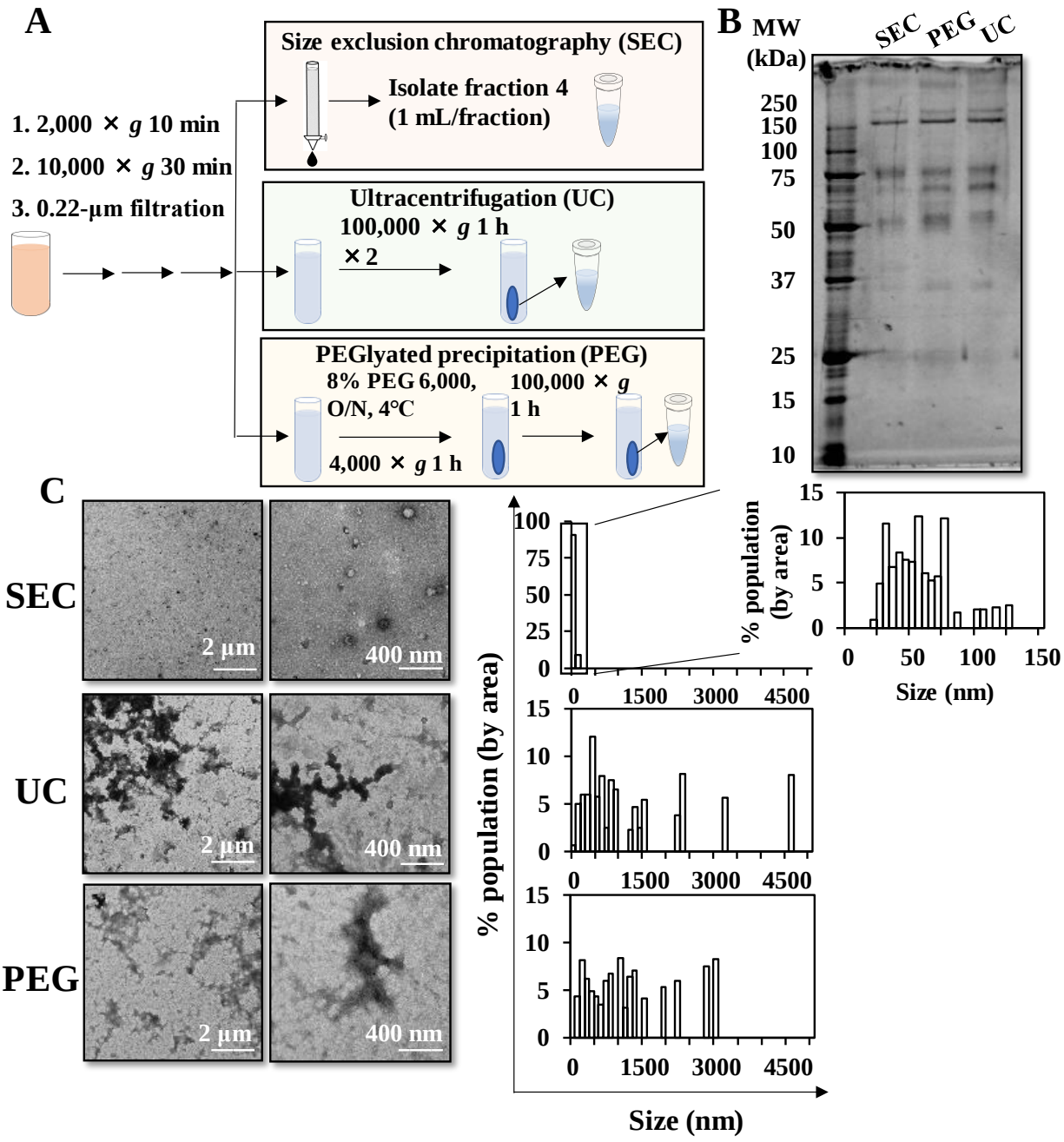

Figure 23. Comparison of methods to isolate sEVs from mouse plasma.

(A) Scheme for sEV isolation from mouse plasma through SEC, UC, and PEG-based isolation. (B) Protein profiles were examined by SDS-PAGE (0.1 µg protein /lane). (C) Morphology was examined by TEM. TEM images in low (left) and high (right) magnification are shown. Representative TEM images were analyzed by Image J software to measure the size histogram.

III-2-3-b. Preparation of gLuc-LA-labeled MP-sEVs.

Next, I tried to optimize the protocol for labeling MP-sEVs using chimeric gLuc proteins. Proteins that can bind target lipids, such as LA (high affinity to phosphatidylserine (PS)), perfringolysin-O (PFG; high affinity to cholesterol), and lysenin (Lys; high affinity to sphingomyelin), were used to prepare gLuc-LA, gLuc-PFG, and gLuc-Lys, respectively (Figure 34A, Supplementary figure 6). After incubating mouse plasma with the chimeric gLuc proteins followed by SEC, the gLuc enzyme activity per sEV-related protein content was 10-fold higher for gLuc-LA compared to that for gLuc-Lys or gLuc-PFG (Figure 34B). Next, labeling stability in mouse serum was examined (Figure 34C-34F). For all the three chimeric gLuc proteins, approximately 80% of initial gLuc enzyme activity was retained after 4 h of incubation. SEC analysis revealed that gLuc-LA-labeled MP-sEVs ($^{gLuc\text{-}LA}$MP-sEVs) were eluted at fraction 4, which corresponded to sEVs, irrespective of the incubation time. In contrast, gLuc enzyme activity was detected in fractions 8–11 after incubating gLuc-PFG- and gLuc-Lys-labeled MP-sEVs in mouse serum, suggesting the release of gLuc-PFG and gLuc-Lys from MP-sEVs. Based on these results, gLuc-LA was selected, and labeling conditions were optimized to prepare $^{gLuc\text{-}LA}$MP-sEVs with high gLuc enzyme activity (Supplementary figure 7, 8). For the final optimized conditions of labeling, gLuc-LA (> 5×10^8 RLU/s) was incubated with mouse plasma (0.5 mL) for > 1 h at 4℃ with gentle agitation. MP-sEV was successfully isolated regardless of gLuc-LA labeling based on the observation of similar sEV-like vesicle by TEM, detection of comparable protein profile and western blotting against sEV markers (CD63, Alix, and HSP70) (Supplementary figure 9). Supplementary figure 10 indicates that gLuc-LA bound to sEVs through LA, which has high affinity for PS enriched on the surface membrane. Then, the possibility of gLuc-LA labeling to LDL/VLDL particles, which are expected to be contaminated in $^{gLuc\text{-}LA}$MP-sEVs-enriched SEC eluate, was evaluated. Immunoprecipitation experiments revealed that gLuc-LA scarcely labeled LDL/VLDL particles (Supplementary figure 11). Moreover, successful labeling of gLuc-LA to MP-sEVs was confirmed by the observed gLuc Ab-coated immunogold on the surface of MP-sEVs based on immunoelectron microscopy (Figure 35A) as well as detection of sEV marker (CD63, Lamp2) of $^{gLuc\text{-}LA}$MP-sEVs loaded on gLuc Ab-coated beads ($^{gLuc\ Ab}$beads) by flow cytometry (Figure 35B). Then, $^{gLuc\text{-}LA}$MP-sEVs in the SEC eluate sample was immunocaptured by $^{gLuc\ Ab}$beads, followed by purification and elution in order to characterize sEVs labeled by gLuc-LA. Figure 35C-35E show that $^{gLuc\text{-}LA}$MP-sEVs were spherical vesicle with approximately 100 nm in diameter and possessed negative charge (-13.5 ± 1.9 mV). The surface charge data of input (-30.5 ± 0.7 mV) and non-captured fraction (-34.5 ± 1.3 mV) is assumed to reflect the surface charge of the contaminated molecules in the SEC eluate (Figure 46E). Protein staining result shows distinct protein composition of $^{gLuc\text{-}LA}$MP-sEVs (Figure 35F).

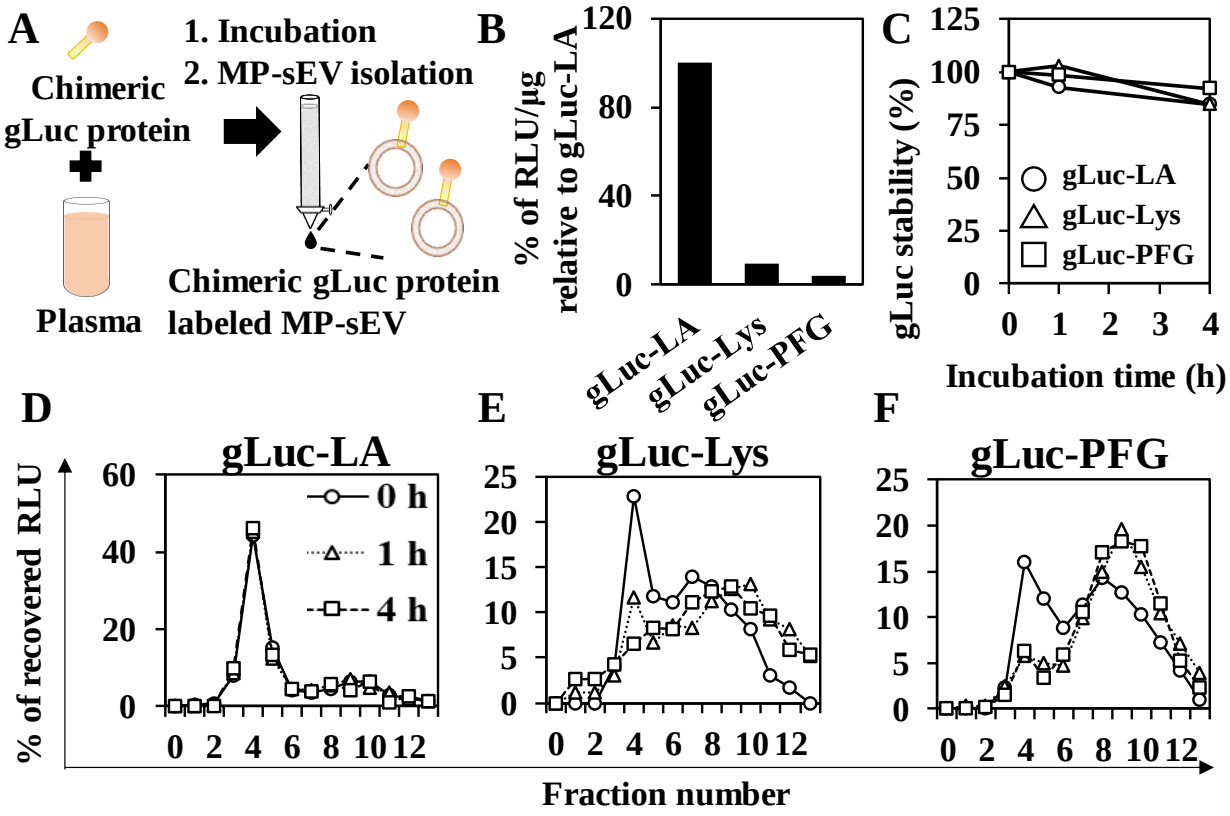

Figure 24. MP-sEV labeling by chimeric gLuc proteins and stability in serum.

(A) Schematic workflow of MP-sEV labeling with chimeric gLuc proteins. (B) The luciferase activity per sEV protein amounts of MP-sEV incubated with approximately 5-7 × 10^9 RLU of gLuc-LA, gLuc-Lys, or gLuc-PFG. The results are expressed as the percentage relative to gLuc-LA. (C) Time-course of gLuc activity for gLuc-LA-, gLuc-PFG-, or gLuc-Lys-labeled MP-sEVs incubated with 10% mouse serum in PBS at 37 ℃. (D)-(F) SEC analysis of (D) gLuc-LA-, (E) gLuc-PFG-, or (F) gLuc-Lys-labeled MP-sEVs incubated with 10% mouse serum in PBS at 37 ℃ for the indicated time periods.

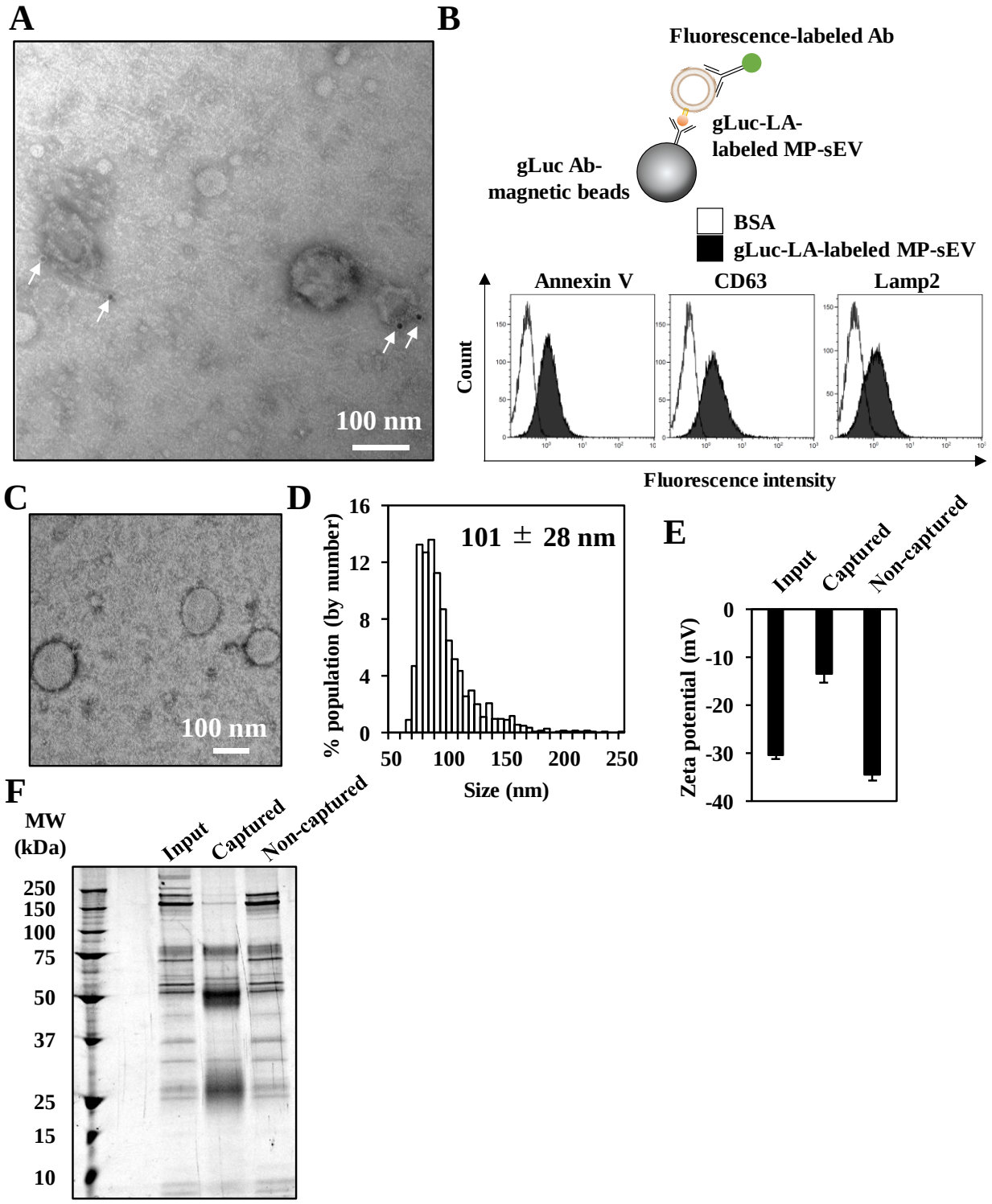

Figure 25. Characterization of $^{gLuc\text{-}LA}$MP-sEVs.

(A) Transmission electron microscopy (TEM) observation of $^{gLuc\text{-}LA}$MP-sEVs stained with protein A-gold nanoparticles (indicated by arrows) after reacting with an anti-gLuc Ab. (B)-(F) $^{gLuc\text{-}LA}$MP-sEVs in the SEC eluate sample was immunocaptured by gLuc Ab-coated magnetic beads. (B) To confirm the sEV capturing by the beads, the sEVs-beads complexes were subsequently stained with the indicated FITC-AnV (high affinity to PS), PE-anti-CD63 Ab, or Alexa fluor 488-anti-Lamp2 Ab and analyzed by flow cytometry. BSA was set as a control sample against the sEV. Then, the sEV was eluted from the beads and psychochemical properties as well as protein composition was identified as follow: (C) sEV morphology by TEM analysis, (D) Size histogram measured by qNano instrument, (E) Zeta potential of sEV, and (F) SDS-PAGE analysis (0.7 μg/lane). The input and non-captured fraction of the immunocapturing was simultaneously analyzed for zeta potential and SDS-PAGE.

III-2-3-c. Macrophage-dependent rapid clearance of systemically injected MP-sEVs from the circulation of mice.

Next, the serum concentration profile of $^{gLuc\text{-}LA}$MP-sEVs after i.v. injection into mice was evaluated. gLuc enzyme activity in the mouse serum treated with $^{gLuc\text{-}LA}$MP-sEVs quickly disappeared with a $t_{1/2\alpha}$ of 6.38 ± 2.81 min, almost irrespective of the investigated doses of MP-sEVs (approximately 3–25 μg MP-sEV protein/dose; Figure 36A). *In vivo* imaging showed that $^{gLuc\text{-}LA}$MP-sEVs mainly distributed to the liver (Figure 36B). Moreover, immunostaining of macrophage ($F4/80^+$ cells) in the liver and microscopic observation indicates that $^{gLuc\text{-}LA}$MP-sEVs was taken up by macrophage in the liver (Figure 36C). To evaluate the role of macrophages in the blood clearance of MP-sEVs, macrophage-depleted mice were prepared via the administration of clodronate liposome. Macrophages were absent from the liver and this depletion was retained from at least day 1 to day 4 after this

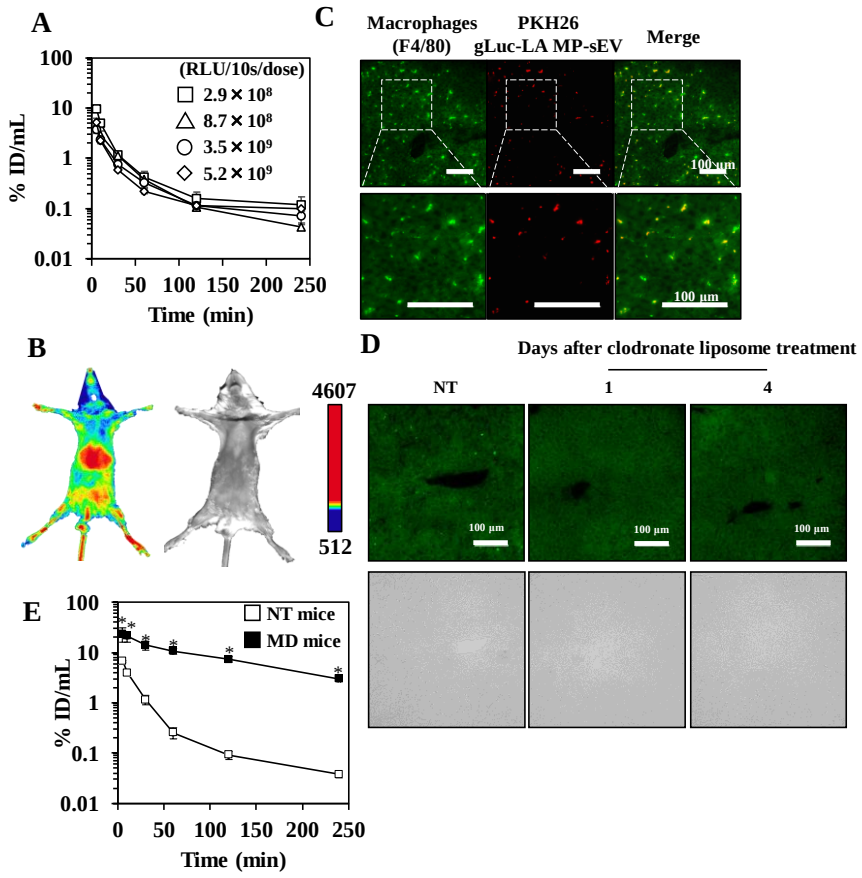

Figure 26. Blood clearance of $^{gLuc\text{-}LA}$MP-sEVs from circulation in NT- and MD- mice.

(A) The dose effect on the time-course of serum concentrations of gLuc activity after the i.v. administration of gLuc-LA-labeled MP-sEVs into NT mice. The dose was expressed as gLuc activity per dose (RLU/10s/dose). Protein dose for 2.9×10^8, 5.2×10^9, 8.7×10^8, and 3.5×10^9 RLU/10s/dose are 3, 7.8, 8.5 and 25 μg/dose, respectively. Results are expressed as the mean of the percentage of the administered dose/mL (% ID/mL) ± SD (n = 3). (B) NT mice were treated with $^{gLuc\text{-}LA}$MP-sEVs. The MP-sEVs were imaged 5 min after i.v. administration of MP-sEVs through a bolus i.v. administration of coelenterazine (a gLuc substrate). The chemiluminescence was detected. Left; chemiluminescence image. Right; bright field image. (C) Cellular uptake of $^{gLuc\text{-}LA}$MP-sEVs in the liver. The MP-sEVs were labeled with PKH26, followed by i.v. administration into mice. Four hours after the injection, the liver was collected and cut into cryostat section. The section was stained with F4/80-specific Ab and observed by fluorescence microscopy. (D) Immunofluorescence staining of liver macrophages after clodronate-encapsulated liposome treatment. Upper images: the green channel corresponds to F4/80-specific Ab-derived signals. Lower images: bright field. (E) Time-course of serum concentrations of gLuc activity after the i.v. administration of gLuc-LA-labeled MP-sEVs (9.1×10^8 RLU/10s/dose; approximately 1 μg MP-sEV protein/dose) into NT mice (open symbols) or MD mice (closed symbols). Results are expressed as the mean of the percentage of the administered dose/mL (% ID/mL) ± SD (n = 3). *$p < 0.05$ versus NT mice.

protocol (Figure 36D). Macrophage depletion retarded the rate of the decline in gLuc enzyme activity in the serum (Figure 36E). Next, as MP-sEVs are composed of a heterogenous population of particles with different physiochemical properties, pharmacokinetics might differ depending on the subpopulation of MP-sEVs. To investigate this possibility, $^{gLuc\text{-}LA}$MP-sEVs (Total sEVs) were further fractionated into low-density (named "LD-sEV"; 1.00–1.07 g/mL) and high-density ("HD-sEV"; 1.07–1.21 g/mL) groups by density gradient centrifugation (DGC). Similar to the Total sEVs fraction, LD-sEVs and HD-sEVs quickly disappeared from circulation after i.v. administration (Supplementary figure 12).

III-2-3-d. Increased MP-sEV concentration after macrophage depletion.

Next, the MP-sEV concentration in non-treated (NT) and macrophage-depleted (MD) mice was measured. As MP-sEV samples isolated by SEC were contaminated with LDL particles (Supplementary figure 11A), these samples were subjected to DGC in order to remove LDL particles based on differences in density (LDL, 1.01–1.06 g/mL versus sEVs, 1.08–1.21 g/mL, Figure 37A). A typical density profile for each fraction after centrifugation is shown on Figure 37B. In this case, fractions 5–10 were collected for sEV-related protein analysis and quantitation. After successful depletion of LDL was confirmed (Figure 37C-37E), sEV was captured by Tim4 (high affinity to PS on the sEV membrane)-coated beads (^{Tim4}beads) and protein amount as well as sEV marker of the sEV-^{Tim4}beads complexes (captured fraction) were analyzed. Figure 37F-37H indicates that more than 90% of the protein in the SEC+DGC treated sample was associated with sEVs interacted with ^{Tim4}beads, suggesting that the protein amount mostly reflected the sEV-related protein amount. After identification of sEV from NT and MD mice (Figure 38A-38D), it was revealed that macrophage depletion approximately tripled the amount of MP-sEV-related protein (Figure 38E). Then, proteomic analysis of sEV-related proteins from of NT and MD mice was conducted. LC-MS/MS was performed in triplicate for each sample and commonly identified proteins were selected for downstream analysis (Figure 39A). Identified proteins were ranked based on a volcano plot according to their statistical p-value and their relative difference in abundance (Figure 39B). Eighty-one spots (half of the total identified proteins) were selected based on the magnitude of response (more than 2-fold) and the statistical significance ($P < 0.05$). The selected proteins were then analyzed by clustering and gene ontology enrichment analysis to identify enriched biological process compared to the genome frequency (Figure 39C, 39D). The only up-regulated term was "Cell adhesion", whereas the down-regulated terms included "Complement activation", "Innate immune response", and "Immune system process".

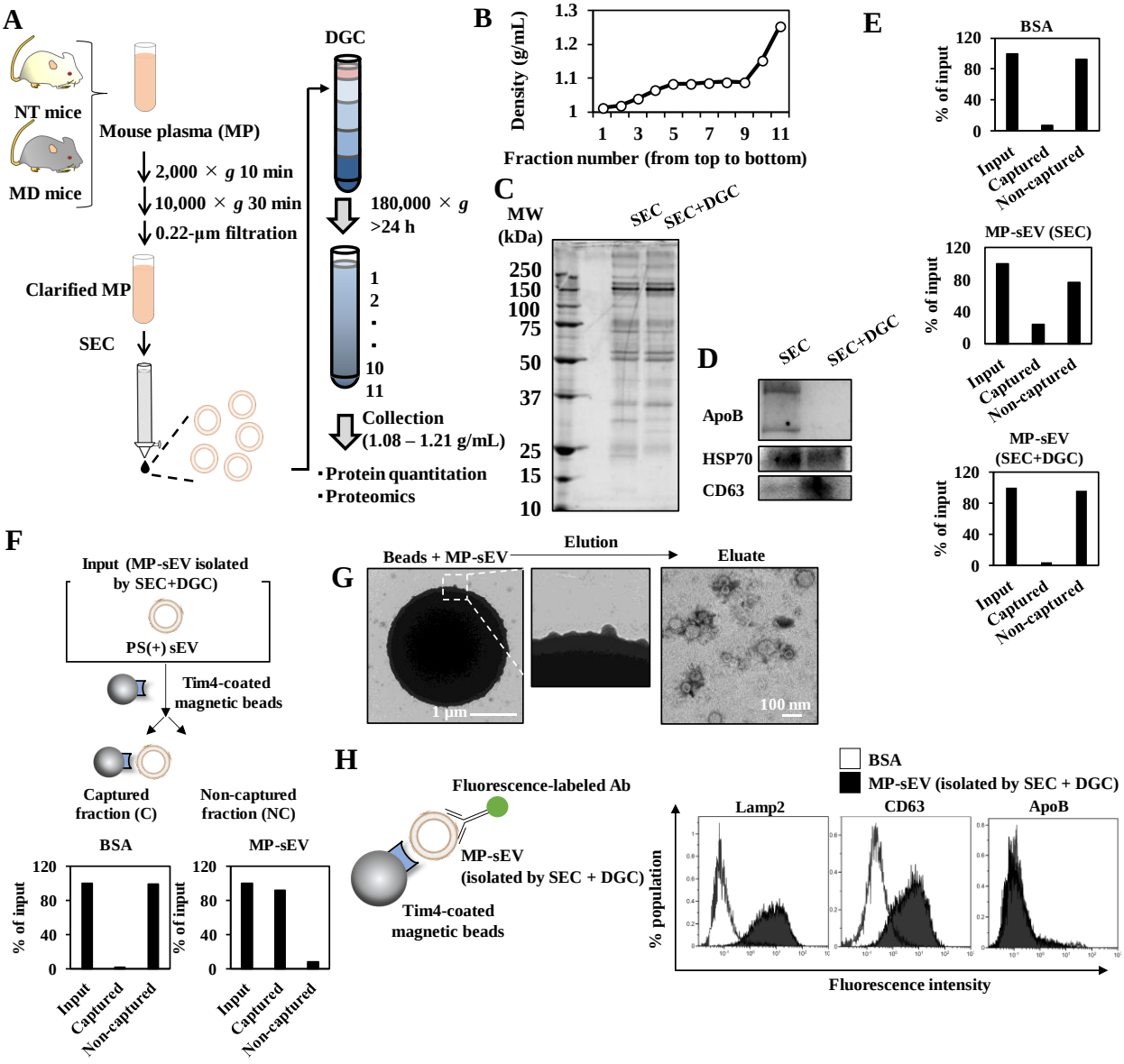

Figure 27. Verification of highly purified MP-sEVs after DGC.

(A) Scheme for the isolation of highly purified MP-sEVs from NT or MD mice. (B) Typical density profile of each fraction from top to bottom after density gradient centrifugation. (C) MP-sEVs isolated only through SEC or SEC followed by DGC (SEC+DGC) was run in SDS-PAGE (1.0 μg protein/lane). The gel was stained with Lumitein™ Protein Gel reagent to visualize the protein profile. (D) Another gel was proceeded to western blot analysis to detect the indicated protein. (E) To quantitatively analyze the remaining ApoB in the MP-sEVs isolated by SEC only or SEC + DGC method on a protein-based quantitation, the remaining ApoB was pulled down by anti-ApoB Ab-coated magnetic beads. The protein amount of non-captured fraction was measured. The protein amount in the captured fraction was calculated by subtracting the protein amount of non-captured fraction from that of input. (F) MP-sEV isolated through SEC + DGC method was loaded onto Tim4-coated magnetic beads. (G) MP-sEV loaded on the beads was confirmed by TEM observation. Then, the protein balance of non-captured fraction and captured fraction was analyzed. (H) The sEV-beads complexes were stained with Alexa fluor 488-Lamp2 Ab, PE-CD63 Ab, or ApoB Ab (primary Ab) + Alexa fluor 488 secondary Ab and analyzes by flow cytometry. BSA was set as a control sample against the sEV.

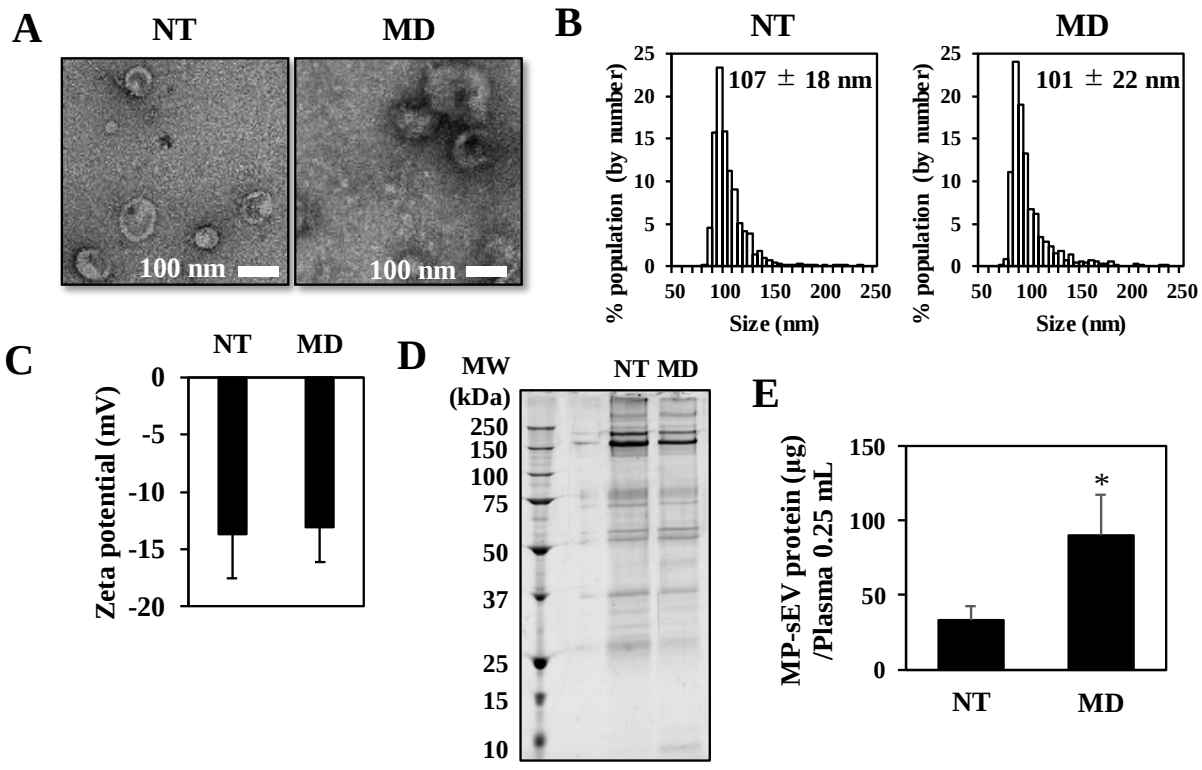

Figure 28. Characterization of MP-sEVs from NT- and MD-mice.

(A) TEM images of MP-sEVs from NT- (left) and MD (right)-mice. (B) Size histogram of MP-sEVs from NT- (left) and MD (right)-mice measured by qNano. (C) Zeta potential of MP-sEVs from NT- and MD-mice measured by a zetasizer. (D) Protein profiles of MP-EVs from NT- and MD-mice examined by SDS-PAGE (1.0 µg protein/lane). (E) Quantification of sEV amounts isolated from NT and MD mice, as estimated by protein quantification. Results are expressed as the mean ± SD (n = 3). *$p < 0.05$ versus NT mice.

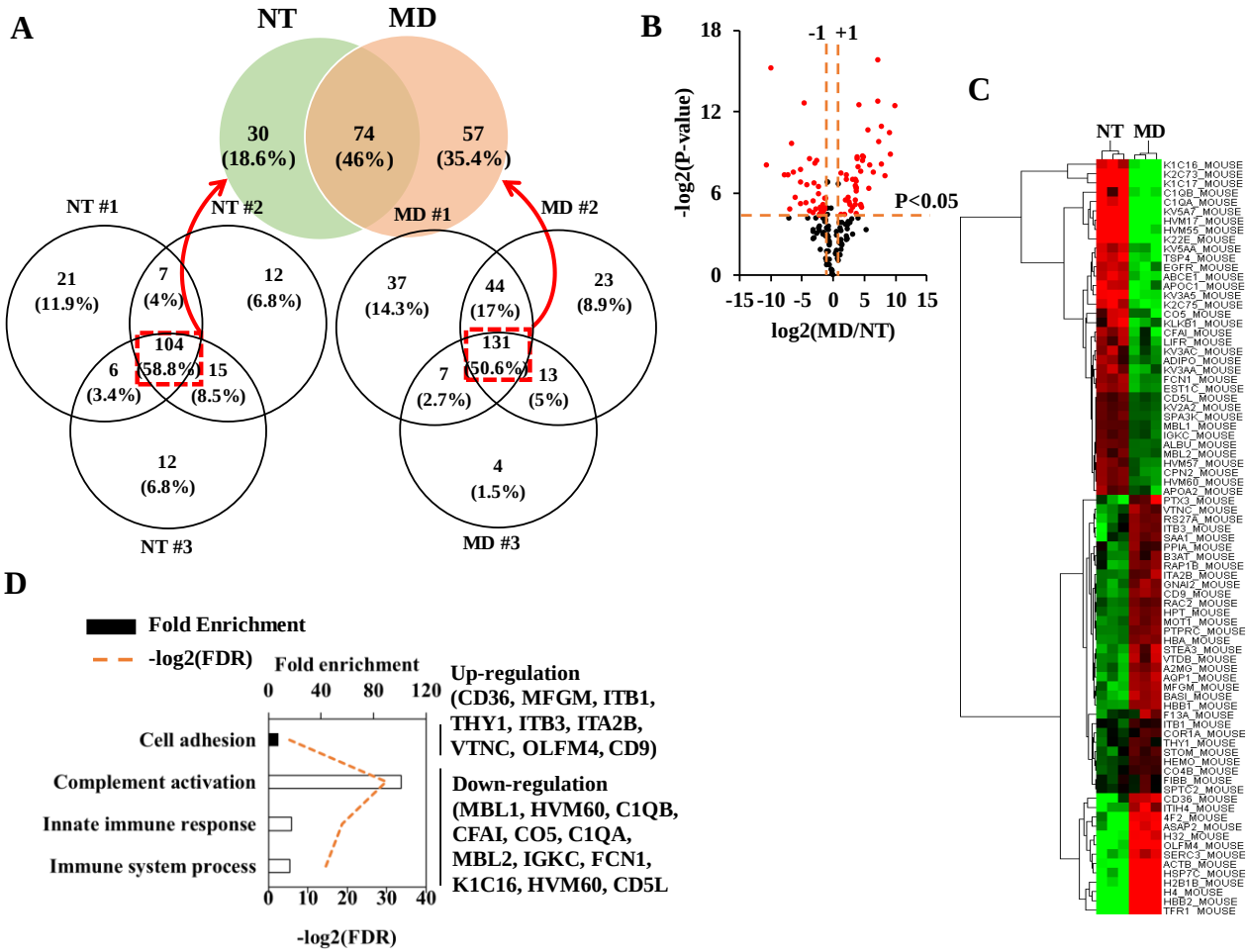

Figure 29. Proteomic analysis of MP-sEVs from NT and MD mice.

(A) Venn diagram of proteins detected in the two samples. (B) Identified proteins were ranked in a volcano plot according to their statistical P-value (y-axis) and their relative abundance ratios ($\log_2$ fold-change, x-axis) between MP-sEVs from NT and MD mice. Red dots indicate the proteins with both P value < 0.05 and $\log_2$ fold-change < −1 or > 1). (C) Heat map of proteins of MP-sEVs from NT- and MD-mice based on proteomic analysis. (D) Gene ontology enrichment analysis for up-regulated (closed bar) and down-regulated proteins (open bar) after macrophage depletion. FDR values < 0.05 are listed. The related genes are listed to the right.

III-2-3-e. Pharmacokinetics of i.v. infusion in a two-compartment model.

Figure 40 shows the results of PK analysis based on i.v. infusion using a two-compartment model. The k_0 value [MP-sEV secretion rate constant (μg/mL)] was calculated by substituting the experimental values [k_{el}, MP-sEV clearance rate constant (min^{-1}) in NT mice, C_{sEV}, MP-sEV concentration in blood (μg/mL) in NT mice, and V_c, volume of distribution (mL) in NT mice] for equation (13) described in materials and methods. The k_0 value was 17.9 μg/min, which indicates that approximately 18 μg of MP-sEVs is secreted from various origins into the plasma per minute. Next, assuming that clodronate liposome treatment had little effect on sEV-producing cells except macrophages, k_0 in addition to k_{el}' [MP-sEV clearance rate constant (min^{-1}) in MD mice] and V_c' [volume of distribution (mL) in MD mice] values were used to simulate the C_{sEV}' value with an assumption that macrophage depletion did not change the sEV secretion rate as it was reported that most sEVs in the blood are derived from hematopoietic cells[115]. The simulated value was 453 μg/mL, which was comparable to the experimental C_{sEV}' value [MP-sEV concentration in blood (μg/mL) in MD mice, 361 ± 108 μg/ mL].

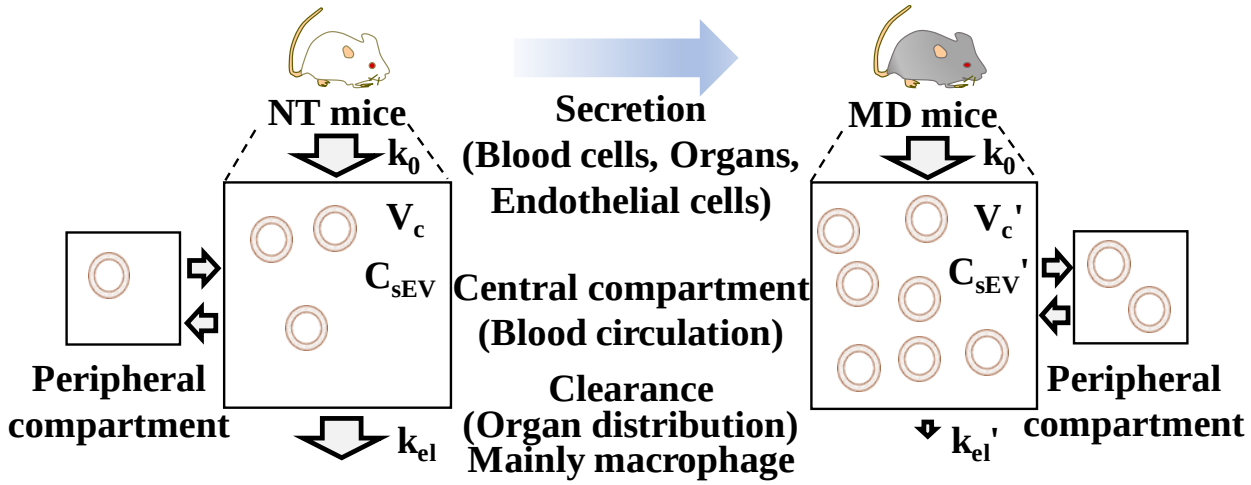

NT mice	Parameters	MD mice
1.09	k_{el} or k_{el}' (min^{-1})	0.00708
132 ± 37	C_{sEV} or C_{sEV}' (measured) (μg/mL)	361 ± 108
	C_{sEV}' (simulated) (μg/mL)	453
0.125	V_c or V_c' (mL)	3.8
17.9	k_0 (μg/min) (simulated)	17.9

Figure 30. PK analysis of the secretion/clearance balance of MP-sEVs based on i.v. infusion in a two-compartment model.

The image above shows the schematic concept. MP-sEVs are secreted from various cells or organs. Under the assumption of this model, the MP-sEVs are secreted into plasma based on zero-order kinetics. MP-sEV clearance from circulation is assumed to follow first-order kinetics. k_{el} or k_{el}': MP-sEV clearance rate constant (min^{-1}). C_{sEV} or C_{sEV}': MP-sEV concentration in blood (μg/mL). V_c or V_c': volume of distribution (mL). k_0: MP-sEV secretion rate constant (μg/min). The k_0 value was assumed to be constant before and after macrophage depletion treatment.

III-2-4. Discussion

Unlike the supernatants of cultured cell lines, blood is a complex mixture of sEVs from various cells, as well as lipoprotein particles, and thus the isolation and labeling of blood sEVs is difficult[105,106,116]. Therefore, estimating the blood clearance of MP-sEVs is very difficult. The proposed method achieves isolation of morphologically intact MP-sEV and highly sensitive, stable, and specific MP-sEV labeling that enabled PK analysis (Figure 33-35, Supplementary figure 5-10). In this section, sEV amount was quantified based on protein amount because measuring protein amount requires rapid and rigid sample processing[117]. On the other hand, attention should be paid to a point that blood sEV concentration estimation is dependent on the method of sEV isolation and quantification method, *i.e.* protein quantification or particle number quantification as summarized by Johnsen et al.[118].

In addition to gLuc-LA, both gLuc-PFG and gLuc-Lys were used to label MP-sEVs; however, these two probes were less sensitive than gLuc-LA and failed to result in stable labeling in the presence of serum (Figure 34). As cholesterol and sphingomyelin are enriched in lipoprotein particles and that lipoproteins are 100-fold more abundant than sEVs in plasma[105,106,116,118], it is assumed that gLuc-PFG- and gLuc-Lys-labeled MP-sEVs were transferred to lipoprotein particles at the point of isolation. These results stress the importance of checking labeling stability before PK studies.

PK analysis clearly demonstrated that macrophages play an important role in the clearance of MP-sEVs from blood circulation (Figure 36). Because MP-sEVs are negatively charged (Figure 35E) and the negative charge of PS in the sEV membrane could be involved in the recognition and clearance of intravenously administered cultured cell-derived sEVs by macrophages[26,51], MP-sEVs might also be recognized and taken up by macrophages through a PS-dependent mechanism. It is also considered that the PK properties might be different among subpopulations of MP-sEVs, as demonstrated previously for cultured cell-derived sEVs[119]. This was partly denied by the results indicating that HD-sEVs and LD-sEVs, as well as Total sEVs, are rapidly cleared from circulation (Supplementary figure 12). Besides, more than 90% of MP-sEV-related protein was detected in Tim4-captured fraction, suggesting that majority of MP-sEV was PS-positive (Figure 37F), which is in agreement with previous studies that showed most of sEVs in blood were positive for PS[120,121]. As gLuc-LA binds to PS-positive MP-sEV that consists majority of whole MP-sEV, I considered that the presented PK data are relevant for the whole MP-sEV population. On the other hand, attention should be paid to the point that MP-sEV population is dependent on the method of MP-sEV isolation[69,118]. As a future study, fractionation of MP-sEVs based on other criteria such as surface markers followed by a PK study would be necessary[122].

Most sEVs in the blood are derived from hematopoietic cells (CD45-positive vesicles)[115]. Other sources would be vascular endothelial cells (CD31-positive) or organs with a discontinuous endothelium such as the liver, pancreas, and bone marrow[81,82]. Measuring the secretion rate of each cell is technologically impossible at present. However, the proposed simulation-based approach is unique in that the secretion rate can be calculated without information regarding the origins of MP-sEVs. Simulation results demonstrated that sEVs are secreted from these cells or organs into the blood at a rate of 18 μg/min (Figure 40). This value appears to be larger compared to results from quantitative *in vitro* secretion analysis recently reported in several articles using a microfluidic device or single cell assay system[108,123]. Further, the secretion rate of MP-sEVs is approximately three-fold higher than that of cell

culture-derived sEVs based on a calculation using reported values[124–126]; specifically, these values were reported as follows: sEV secretion rate from single cell = 100 sEV particles per hour, number of blood cells = 1×10^7 cells per 1 μL of blood, number of sEV particles per sEV protein = 5×10^9 sEV particles per 1 μg of sEV protein. As numerous cell types are involved in sEV secretion and have different secretion rates into the blood *in vivo*, this difference in the secretion rate might imply the limitation of *in vitro* secretion analysis for estimating the sEV secretion rate into blood. My robust approach can overcome this limitation.

To simplify the simulation, it was initially assumed that sEVs are secreted into the blood at the same qualitative level regardless of physiological conditions. Proteomic analysis revealed that 50% of the identified proteins were expressed at the same level, based on P-values and relative abundance ratios, suggesting that, in terms of protein, the quality of MP-sEVs is retained to some extent after macrophage depletion (Figure 38, 39). This might be the reason for the difference in the MP-sEV concentration in MD mice between calculated (453 μg/mL) and experimental values (361 ± 108 μg/mL). Further, the differentially expressed proteins might reflect population changes in sEVs, resulting in differences in several biological processes (Figure 39C, 39D). Interestingly, integrin proteins and complement-related proteins were found to be up-regulated and down-regulated in MP-sEVs from MD mice, respectively. Integrin proteins as well as PS are reported as key molecules for recognition by macrophages in the liver as a PS-independent manner[10,21]. Thus, macrophage depletion might prolong the blood retention time of the integrin-enriched MP-sEV subpopulation. Moreover, macrophages are partly responsible for complement secretion into the blood[127]. Accordingly, the downregulation of complement activation due to macrophage depletion might protect sEVs from complement-mediated vesicle lysis[128], which could also be related to the decreased clearance rate of MP-sEVs in macrophage-depleted mice. Thus, future challenges comprise validating the effects of such protein differences.

As my “balance hypothesis” was validated to some extent (Figure 40), it would be valuable to consider treatment strategies targeting sEVs. For example, in cancer patients, tumor-derived sEVs from various tumor types are known to enter the circulation, reach distant locations, and educate the pre-metastatic niche, which is associated with organotropic metastasis[21,81]. In addition, tumor-derived sEVs in blood circulation induce immune suppression through interaction with immune cells such as T cells in the blood or delivery of anticancer agents enhancing tumor associated immunoresponse[129,130]. Therefore, the removal of tumor-derived sEVs from circulation is expected to be a novel anti-cancer therapy. As such, adaptive dialysis-like affinity platform technology or the administration of Ab against sEVs to decrease tumor-derived sEVs concentrations in the blood have been proposed[131,132]. Based on simulation using parameters obtained in the current study, it was calculated that MP-sEV concentrations return to greater than 90% of steady state levels, from 0, within 30 min after the termination of treatment, suggesting that tumor-derived sEV concentrations in the blood might rapidly recover after such treatments. Thus, for successful treatment, intervention that enables the continuous removal of tumor-derived sEVs from the blood is required to maintain low concentrations. Therefore, removing these types of sEVs from circulation might be challenging as a therapeutic application. Rather, it would be much more reasonable to inhibit sEV secretion from the tumor. Several potent sEV secretion inhibitors have been discovered through cell-based drug screening[133]. However, there are no available animal models to test the efficacy of such drugs *in vivo*. The proposed simulation approach to estimate sEV secretion rates *in vivo* is highly reproducible and could be a valuable tool to validate the *in vivo* efficacy of

candidate sEV secretion inhibitors.

III-2-5. Summary of section 2 of chapter III.

In this chapter, the "balance hypothesis" was validated for the first time using a mouse model. To achieve this, I developed a novel protocol for MP-sEV preparation that is suitable for PK analysis and proposed a simple simulation method for sEV secretion analysis. These findings will help to integrate *in vivo* and *in vitro* knowledge to understand the biological role of sEVs.

III-2-6. Supplementary figures of chapter III.

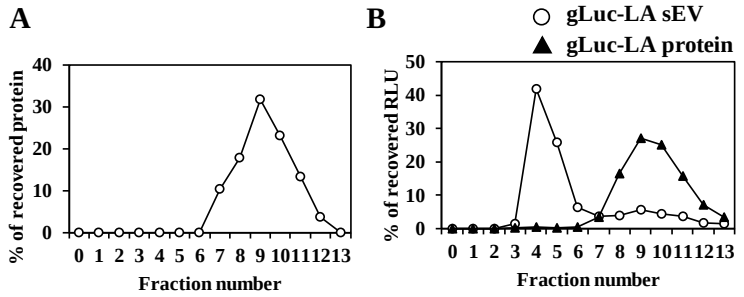

Supplementary figure 5. SEC elution pattern of soluble protein, and gLuc-LA-labeled sEVs isolated form cultured cells.

(A) PBS containing 0.01% BSA (B) gLuc-LA-labeled B16-sEVs (open circle), and gLuc-LA protein (closed triangle) were subjected to the column packed with sepharose 2B, and the eluate was collected (fraction 0). Subsequently, PBS was applied to collect the fraction (1 mL each). The fraction was numbered by collection order.

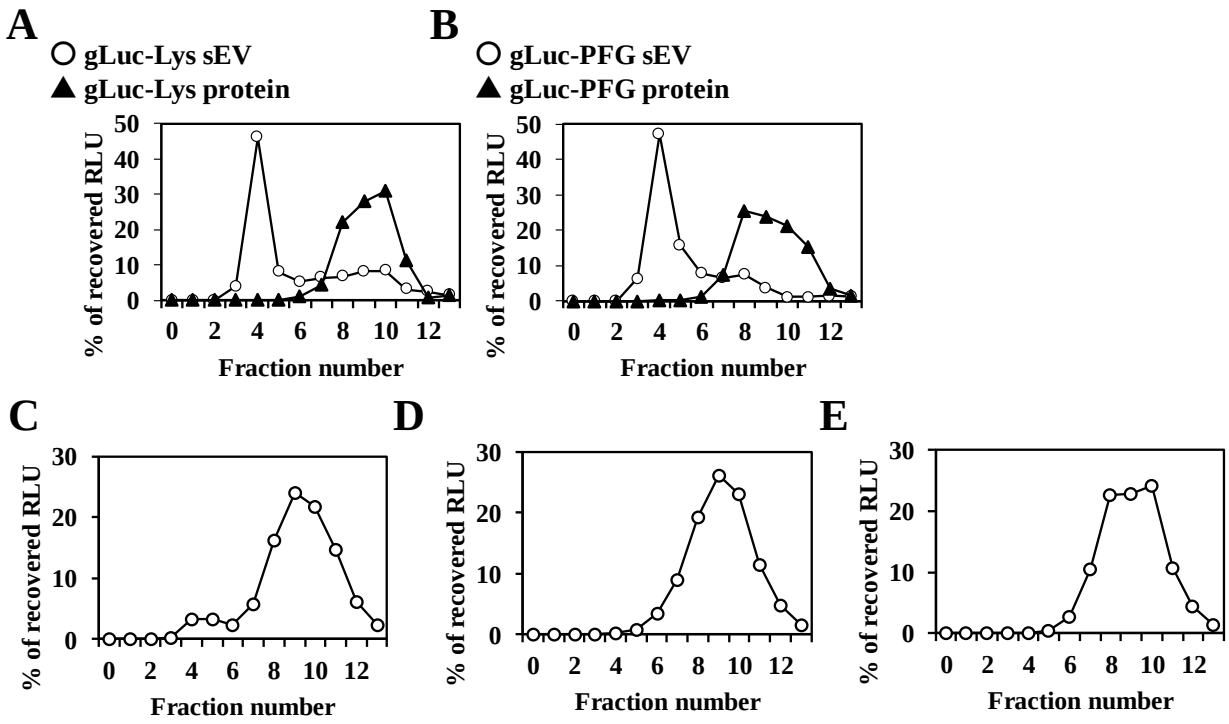

Supplementary figure 6. Typical elution pattern of gLuc-PFG- or gLuc-Lys-labeled MP-sEVs.

(A), (B) Typical size exclusion chromatography (SEC) elution pattern of (A) gLuc-Lys- (open circle) or (B) gLuc-PFG-labeled B16-sEVs (open circle) and (A) gLuc-Lys- (closed triangle) or (B) gLuc-PFG (closed triangle) protein-enriched sample. One milliliter sample was subjected to SEC and the eluate was collected (fraction 0). Subsequently, PBS was applied to collect the fraction (1 mL each). (C)-(E) Mouse plasma was incubated with (C) gLuc-LA-, (D) gLuc-Lys-, or (F) gLuc-PFG-enriched protein, for which the gLuc activity was adjusted to the same level. After incubation, the mixtures were subjected to SEC. The results are shown as the percentage of gLuc activity of each fraction divided by the total recovered gLuc activity.

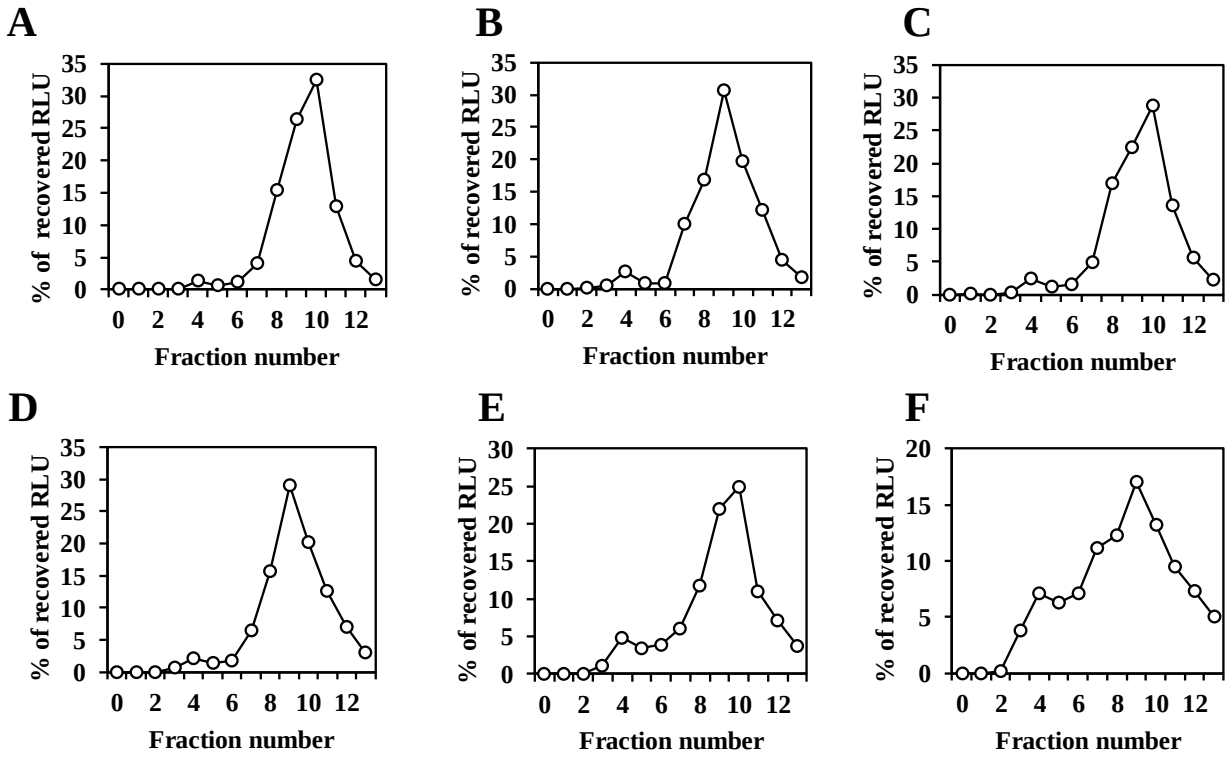

G

Conditions	Total applied gLuc activity (RLU/s/mL)	GLuc enzyme activity of fraction 4 (RLU/s/mL)	Protein concentration of fraction 4 (μg/mL)	GLuc enzyme activity per sEV protein (RLU/s/μg)
A	6.27×10^{10}	2.22×10^{8}	3.44	6.45×10^{7}
B	2.09×10^{10}	1.33×10^{8}	2.78	4.79×10^{7}
C	5.57×10^{9}	2.94×10^{7}	8.12	3.63×10^{6}
D	2.09×10^{8}	1.10×10^{7}	6.20	1.77×10^{6}
E	5.57×10^{8}	1.02×10^{7}	4.89	2.09×10^{6}
F	5.57×10^{7}	1.05×10^{7}	9.02	1.16×10^{6}

Supplementary figure 7. Effect of gLuc-LA protein concentration on the B16-sEV labeling with gLuc-LA.

B16BL6 conditioned medium (0.5 mL) was mixed with of gLuc-LA-enriched samples with different gLuc activities (0.5 mL). Total gLuc activity was as follows: (A) 6.27×10^{10} RLU/s/mL, (B) 2.09×10^{10} RLU/s/mL, (C) 5.57×10^{9} RLU/s/mL, (D) 2.09×10^{8} RLU/s/mL, (E) 5.57×10^{8} RLU/s/mL, and (F) 5.57×10^{7} RLU/s/mL. After incubation overnight at 4 ℃, the mixtures were subjected to size exclusion chromatography (SEC). The gLuc activity of each recovered fraction was measured. The results are shown as the percentage of gLuc activity of each fraction divided by the total recovered gLuc activity. Supplementary figure 7G summarizes the gLuc activities of the sEVs labeled with gLuc-LA under each condition.

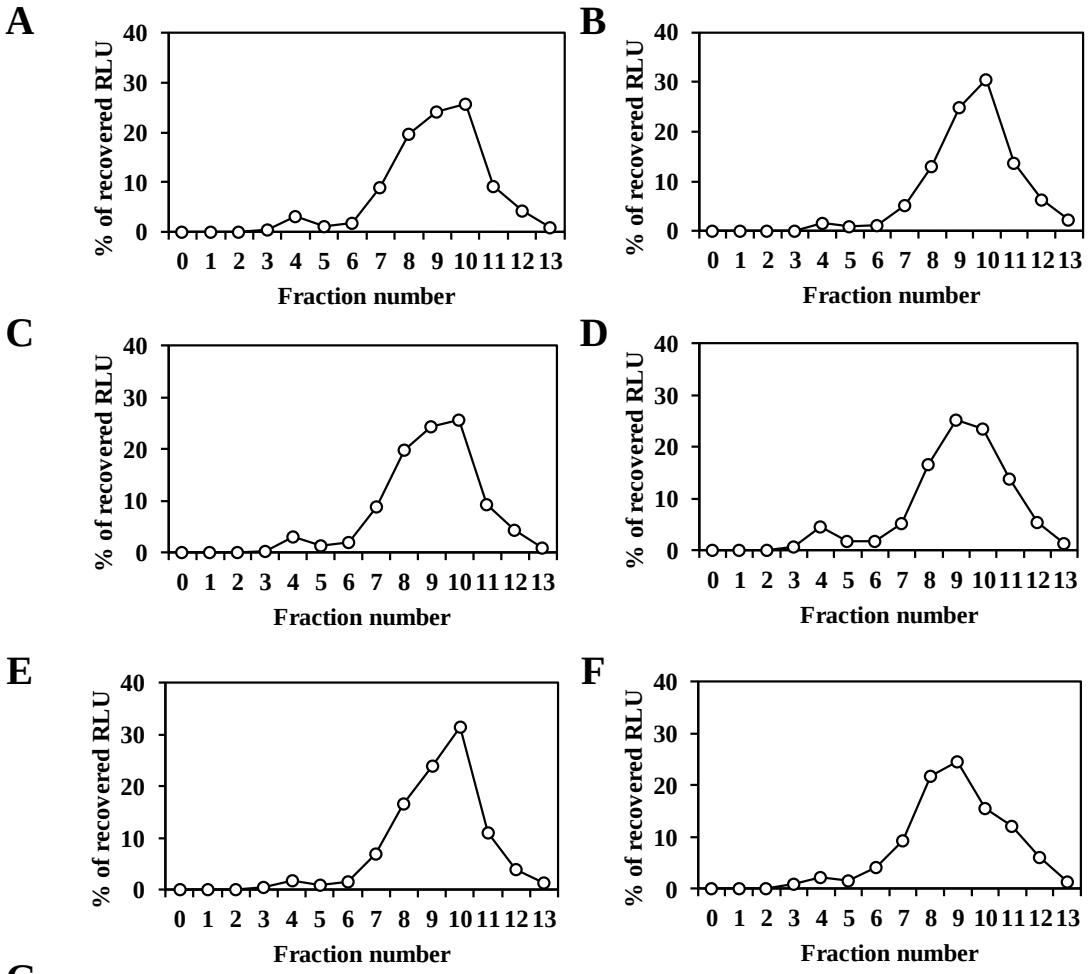

G

Conditions	Incubation temperature	Total applied gLuc activity (RLU/s/mL)	GLuc enzyme activity of fraction 4 (RLU/s/mL)	Protein concentration of fraction 4 (μg/mL)	GLuc enzyme activity per sEV protein (RLU/s/μg)
A	4 ℃	1.85×10^{10}	1.88×10^{8}	3.92	4.63×10^{7}
B	37 ℃	1.85×10^{10}	1.75×10^{8}	4.53	3.73×10^{7}

Conditions	Incubation time	Total applied gLuc activity (RLU/s/mL)	GLuc enzyme activity of fraction 4 (RLU/s/mL)	Protein concentration of fraction 4 (μg/mL)	GLuc enzyme activity per sEV protein (RLU/s/μg)
C	1 h	1.26×10^{10}	3.96×10^{8}	8.95	4.43×10^{7}
D	4 h	1.26×10^{10}	5.74×10^{8}	6.46	8.89×10^{7}
E	12 h	1.19×10^{10}	2.48×10^{8}	1.54	1.61×10^{8}
F	24 h	1.26×10^{10}	3.33×10^{8}	34.6	9.65×10^{6}

Supplementary figure 8. Effect of incubation temperature and incubation time on the B16-sEV labeling with gLuc-LA.

(A), (B) B16BL6 conditioned medium (0.5 mL) was mixed with gLuc-LA-enriched samples of indicated activity (0.5 mL). The mixture was incubated overnight at (A) 4 ℃ or (B) 37 ℃. (C)-(F) The mixture was incubated at 4 ℃ for 1 (C), 4 (D), 12 (E), or 24 h (F). After incubation, the mixtures were subjected into size exclusion chromatography (SEC). The gLuc activity of each recovered fraction was measured. The results are shown as the percentage of gLuc activity of each fraction divided by the total recovered gLuc activity. Supplementary figure 8G summarizes the gLuc activities of the sEVs labeled with gLuc-LA under each condition.

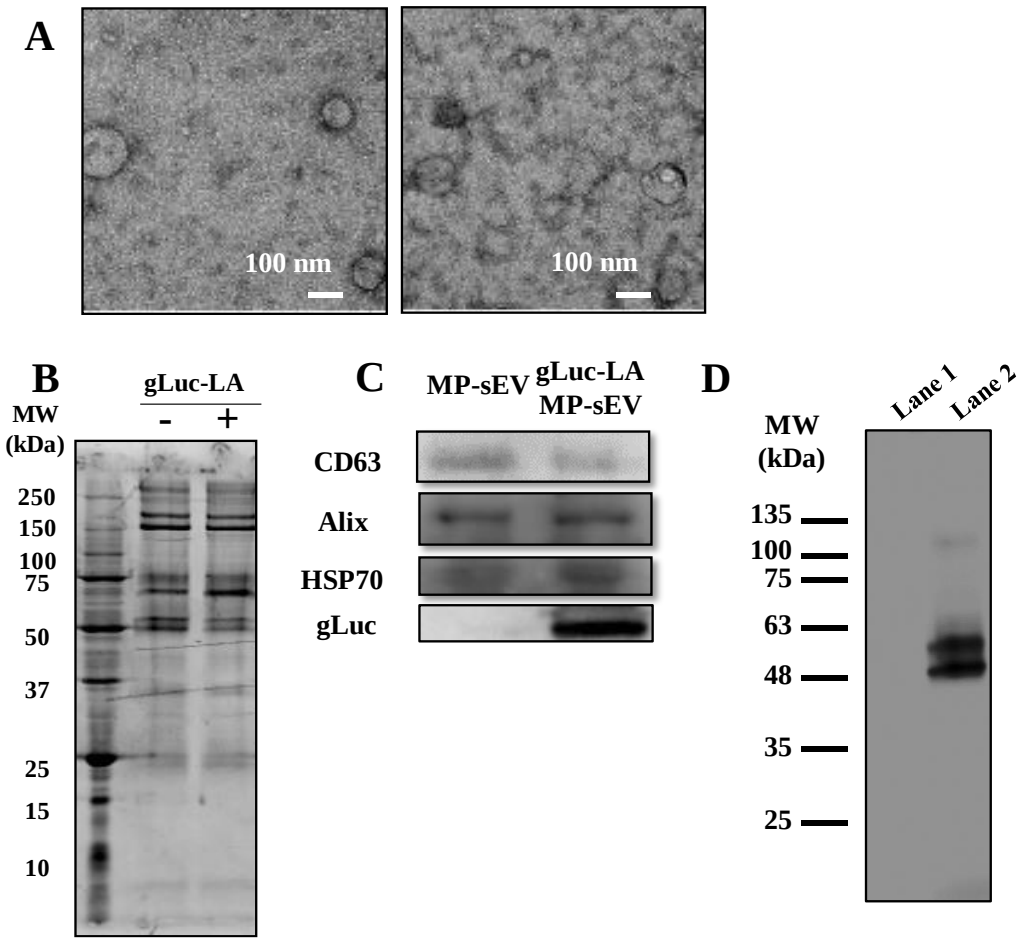

Supplementary figure 9. Characterization of vesicles in the gLuc-LA-labeled mouse plasma-derived sEVs.

(A) TEM images of MP-sEVs (left) and $^{gLuc\text{-}LA}$MP-sEVs (right). (B) Protein profiles of MP-EVs and $^{gLuc\text{-}LA}$MP-sEVs examined by SDS-PAGE (0.5 μg protein/lane). (C) Western blotting analysis of EV marker proteins (CD63, Alix, and HSP70) and gLuc protein in MP-sEVs and $^{gLuc\text{-}LA}$MP-sEVs. (D) gLuc zymography of gLuc-LA-labeled MP-sEVs. Lane 1:MP-sEVs; Lanes 2: $^{gLuc\text{-}LA}$MP-sEVs.

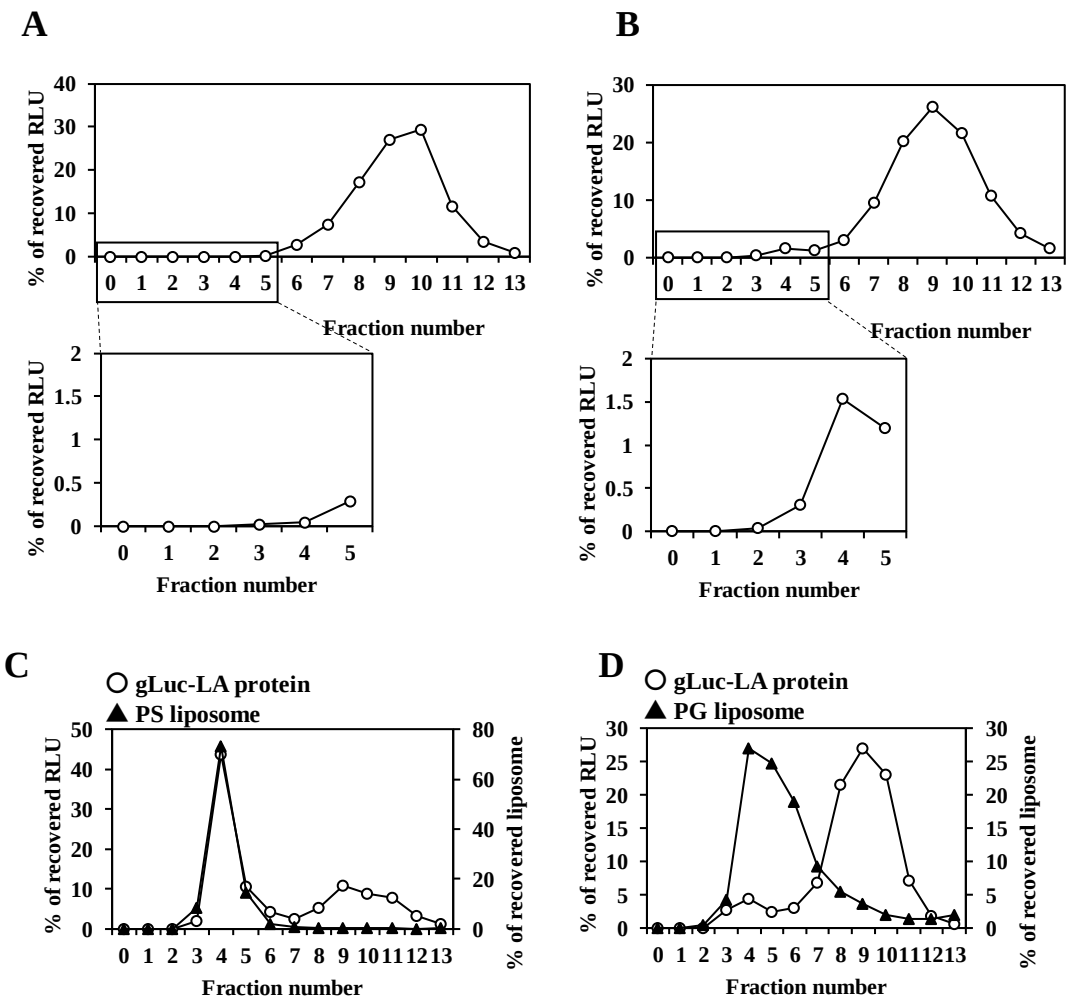

Supplementary figure 10. sEV labeling with gLuc-LA protein based on the affinity of LA to PS.

(A), (B) B16BL6 conditioned medium (0.5 mL) was mixed with (A) gLuc or (B) gLuc-LA-enriched samples (0.5 mL, approximately 5×10^9 RLU). After incubation, the mixtures were subjected into size exclusion chromatography (SEC). The gLuc activity of each recovered fraction was measured. The results are shown as the percentage of gLuc activity of each fraction divided by the total recovered gLuc activity. In a separate set of experiments, (C) PS liposomes, or (D) Phosphatidylglycerol (PG) liposomes were mixed with gLuc-LA-enriched sample. After incubation, the mixtures were subjected to SEC. The gLuc activity and liposome concentration of each recovered fraction was measured. The results are expressed as the percentage of gLuc activity (open circle) and liposome concentration (closed triangle) divided by the total recovered gLuc activity and liposome concentration, respectively.

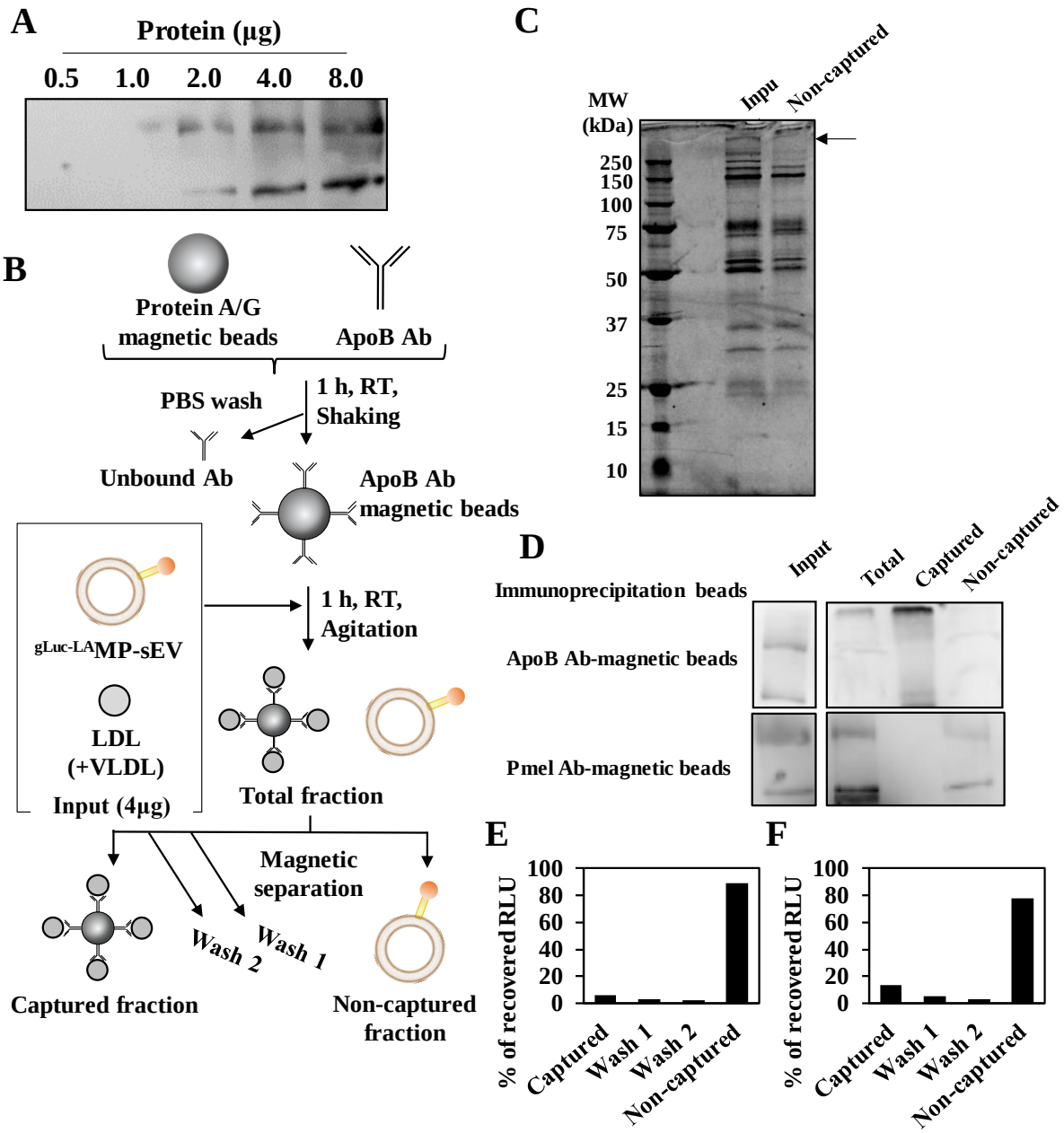

Supplementary figure 11. gLuc-LA did not label LDL/VLDL co-isolated in MP-sEV sample.

(A) Western blotting analysis of MP-sEVs. MP-sEVs (0.5–8.0 μg) were loaded into SDS-PAGE and ApoB100 (LDL marker protein) was detected by western blotting using an anti-ApoB100 Ab. (B) Schematic workflow for the immunocapture of LDL/VLDL from MP-sEV samples, which contain the bulk of LDL/VLDL nanoparticles. (C) Protein staining of input and non-captured fractions by SDS-PAGE (1.0 μg protein/lane). (D) Western blotting analysis of captured and non-captured fractions. ApoB100 was detected by western blotting. As a control immunocapturing, $^{gLuc\text{-}LA}$MP-sEVs was immunocaptured by gLuc-Ab conjugated magnetic beads, followed by ApoB100 detection in each fraction. (E) and (F) gLuc distribution after immunocapture using (E) anti-Pme1 Ab (as a negative control Ab) or (F) anti-ApoB100 Ab-coated magnetic beads. The results are shown as the percentage of gLuc activity of each fraction divided by the total recovered gLuc activity.

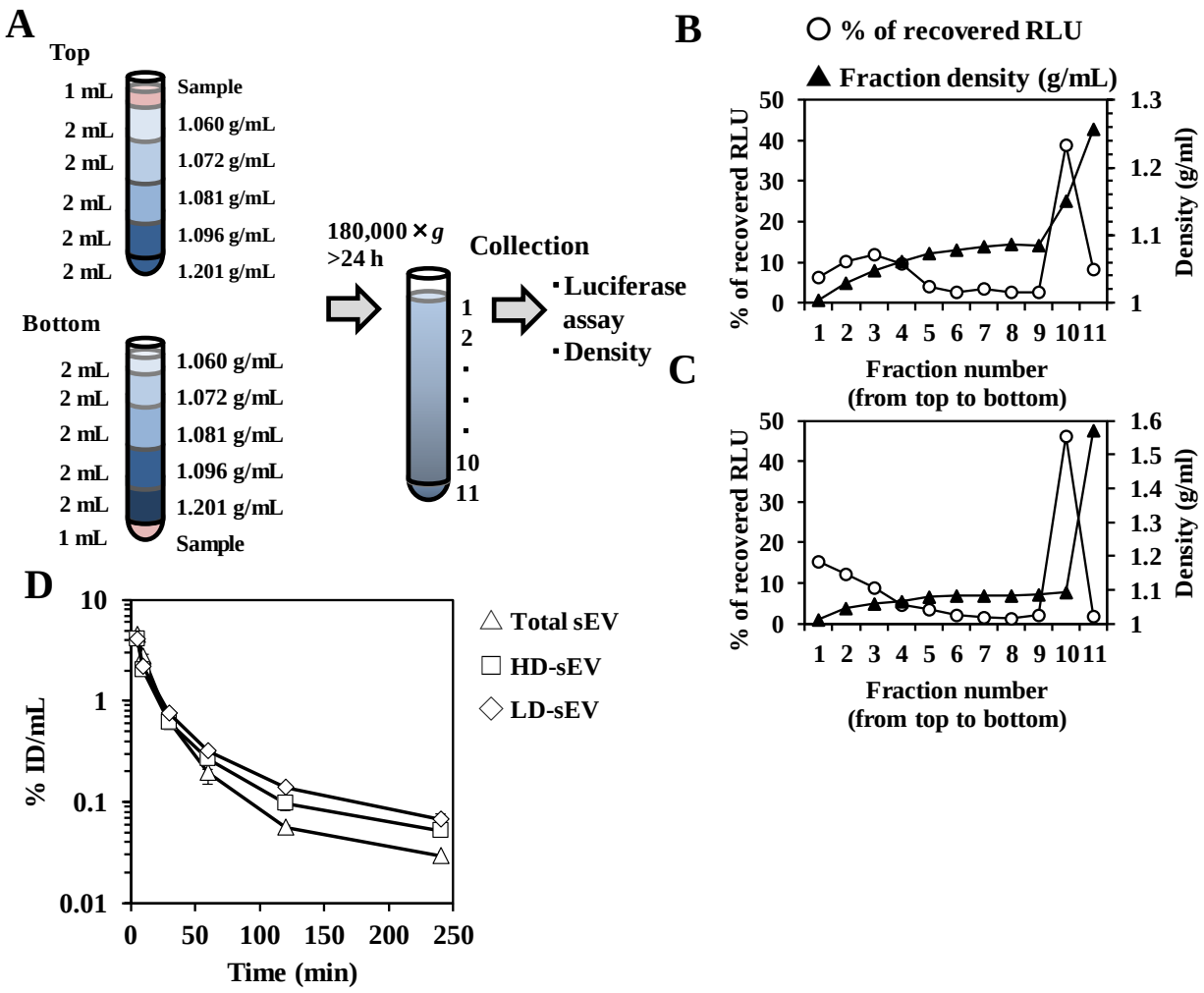

Supplementary figure 12. Fractionation of MP-sEV by DGC and blood clearance after i.v. administration.

(A) Schematic workflow for the fractionation of $^{gLuc\text{-}LA}$MP-sEVs by DGC. sEV samples were loaded at the (B) top or (C) bottom of the Optiprep buffer. The typical density profiles and gLuc activity of each fraction from top to bottom are shown. The results are shown as the percentage of gLuc activity of each fraction divided by the total recovered gLuc activity. The fractions were separated into high-density sEV (HD-sEV; density > 1.08 g/mL) and low-density sEV (LD-sEV; density < 1.08 g/mL) groups based on density. "Total sEV" represents the input $^{gLuc\text{-}LA}$MP-sEVs. (D) Blood clearance of gLuc-LA-labeled Total sEV (triangle), HD-sEV (square), and LD-sEV (diamond) preparations after i.v. administration into mice. Results are expressed as the mean of the percentage of injected dose/mL (% ID/mL) ± SD (n = 3).

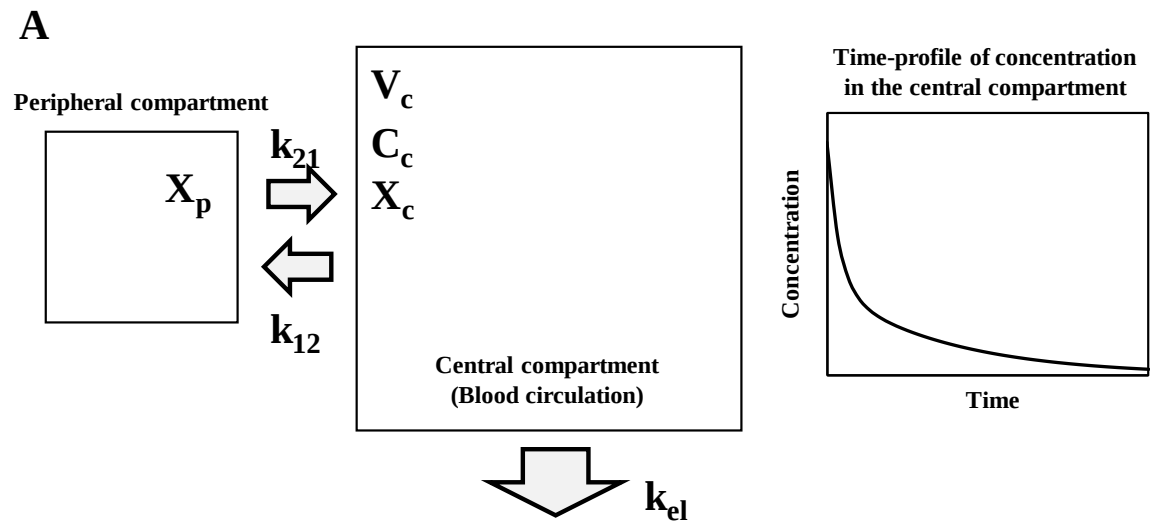

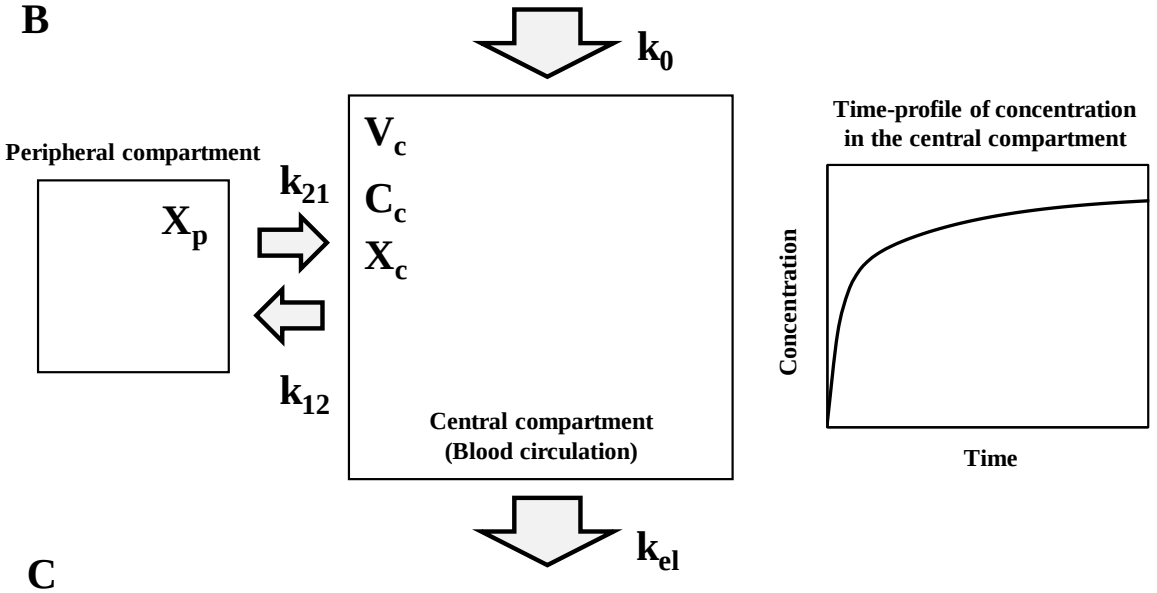

C

Sample	Treated mice	A	α	B	β	V_c (mL)	k_{21} (min^{-1})	k_{12} (min^{-1})	k_{el} (min^{-1})
$^{gLuc\text{-}LA}$MP-sEV from NT mice	NT mice	798	1.24	5.02	0.0535	0.125	0.0609	0.144	1.09
$^{gLuc\text{-}LA}$MP-sEV from MD mice	MD mice	12.3	0.00544	5.61	0.0207	5.59	0.0159	0.00316	0.00708

Supplementary figure 13. Schematic image of PK analysis by two-compartment model.

(A) Two-compartment model with intravenous bolus administration (left). Typical profile of serum-drug level versus time for this model is shown (right). (B) Two-compartment model with intravenous infusion (left). Typical profile of serum-drug level versus time for this model is shown (right). (C) PK parameters of gLuc-LA-labeled MP-sEV from NT mice or MD mice after i.v. injection into NT mice or MD mice, respectively.

CHAPTER IV

Discovery of novel long circulating small extracellular vesicle through escape from macrophage uptake

IV-1. Summary of chapter IV

Although the understanding of the biology, function and translational potential of sEV is expanding rapidly, the macrophage-dependent rapid blood clearance of blood-derived as well as cultured cell-derived sEV with a blood half-life less than 10 min have hindered further research progresses[26,113]. As recently highlighted by many sEV researchers, cells can release heterogenous sEVs with distinct biological properties[134]. Fractionation of sEV by size, or density followed by characterization revealed that *in vivo* fate of sEV can be slightly different depending on the subpopulations[119]. These findings raise possibility that sEV subpopulation with long blood circulation might exist. However, current approaches still limited identification of such sEV subpopulations. For the successful discovery of sEV subpopulation with long blood circulation, several challenges need to be overcome, such as information of promising markers which is critical for the sEV clearance from the blood and establishing protocol for distinct sEV fractionation and identification.

In chapter III, I evaluated how lipid on the sEV membrane affected sEV rapid blood clearance after i.v. administration[51]. Combined with the previous report on how surface protein on the sEV membrane is involved in the sEV clearance from blood, I investigated whether there is an sEV subpopulation that shows long blood circulation in this chapter. As a result, I have discovered and characterized such an sEV subpopulation in terms of the *in vivo* fate (blood clearance, and biodistribution) as well as the physicochemical & biological properties. These findings will help to integrate *in vivo* and *in vitro* knowledge to understand the biological role of sEVs.

CONCLUSION

sEV is a cell-derived lipid nanoparticle which encapsulates nucleic acids and proteins inside the vesicle. Ever since the discovery that sEV can transfer the cargos to the remote recipient cells, sEV has recently been expected as a novel therapeutics or drug carrier. One of the most important issues is the development of sEV-based therapeutics based on elucidation and regulation of PK properties. My laboratory has previously found that sEVs are efficiently taken up by macrophages, one of the APCs. Thus, my laboratory has studied to utilize tumor cell-derived sEV which carry tumor antigens for cancer vaccine.

Based on these research backgrounds, in chapter I, the *in vivo* fate of tumor cell-derived sEV after intratumoral administration was investigated. Since it was found that tumor cell-derived sEV was delivered to non-APCs instead of APCs, selective delivery of tumor cell-derived sEV to APCs was set as a challenging issue. I developed micrometer-sized sEV assembly which can selectively be delivered to APCs and can induce strong anti-tumor immunity.

In chapter II, DC-sEV was considered for cancer vaccine. The immunostimulatory activated-DC_{OVA}-sEV interacted with macrophages, DCs, and T cells to boost both innate and adaptive immunity. The activated-DC_{OVA}-sEV strongly activated the macrophages and dendritic cells in a TLR4-dependent mechanism. The APC-dependent mechanism was the primary pathway for T cell activation compared to the APC-independent mechanism. These result suggest that DC-sEV could be used as a cancer vaccine material which could elicit strong anti-tumor immunity.

Next, in order to control the PK properties of sEV and develop sEV-based versatile therapeutics or drug carrier, in chapter III, I elucidated the novel PK properties and its mechanism. It was found that PS in the cultured-cell-derived sEV surface is responsible for the recognition and uptake of sEV by macrophages. MP-sEV shows macrophage-dependent rapid clearance from blood circulation after i.v. administration, suggesting MP-sEV was recognized and taken up by macrophages by similar mechanism as cultured-cell-derived sEV.

In chapter IV, a novel $PS^{(-)}$-sEV subpopulation which escapes from macrophage uptake and shows long blood half-life was discovered. $PS^{(-)}$-sEV circulates the blood with a $t_{1/2\alpha}$ of 3 h. $PS^{(-)}$-sEV was estimated to exist at around 10% of the bulk sEV populations derived from a cultured cell. Moreover, it was found that such $PS^{(-)}$-sEVs were also discovered in mouse plasma and were *in vivo* selected by macrophages in the liver.

The obtained results contribute to the understanding on the PK properties of sEV and to the development of sEV-based therapeutics or drug carrier.

REFERENCES

1. Bianconi, E. *et al.* An estimation of the number of cells in the human body. *Ann. Hum. Biol.* **40**, 463–471 (2013).
2. McCoy, A. N. & Tan, S. Y. on. Otto Loewi (1873-1961): Dreamer and Nobel laureate. *Singapore Med. J.* **55**, 3–4 (2014).
3. Harding, C., Heuser, J. & Stahl, P. Receptor-mediated endocytosis of transferrin and recycling of the transferrin receptor in rat reticulocytes. *J. Cell Biol.* **97**, 329–339 (1983).
4. Harding, C. V., Heuser, J. E. & Stahl, P. D. Exosomes: Looking back three decades and into the future. *J. Cell Biol.* **200**, 367–371 (2013).
5. Raposo, G. *et al.* B lymphocytes secrete antigen-presenting vesicles. *J. Exp. Med.* **183**, 1161–1172 (1996).
6. Valadi, H. *et al.* Exosome-mediated transfer of mRNAs and microRNAs is a novel mechanism of genetic exchange between cells. *Nat. Cell Biol.* **9**, 654–659 (2007).
7. Alvarez-Erviti, L. *et al.* Delivery of siRNA to the mouse brain by systemic injection of targeted exosomes. *Nat. Biotechnol.* **29**, 341–345 (2011).
8. Murphy, D. E. *et al.* Extracellular vesicle-based therapeutics: natural versus engineered targeting and trafficking. *Exp. Mol. Med.* **51**, (2019).
9. Pitt, J. M. *et al.* Dendritic Cell–Derived Exosomes as Immunotherapies in the Fight against Cancer. *J. Immunol.* **193**, 1006–1011 (2014).
10. Morishita, M., Takahashi, Y., Nishikawa, M. & Takakura, Y. Pharmacokinetics of Exosomes—An Important Factor for Elucidating the Biological Roles of Exosomes and for the Development of Exosome-Based Therapeutics. *J. Pharm. Sci.* **106**, 2265–2269 (2017).
11. Sadovska, L., Santos, C. B., Kalniņa, Z. & Linē, A. Biodistribution, Uptake and Effects Caused by Cancer-Derived Extracellular Vesicles. *J. Circ. Biomarkers* **4**, 1–15 (2015).
12. Wiklander, O. P. B. *et al.* Extracellular vesicle in vivo biodistribution is determined by cell source, route of administration and targeting. *J. Extracell. Vesicles* **4**, 1–13 (2015).

13. Coulie, P. G., Van Den Eynde, B. J., Van Der Bruggen, P. & Boon, T. Tumour antigens recognized by T lymphocytes: At the core of cancer immunotherapy. *Nat. Rev. Cancer* **14**, 135–146 (2014).

14. Sun, Y. & Liu, J. Potential of cancer cell-derived exosomes in clinical application: A review of recent research advances. *Clin. Ther.* **36**, 863–872 (2014).

15. Morishita, M., Takahashi, Y., Matsumoto, A., Nishikawa, M. & Takakura, Y. Exosome-based tumor antigens–adjuvant co-delivery utilizing genetically engineered tumor cell-derived exosomes with immunostimulatory CpG DNA. *Biomaterials* **111**, 55–65 (2016).

16. Morishita, M., Takahashi, Y., Nishikawa, M., Ariizumi, R. & Takakura, Y. Enhanced Class i Tumor Antigen Presentation via Cytosolic Delivery of Exosomal Cargos by Tumor-Cell-Derived Exosomes Displaying a pH-Sensitive Fusogenic Peptide. *Mol. Pharm.* **14**, 4079–4086 (2017).

17. Morishita, M. *et al.* Quantitative analysis of tissue distribution of the B16BL6-derived exosomes using a streptavidin-lactadherin fusion protein and Iodine-125-Labeled biotin derivative after intravenous injection in mice. *J. Pharm. Sci.* **104**, 705–713 (2015).

18. Suchorska, W. M. & Lach, M. S. The role of exosomes in tumor progression and metastasis (Review). *Oncol. Rep.* **35**, 1237–1244 (2016).

19. Costa-Silva, B. *et al.* Pancreatic cancer exosomes initiate pre-metastatic niche formation in the liver. *Nat. Cell Biol.* **17**, 816–826 (2015).

20. Peinado, H. *et al.* Melanoma exosomes educate bone marrow progenitor cells toward a pro-metastatic phenotype through MET. *Nat. Med.* **18**, 883–891 (2012).

21. Hoshino, A. *et al.* Tumour exosome integrins determine organotropic metastasis. *Nature* **527**, 329–335 (2015).

22. Tominaga, N. *et al.* Brain metastatic cancer cells release microRNA-181c-containing extracellular vesicles capable of destructing blood-brain barrier. *Nat. Commun.* **6**, (2015).

23. Ge, R., Tan, E., Sharghi-Namini, S. & Asada, H. H. Exosomes in cancer microenvironment and beyond: Have we overlooked these extracellular messengers? *Cancer Microenviron.* **5**, 323–332 (2012).

24. Kahlert, C. & Kalluri, R. Exosomes in tumor microenvironment influence cancer progression and metastasis. *J.*

Mol. Med. **91**, 431–437 (2013).

25. Takahashi, Y. *et al.* Visualization and in vivo tracking of the exosomes of murine melanoma B16-BL6 cells in mice after intravenous injection. *J. Biotechnol.* **165**, 77–84 (2013).

26. Imai, T. *et al.* Macrophage-dependent clearance of systemically administered B16BL6-derived exosomes from the blood circulation in mice. *J. Extracell. Vesicles* **4**, 1–8 (2015).

27. Baldin, V., Lukas, J., Marcote, M. J., Pagano, M. & Draetta, G. Cyclin D1 is a nuclear protein required for cell cycle progression in G1. *Genes Dev.* **7**, 812–821 (1993).

28. Cory, S., Huang, D. C. S. & Adams, J. M. The Bcl-2 family: Roles in cell survival and oncogenesis. *Oncogene* **22**, 8590–8607 (2003).

29. Swanton, E., Savory, P., Cosulich, S., Clarke, P. & Woodman, P. Bcl-2 regulates a caspase-3/caspase-2 apoptotic cascade in cytosolic extracts. *Oncogene* **18**, 1781–1787 (1999).

30. Hennessy, B. T., Smith, D. L., Ram, P. T., Lu, Y. & Mills, G. B. Exploiting the PI3K/AKT pathway for cancer drug discovery. *Nat. Rev. Drug Discov.* **4**, 988–1004 (2005).

31. Altieri, D. C. Survivin, cancer networks and pathway-directed drug discovery. *Nat. Rev. Cancer* **8**, 61–70 (2008).

32. Ito, T. *et al.* Survivin promotes cell proliferation in human hepatocellular carcinoma. *Hepatology* **31**, 1080–1085 (2000).

33. Wang, H. W., Sharp, T. V., Koumi, A., Koentges, G. & Boshoff, C. Characterization of an anti-apoptotic glycoprotein encoded by Kaposi's sarcoma-associated herpesvirus which resembles a spliced variant of human survivin. *EMBO J.* **21**, 2602–2615 (2002).

34. Yang, L., Wu, X. H., Wang, D., Luo, C. L. & Chen, L. X. Bladder cancer cell-derived exosomes inhibit tumor cell apoptosis and induce cell proliferation in vitro. *Mol. Med. Rep.* **8**, 1272–1278 (2013).

35. Luberto, C. *et al.* Inhibition of tumor necrosis factor-induced cell death in MCF7 by a novel inhibitor of neutral sphingomyelinase. *J. Biol. Chem.* **277**, 41128–41139 (2002).

36. Essandoh, K. *et al.* Blockade of exosome generation with GW4869 dampens the sepsis-induced inflammation and cardiac dysfunction. *Biochim. Biophys. Acta - Mol. Basis Dis.* **1852**, 2362–2371 (2015).

37. Guo, B. B., Bellingham, S. A. & Hill, A. F. The neutral sphingomyelinase pathway regulates packaging of the prion protein into exosomes. *J. Biol. Chem.* **290**, 3455–3467 (2015).

38. Li, J. *et al.* Exosomes mediate the cell-to-cell transmission of IFN-α-induced antiviral activity. *Nat. Immunol.* **14**, 793–803 (2013).

39. Rohner, N. A. & Thomas, S. N. Melanoma growth effects on molecular clearance from tumors and biodistribution into systemic tissues versus draining lymph nodes. *J. Control. Release* **223**, 99–108 (2016).

40. Weis, S. M. & Cheresh, D. A. Tumor angiogenesis: Molecular pathways and therapeutic targets. *Nat. Med.* **17**, 1359–1370 (2011).

41. Hazan-Halevy, I. *et al.* Cell-specific uptake of mantle cell lymphoma-derived exosomes by malignant and non-malignant B-lymphocytes. *Cancer Lett.* **364**, 59–69 (2015).

42. Rana, S., Yue, S., Stadel, D. & Zöller, M. Toward tailored exosomes: The exosomal tetraspanin web contributes to target cell selection. *Int. J. Biochem. Cell Biol.* **44**, 1574–1584 (2012).

43. Raimondo, S. *et al.* Chronic myeloid leukemia-derived exosomes promote tumor growth through an autocrine mechanism. *Cell Commun. Signal.* **13**, 1–12 (2015).

44. Bachmann, M. F. & Jennings, G. T. Vaccine delivery: A matter of size, geometry, kinetics and molecular patterns. *Nat. Rev. Immunol.* **10**, 787–796 (2010).

45. Weissleder, R., Nahrendorf, M. & Pittet, M. J. Imaging macrophages with nanoparticles. *Nat. Mater.* **13**, 125–138 (2014).

46. Pradal, J. *et al.* Effect of particle size on the biodistribution of nano- and microparticles following intra-articular injection in mice. *Int. J. Pharm.* **498**, 119–129 (2016).

47. Feng, Q. *et al.* Self-Assembly of Gold Nanoparticles Shows Microenvironment-Mediated Dynamic Switching and Enhanced Brain Tumor Targeting. *Theranostics* **7**, 1875–1889 (2017).

48. Chou, L. Y. T., Zagorovsky, K. & Chan, W. C. W. DNA assembly of nanoparticle superstructures for controlled biological delivery and elimination. *Nat. Nanotechnol.* **9**, 148–155 (2014).

49. Mizukami, Y. *et al.* Regulation of the Distribution of Cells in Mixed Spheroids by Altering Migration Direction.

Tissue Eng. - Part A **25**, 390–398 (2019).

50. Matsumoto, A. *et al.* Accelerated growth of B16BL6 tumor in mice through efficient uptake of their own exosomes by B16BL6 cells. *Cancer Sci.* **108**, 1803–1810 (2017).

51. Matsumoto, A. *et al.* Role of Phosphatidylserine-Derived Negative Surface Charges in the Recognition and Uptake of Intravenously Injected B16BL6-Derived Exosomes by Macrophages. *J. Pharm. Sci.* **106**, 168–175 (2017).

52. Xin, Q. *et al.* Subunit Vaccine Consisting of Multi-Stage Antigens Has High Protective Efficacy against Mycobacterium tuberculosis Infection in Mice. *PLoS One* **8**, 1–12 (2013).

53. Moon, H. J. *et al.* Mucosal immunization with recombinant influenza hemagglutinin protein and poly gamma-glutamate/chitosan nanoparticles induces protection against highly pathogenic influenza A virus. *Vet. Microbiol.* **160**, 277–289 (2012).

54. Chen, W. *et al.* Efficient induction of comprehensive immune responses to control pathogenic E. coli by clay nano-adjuvant with the moderate size and surface charge. *Sci. Rep.* **7**, 1–12 (2017).

55. Mirkin, C. A., Letsinger, R. L., Mucic, R. C. & Storhoff, J. J. A DNA-based method for rationally assembling nanoparticles into macroscopic materials. *Nature* **382**, 607–609 (1996).

56. Chan, Y. H. M., Van Lengerich, B. & Boxer, S. G. Effects of linker sequences on vesicle fusion mediated by lipid-anchored DNA oligonucleotides. *Proc. Natl. Acad. Sci. U. S. A.* **106**, 979–984 (2009).

57. Dave, N. & Liu, J. Programmable assembly of DNA-functionalized liposomes by DNA. *ACS Nano* **5**, 1304–1312 (2011).

58. Mulcahy, L. A., Pink, R. C. & Carter, D. R. F. Routes and mechanisms of extracellular vesicle uptake. *J. Extracell. Vesicles* **3**, (2014).

59. Stern, S. T., Adiseshaiah, P. P. & Crist, R. M. Autophagy and lysosomal dysfunction as emerging mechanisms of nanomaterial toxicity. *Part. Fibre Toxicol.* **9**, 1 (2012).

60. Canton, J. Macropinocytosis: New insights into its underappreciated role in innate immune cell surveillance. *Front. Immunol.* **9**, 1–8 (2018).

61. Mathers, A. R. & Larregina, A. T. Professional antigen-presenting cells of the skin. *Immunol. Res.* **36**, 127–136 (2006).

62. Srinivasan, S., Vannberg, F. O. & Dixon, J. B. Lymphatic transport of exosomes as a rapid route of information dissemination to the lymph node. *Sci. Rep.* **6**, 1–14 (2016).

63. Kim, S. H., Bianco, N. R., Shufesky, W. J., Morelli, A. E. & Robbins, P. D. Effective Treatment of Inflammatory Disease Models with Exosomes Derived from Dendritic Cells Genetically Modified to Express IL-4. *J. Immunol.* **179**, 2242–2249 (2007).

64. Nibbs, R. J. B. & Graham, G. J. Immune regulation by atypical chemokine receptors. *Nat. Rev. Immunol.* **13**, 815–829 (2013).

65. Jones, S. A. & Jenkins, B. J. Recent insights into targeting the IL-6 cytokine family in inflammatory diseases and cancer. *Nat. Rev. Immunol.* **18**, 773–789 (2018).

66. Bunggulawa, E. J. *et al.* Recent advancements in the use of exosomes as drug delivery systems 06 Biological Sciences 0601 Biochemistry and Cell Biology. *J. Nanobiotechnology* **16**, 1–13 (2018).

67. Akiyama, Y., Shikagawa, H., Kanayama, N., Takarada, T. & Maeda, M. Modulation of Interparticle Distance in Discrete Gold Nanoparticle Dimers and Trimers by DNA Single-Base Pairing. *Small* **11**, 3153–3161 (2015).

68. Trantakis, I. A., Bolisetty, S., Mezzenga, R. & Sturla, S. J. Reversible aggregation of DNA-decorated gold nanoparticles controlled by molecular recognition. *Langmuir* **29**, 10824–10830 (2013).

69. Théry, C. *et al.* Minimal information for studies of extracellular vesicles 2018 (MISEV2018): a position statement of the International Society for Extracellular Vesicles and update of the MISEV2014 guidelines. *J. Extracell. Vesicles* **7**, (2018).

70. Hernández-Ainsa, S. *et al.* Controlling the reversible assembly of liposomes through a multistimuli responsive anchored DNA. *Nano Lett.* **16**, 4462–4466 (2016).

71. Viaud, S. *et al.* Dendritic cell-derived exosomes for cancer immunotherapy: What's next? *Cancer Res.* **70**, 1281–1285 (2010).

72. Damo, M., Wilson, D. S., Simeoni, E. & Hubbell, J. A. TLR-3 stimulation improves anti-tumor immunity elicited

by dendritic cell exosome-based vaccines in a murine model of melanoma. *Sci. Rep.* **5**, 1–15 (2015).

73. Wahlund, C. J. E. *et al.* Exosomes from antigen-pulsed dendritic cells induce stronger antigen-specific immune responses than microvesicles in vivo. *Sci. Rep.* **7**, 1–9 (2017).

74. Zitvogel L, Regnault A, Lozier A, Wolfers J, Flament C, Tenza D, Ricciardi-Castagnoli P, Raposo G, A. S. *et al.* Eradication of established murine tumors using a novel cell-free vaccine: dendritic cell-derived exosomes. *Nat. Med.* **4**, 594–600 (1998).

75. Vacchelli, E. *et al.* Trial Watch: Dendritic cell-based interventions for cancer therapy. *Oncoimmunology* **2**, (2013).

76. Moynihan, K. D. & Irvine, D. J. Roles for innate immunity in combination immunotherapies. *Cancer Res.* **77**, 5215–5221 (2017).

77. Demaria, O. *et al.* Harnessing innate immunity in cancer therapy. *Nature* **574**, 45–56 (2019).

78. Hoves, S. *et al.* Rapid activation of tumor-associated macrophages boosts preexisting tumor immunity. *J. Exp. Med.* **215**, 859–876 (2018).

79. Hiltbrunner, S. *et al.* Exosomal cancer immunotherapy is independent of MHC molecules on exosomes. *Oncotarget* **7**, 38707–38717 (2016).

80. Charoenviriyakul, C. *et al.* Cell type-specific and common characteristics of exosomes derived from mouse cell lines: Yield, physicochemical properties, and pharmacokinetics. *Eur. J. Pharm. Sci.* **96**, 316–322 (2017).

81. Bakhshandeh, B., Kamaleddin, M. & Aalishah, K. A Comprehensive Review on Exosomes and Microvesicles as Epigenetic Factors. *Curr. Stem Cell Res. Ther.* **12**, 31–36 (2016).

82. Wu, M. *et al.* Isolation of exosomes from whole blood by integrating acoustics and microfluidics. *Proc. Natl. Acad. Sci. U. S. A.* **114**, 10584–10589 (2017).

83. Wu, Y., Tibrewal, N. & Birge, R. B. Phosphatidylserine recognition by phagocytes: a view to a kill. *Trends Cell Biol.* **16**, 189–197 (2006).

84. Terpstra, V. & Van Berkel, T. J. C. Scavenger receptors on liver Kupffer cells mediate the in vivo uptake of oxidatively damaged red blood cells in mice. *Blood* **95**, 2157–2163 (2000).

85. Fadok, V. A. *et al.* A receptor for phosphatidylserine-specific clearance of apoptotic cells. *Nature* **405**, 85–90

(2000).

86. Subra, C., Laulagnier, K., Perret, B. & Record, M. Exosome lipidomics unravels lipid sorting at the level of multivesicular bodies. *Biochimie* **89**, 205–212 (2007).

87. Llorente, A. *et al.* Molecular lipidomics of exosomes released by PC-3 prostate cancer cells. *Biochim. Biophys. Acta - Mol. Cell Biol. Lipids* **1831**, 1302–1309 (2013).

88. Kiyota, T. *et al.* Enhancement of anticancer effect of interferon-γ gene transfer against interferon-γ-resistant tumor by depletion of tumor-associated macrophages. *Mol. Pharm.* **11**, 1542–1549 (2014).

89. Yamashita, T., Takahashi, Y., Nishikawa, M. & Takakura, Y. Effect of exosome isolation methods on physicochemical properties of exosomes and clearance of exosomes from the blood circulation. *Eur. J. Pharm. Biopharm.* **98**, 1–8 (2016).

90. Escrevente, C., Keller, S., Altevogt, P. & Costa, J. Interaction and uptake of exosomes by ovarian cancer cells. *BMC Cancer* **11**, (2011).

91. Zhang, G., Gurtu, V., Kain, S. R. & Yan, G. Early detection of apoptosis using a fluorescent conjugate of annexin V. *Biotechniques* **23**, 525–531 (1997).

92. Bennett, M. R., Gibson, D. F., Schwartz, S. M. & Tait, J. F. Binding and phagocytosis of apoptotic vascular smooth muscle cells is mediated in part by exposure of phosphatidylserine. *Circ. Res.* **77**, 1136–1142 (1995).

93. Wang, Q., Ju, X., Zhou, Y. & Chen, K. Necroptotic cells release find-me signal and are engulfed without proinflammatory cytokine production. *Vitr. Cell. Dev. Biol. - Anim.* **51**, 1033–1039 (2015).

94. Driscoll, W. S., Vaisar, T., Tang, J., Wilson, C. L. & Raines, E. W. Macrophage ADAM17 deficiency augments CD36-dependent apoptotic cell uptake and the linked anti-inflammatory phenotype. *Circ. Res.* **113**, 52–61 (2013).

95. Kobayashi, N. *et al.* TIM-1 and TIM-4 Glycoproteins Bind Phosphatidylserine and Mediate Uptake of Apoptotic Cells. *Immunity* **27**, 927–940 (2007).

96. Tian, L. *et al.* P85α recruitment by the CD300f phosphatidylserine receptor mediates apoptotic cell clearance required for autoimmunity suppression. *Nat. Commun.* **5**, 1–15 (2014).

97. Henson, D. L. B. and P. M. Apoptotic Cell Recognition: Will the Real Phosphatidylserine Receptor(s) Please

Stand up? *Curr. Biol.* **18**, 76–79 (2008).

98. Graham, D. K., Deryckere, D., Davies, K. D. & Earp, H. S. The TAM family: Phosphatidylserine-sensing receptor tyrosine kinases gone awry in cancer. *Nat. Rev. Cancer* **14**, 769–785 (2014).

99. Moghimi, S. M. & Hunter, A. C. Recognition by macrophages and liver cells of opsonized phospholipid vesicles and phospholipid headgroups. *Pharmaceutical Research* vol. 18 1–8 (2001).

100. Rigotti, A., Acton, S. L. & Krieger, M. The class B scavenger receptors SR-BI and CD36 are receptors for anionic phospholipids. *Journal of Biological Chemistry* vol. 270 16221–16224 (1995).

101. Mebius, R. E. & Kraal, G. Structure and function of the spleen. *Nature Reviews Immunology* vol. 5 606–616 (2005).

102. Saunderson, S. C., Dunn, A. C., Crocker, P. R. & McLellan, A. D. CD169 mediates the capture of exosomes in spleen and lymph node. *Blood* **123**, 208–216 (2014).

103. Charoenviriyakul, C., Takahashi, Y., Morishita, M., Nishikawa, M. & Takakura, Y. Role of Extracellular Vesicle Surface Proteins in the Pharmacokinetics of Extracellular Vesicles. *Mol. Pharm.* **15**, 1073–1080 (2018).

104. Blanco, E., Shen, H. & Ferrari, M. Principles of nanoparticle design for overcoming biological barriers to drug delivery. *Nat. Biotechnol.* **33**, 941–951 (2015).

105. Karimi, N. *et al.* Detailed analysis of the plasma extracellular vesicle proteome after separation from lipoproteins. *Cell. Mol. Life Sci.* **75**, 2873–2886 (2018).

106. Simonsen, J. B. Pitfalls associated with lipophilic fluorophore staining of extracellular vesicles for uptake studies. *J. Extracell. Vesicles* **8**, (2019).

107. Gudbergsson, J. M., Johnsen, K. B., Skov, M. N. & Duroux, M. Systematic review of factors influencing extracellular vesicle yield from cell cultures. *Cytotechnology* **68**, 579–592 (2016).

108. Verweij, F. J. *et al.* Quantifying exosome secretion from single cells reveals a modulatory role for GPCR signaling. *J. Biol. Chem.* **217**, 1129–1142 (2018).

109. Hong, C. S., Funk, S., Muller, L., Boyiadzis, M. & Whiteside, T. L. Isolation of biologically active and morphologically intact exosomes from plasma of patients with cancer. *J. Extracell. Vesicles* **5**, 1–11 (2016).

110. Lauer, M. E. *et al.* Cholesteryl ester transfer between lipoproteins does not require a ternary tunnel complex with CETP. *J. Struct. Biol.* **194**, 191–198 (2016).

111. Sódar, B. W. *et al.* Low-density lipoprotein mimics blood plasma-derived exosomes and microvesicles during isolation and detection. *Sci. Rep.* **6**, 1–12 (2016).

112. Wagner, J. G. Linear pharmacokinetic equations allowing direct calculation of many needed pharmacokinetic parameters from the coefficients and exponents of polyexponential equations which have been fitted to the data. *J. Pharmacokinet. Biopharm.* **4**, 443–467 (1976).

113. Yamaoka, K., Tanigawara, Y., Nakagawa, T. & Uno, T. A pharmacokinetic analysis program (multi) for microcomputer. *J. Pharmacobiodyn.* **4**, 879–885 (1981).

114. Rappsilber, J., Mann, M. & Ishihama, Y. Protocol for micro-purification, enrichment, pre-fractionation and storage of peptides for proteomics using StageTips. *Nat. Protoc.* **2**, 1896–1906 (2007).

115. Trubey, C. M. *et al.* Quantitation of HLA Class II Protein Incorporated into Human Immunodeficiency Type 1 Virions Purified by Anti-CD45 Immunoaffinity Depletion of Microvesicles. *J. Virol.* **77**, 12699–12709 (2003).

116. Simonsen, J. B. What Are We Looking At? Extracellular Vesicles, Lipoproteins, or Both? *Circ. Res.* **121**, 920–922 (2017).

117. Hartjes, T. A., Mytnyk, S., Jenster, G. W., van Steijn, V. & van Royen, M. E. Extracellular vesicle quantification and characterization: Common methods and emerging approaches. *Bioengineering* **6**, (2019).

118. Johnsen, K. B., Gudbergsson, J. M., Andresen, T. L. & Simonsen, J. B. What is the blood concentration of extracellular vesicles? Implications for the use of extracellular vesicles as blood-borne biomarkers of cancer. *Biochim. Biophys. Acta - Rev. Cancer* **1871**, 109–116 (2019).

119. Zhang, H. *et al.* Identification of distinct nanoparticles and subsets of extracellular vesicles by asymmetric flow field-flow fractionation. *Nat. Cell Biol.* **20**, 332–343 (2018).

120. Wei, H., Malcor, J. D. M. & Harper, M. T. Lipid rafts are essential for release of phosphatidylserine-exposing extracellular vesicles from platelets. *Sci. Rep.* **8**, 1–11 (2018).

121. Rak, J. Extracellular vesicles - biomarkers and effectors of the cellular interactome in cancer. *Front. Pharmacol.*

4 MAR, 1–14 (2013).

122. Sharma, P. *et al.* Immunoaffinity-based isolation of melanoma cell-derived exosomes from plasma of patients with melanoma. *J. Extracell. Vesicles* **7**, (2018).

123. Son, K. J. *et al.* Microfluidic compartments with sensing microbeads for dynamic monitoring of cytokine and exosome release from single cells. *Analyst* **141**, 679–688 (2016).

124. Chiu, Y. J., Cai, W., Shih, Y. R. V., Lian, I. & Lo, Y. H. A single-cell assay for time lapse studies of exosome secretion and cell behaviors. *Small* **12**, 3658–3666 (2016).

125. Nemzek, J. A., Bolgos, G. L., Williams, B. A. & Remick, D. G. Differences in normal values for murine white blood cell counts and other hematological parameters based on sampling site. *Inflamm. Res.* **50**, 523–527 (2001).

126. Webber, J. & Clayton, A. How pure are your vesicles? *J. Extracell. Vesicles* **2**, (2013).

127. Ezekowitz, R. A. B., Sim, R. B., Hill, M. & Gordon, S. Local opsonization by secreted macrophage complement components: Role of receptors for complement in uptake of zymosan. *J. Exp. Med.* **159**, 244–260 (1984).

128. Clayton, A., Harris, C. L., Court, J., Mason, M. D. & Morgan, B. P. Antigen-presenting cell exosomes are protected from complement-mediated lysis by expression of CD55 and CD59. *Eur. J. Immunol.* **33**, 522–531 (2003).

129. Hong, C. S. *et al.* Circulating exosomes carrying an immunosuppressive cargo interfere with cellular immunotherapy in acute myeloid leukemia. *Sci. Rep.* **7**, 1–10 (2017).

130. Lv, L. H. *et al.* Anticancer drugs cause release of exosomes with heat shock proteins from human hepatocellular carcinoma cells that elicit effective natural killer cell antitumor responses in vitro. *J. Biol. Chem.* **287**, 15874–15885 (2012).

131. Marleau, A. M., Chen, C. S., Joyce, J. A. & Tullis, R. H. Exosome removal as a therapeutic adjuvant in cancer. *J. Transl. Med.* **10**, 1 (2012).

132. Nishida-Aoki, N. *et al.* Disruption of Circulating Extracellular Vesicles as a Novel Therapeutic Strategy against Cancer Metastasis. *Mol. Ther.* **25**, 181–191 (2017).

133. Datta, A. *et al.* High-Throughput screening identified selective inhibitors of exosome biogenesis and secretion:

A drug repurposing strategy for advanced cancer. *Sci. Rep.* **8**, 1–13 (2018).

134. Kowal, J. *et al.* Proteomic comparison defines novel markers to characterize heterogeneous populations of extracellular vesicle subtypes. *Proc. Natl. Acad. Sci. U. S. A.* **113**, E968–E977 (2016).